

Numerical Modelling of Detonation and Ignition of Condensed Phase Explosives



Simon David Wilkinson

Hughes Hall

University of Cambridge

March, 2019

This thesis is submitted for the degree of Doctor of Philosophy.

Dedicated to the memory of my grandparents, Nonna and Bappa, who passed away before this thesis was completed.

Declaration

This thesis is the result of my own work and includes nothing which is the outcome of work done in collaboration except as declared in the Preface and specified in the text. It is not substantially the same as any that I have submitted, or, is being concurrently submitted for a degree or diploma or other qualification at the University of Cambridge or any other University or similar institution except as declared in the Preface and specified in the text. I further state that no substantial part of my thesis has already been submitted, or, is being concurrently submitted for any such degree, diploma or other qualification at the University of Cambridge or any other University or similar institution except as declared in the Preface and specified in the text. It does not exceed the prescribed word limit for the relevant Degree Committee.

Simon Wilkinson, March 2019

Numerical Modelling of Detonation and Ignition of Condensed Phase Explosives

Simon Wilkinson

A good understanding of the physical properties of explosives is essential for their safe and efficient usage. Numerical simulations have proven to be an excellent tool with which to develop and verify models which describe both ignition and detonation of explosives.

The objective of this work is to improve the robustness and accuracy of numerical simulations of both ideal and non-ideal explosives. Much of the complexity of the detonation phenomenon arises due to the finite width of the reaction zone, which causes the properties of the detonation wave to deviate from the predictions of the ZND model. If numerical models are to predict the attributes of the explosive to greater accuracy, then the dynamics of the reaction zone must be adequately resolved. This thesis also reviews the scientific literature in order to contextualise the developments presented here.

The approach taken in this thesis is to describe the thermodynamics in the reaction zone as a mixture of reactants and products which exist at pressure and thermal equilibrium. To this end, mechanical equations of state of Mie-Grüneisen form are developed with extensions, which allow the temperature to be evaluated appropriately, and the temperature equilibrium condition to be applied robustly. Furthermore the snow plow model is used to capture the effect of porosity.

The methodology is applied to predict the velocity of compliantly confined detonation waves. Once reaction rates are calibrated for unconfined detonation velocities, simulations of confined rate sticks and slabs are performed, and the experimental detonation velocities are matched without further parameter alteration, demonstrating the predictive capability of our simulations. We apply the same methodology to both the non-ideal explosive EM120D (an ANE or ammonium nitrate based emulsion) and the comparatively ideal TATB based explosive PBX 9502. Furthermore, this thesis presents a novel methodology to use gauge data from shock initiation experiments to calculate values for the reaction rate. The methodology can be applied to determine rate law parameters without the use of computationally intensive hydrocode simulations. The validity and limitations of this approach are demonstrated through its application to simulated gauge data for an idealized explosive. The resulting rate law is then used in simulations of shock to detonation transition, and confined detonation waves of the TATB based explosive PBX 9502. Comparison of the results with experimental data is favourable.

Acknowledgements

Many thanks go to my supervisors Dr. Nikos Nikiforakis and Dr. Louisa Michael. Thanks are also due to Prof. Martin Braithwaite, Dr. Alan Minchinton, Dr. Mark Short, Dr. Carlos Chiquete, Dr. Tariq Aslam for useful discussions.

I would also like to thank the Laboratory of Scientific Computing group, especially Dr. Philip Blakely for help with programming and the use of LSC-AMR. I am also grateful to the EPSRC CDT of Computational Modelling of Materials Science for funding.

Finally I thank my family and friends for supporting me.

Contents

1	Introduction	1
1.1	Background	1
1.2	Outline	8
1.3	Novel Contributions of this Thesis	10
1.4	Publications	11
2	Literature Review	13
2.1	Equations of State	13
2.1.1	Fundamentals	13
2.1.2	Reactants	21
2.1.3	Products	26
2.2	Reaction Rate Models	31
2.2.1	Construction and Calibration of Reaction Rate Models	31
2.2.2	Homogeneous and Heterogeneous Explosives	37
2.3	Discussion	41
3	Equations of State	45
3.1	Introduction	45
3.2	Mie-Grüneisen	46
3.3	Products	50
3.4	Reactants	57
3.5	Porosity Model	59
3.6	Temperature of Reactants in the Expansion Regime	61
3.7	Closure Rules for Coexistence of Materials	64
3.8	Sound speed in the Mixture of Materials	68
3.9	Approach for robust solution of the root-finding problem	69
3.10	Conclusions	72
4	ZND Waves	75
4.1	Introduction	75
4.2	Inert Shock Waves	75
4.3	Reactive Shock Waves	79
4.4	The Reaction Zone	82
4.5	Conclusions	90

5	Detonation Modelling	93
5.1	Formulations for multi-material fluid simulations	93
5.2	MiNi16 Formulation	97
5.3	Numerical Methods	101
5.4	Rotational Symmetry	102
5.5	Validation	102
5.5.1	Riemann Tests	102
5.5.2	Shock Speed	105
5.5.3	Detonation Waves in 1D	107
5.6	Evaluating the detonation velocity	110
5.7	Predictive Modelling of Detonation Waves in Rate Sticks and Slabs .	111
5.7.1	Simulation Setup	111
5.7.2	Calibration of the Reaction Rate for EM120D	115
5.7.3	Calibration of the Reaction Rate for PBX 9502	123
5.8	Conclusions	125
6	Direct Calibration of Reaction Rate Models	127
6.1	Introduction	127
6.2	Methodology	130
6.3	Proof of Concept	135
6.4	Application to PBX 9502	139
6.5	Validation	142
6.6	Reaction Zone Width	144
6.7	Results	146
6.8	Conclusions	148
7	Conclusions	151
A	Derivation of the Shock Mie-Grüneisen Equation of State	156
B	Derivation of Davis Equation of State	158
C	Volume and Mass Fractions for Parametrising Multiphase Fluids	160

List of Figures

1.1	The pressure in a ZND wave propagating through the domain to the right is shown. The red curve shows the portion by mass of the explosive consisting of reactants, i.e. the portion which is not yet burned. The values of the pressure and reaction zone width are representative of the ammonium nitrate based emulsion explosive EM120D.	2
1.2	This image shows the density field for a cut out of a rate stick. The confining material (air) is not shown. The cylindrical shape of the unburned rate stick is visible on the right. The shock wave is identifiable as the area with the highest density. The gaseous products expand to low density behind the shock wave.	3
3.1	The form chosen for $T_{S_{CJ}}$ ensures that the Grüneisen gamma is bounded and well behaved in both the limit of large volume and the limit of large density. The values plotted here are for the EoS of the products of PBX 9502, the parameters of which are presented in Table 3.2.	53
3.2	A fit to the principal isentrope from <i>IDeX</i> for PBX 9502. The principal isentrope data are given as blue dots. The fit (red) is the sum of the power law (cyan) and the exponential curve (green). The energy reference curve also includes a non-zero constant, Q , corresponding to the energy content of the explosive. Note how the fitting parameters are chosen such that the exponential term only plays a role in the small volume regime.	55
3.3	A fit to the principal isentrope from <i>IDeX</i> for EM120D.	56
3.4	The EoS calibrated using the ideal detonation code data is used to calculate the Crussard curve for PBX 9502. It matches the experimental data from Tang et al. [123] reasonably well. The CJ state is at the intersection of the Crussard curve with the Rayleigh line. . . .	57
3.5	The isentrope through the initial state is shown in green. The empty marker indicates the neat specific volume. The porosity model means that the isentrope is flat in between the initial the specific volume and the neat specific volume. For smaller volumes, the difference in pressure between an isentropic compression and following a shock wave is evident.	59

3.6 Comparison of Hugoniot curves when using the porosity model, and when using the standard EoS for neat materials. The EoS models are compared with experimental data for PBX 9502 [37, 49]. Both EoS models are calibrated using the same volume-pressure Hugoniot data. The predicted temperatures at each volume increase as a result of using the porosity model. 62

3.7 The relationship between shock velocity and flow velocity is affected by the porosity model. The linear relationship curves towards zero for weak shocks. In the limit of small shocks, this is clearly not valid, however for moderate shocks this curve fits the data well [37, 49]. . . 62

3.8 The dashed lines indicate where the restrictions on the domain are applied. The blue dashed lines indicate the limitation imposed by the equation of state for material β . The red dashed lines are the equivalent for material α . The black arrow indicates the region of the domain that will yield physical solutions. The left hand plot uses specific volumes while the right plot is in terms of density. 72

4.1 The Hugoniot curve and Crussard curve are shown in pressure volume space. The dotted line is the Rayleigh line, which is tangent to the Crussard curve. This corresponds to the slowest wave which intersects the Crussard curve. The intersection of the Rayleigh line with the Crussard curve is the CJ state. The von Neumann state is at the intersection of the Rayleigh line with the Hugoniot curve. This plot uses the equations of state for EM120D as presented in Chapter 3. 80

4.2 The partial burn Hugoniot curves for EM120D are plotted for several values of λ . Note that the curve for $\lambda = 1$ corresponds to the Hugoniot of the inert reactants, while the $\lambda = 0$ curve is the Crussard curve corresponding to a complete reaction. 84

4.3 The markers indicate the evolution of the state in pressure-volume space across the reaction zone of a ZND wave in PBX 9502. The red and green markers represent the state of the reactants and products respectively. The black lines represent the paths expected for heat isolation, in which case the reactants and products evolve isentropically. The blue line represents the path of the explosive mixture, which follows the Rayleigh line. 87

4.4 The temperature in the reaction zone as a function of the mass fraction of the explosive, λ , which consists of reactants. Note that as the reaction proceeds, the mass fraction goes from 1 to 0. 88

4.5 The one-dimensional ZND wave for EM120D is presented as for Figure 4.3. In this case the temperature equilibrium condition leads to more heat transfer between the reactants and products. 89

List of Figures

4.6	The temperatures in the reaction zone of EM120D are more disparate than what is predicted for PBX9502. In this case the temperature equilibrium condition leads to significantly lowered temperatures in the reactants than a heat isolation closure condition.	89
4.7	The temperatures in the reaction zone for EM120D are presented again, but this time with an increased heat capacity for the reactants. This has the effect of lowering the von Neumann spike temperature. In contrast to Figure 4.6, there is significantly less heat transfer in this case.	90
5.1	The waves originating from the discontinuity of the Riemann problem are plotted in space and time. The contact discontinuity is shown with a dashed line. The solid lines indicate the propagation of rarefaction waves or shock waves across which the flow velocity and pressure change.	103
5.2	Riemann test to verify the implementation of the products equation of state for EM120D. The numerical results (red markers) can be compared with the exact solution (black line).	106
5.3	Riemann test to verify the implementation of the equation of state for the porous reactants of EM120D. The numerical results (red markers) can be compared with the exact solution (black line).	106
5.4	Comparison of the shock velocity to flow velocity relationship predicted by the Rankine-Hugoniot conditions with numerical results. The bar chart shows the error between the analytically calculated shock speed and the numerical values.	107
5.5	The cyan markers indicate the evolution of the state in pressure-volume space across the ZND wave of PBX 9502. The red and green markers represent the state of the reactants and products respectively. The black lines represent the predicted paths which are calculated analytically.	109
5.6	The one-dimensional ZND wave for EM120D is presented as for Figure 5.5.	109
5.7	The numerical solution for a one dimensional detonation wave in PBX 9502 is plotted for a range of resolutions.	110
5.8	The convergence criteria for EM120D is evaluated in the same manner as for PBX 9502 in Figure 5.7.	111
5.9	Sample data showing the position of a shock wave from a finite volume simulation. The position of the shock wave illustrated by the red line is chosen such that the total mass over the domain is unchanged.	112
5.10	Time progression of air confined EM120D. Times are 0, 16 μ s, 32 μ s, 50 μ s.	114

5.11 The pressure is plotted for a detonation wave propagating upwards in a EM120D rate stick of radius 25mm confined by air. The black line indicates the explosive-air interface, while the red contour serves to show the boundary of the detonation driving zone (DDZ). The detonation velocity was measured to be $5274 \pm 10\text{ms}^{-1}$, significantly slower than the ideal detonation velocity of 6389ms^{-1} 116

5.12 The pressure is plotted for a detonation in EM120D confined by concrete. The interface between explosive and confiner is shown in black, while the red line shows the boundary of the DDZ. The detonation wave speed for this radius (25mm) was $5486 \pm 10\text{ms}^{-1}$, faster than the rate stick confined by air (Figure 5.11). 117

5.13 This plots shows a detonation wave in a rate stick of EM120D confined by steel. The wave is qualitatively similar to Figure 5.12, however the deflection of the explosive-confiner interface (black) is even less, due to the higher acoustic impedance of steel. The detonation wave was faster still at $5940 \pm 10\text{ms}^{-1}$ 118

5.14 The pressure distribution in a detonation rate stick of PBX 9502 with radius 8mm confined by air is plotted. The wave is qualitatively similar to what was observed for EM120D (Figure 5.11), however the pressure is significantly larger, and the shock front is noticeably flatter despite the rate stick having a lower diameter. 119

5.15 The plot shows the radial dependence of the VoD for rate sticks of EM120D. The lines interpolate the numerical results (square markers) using Eyring fits. The circular markers with error bars are the experimental data [39]. The experimental data for unconfined rate sticks that were used for the calibration are highlighted with magenta markers. 122

5.16 The dependence of the VoD with size is presented for both rate sticks and slabs. The lines are Eyring fits through the simulation data (square markers), while the markers represent the experimental data [63]. Note that for slabs the x axis represents the inverse thickness, where the thickness is measured across the whole slab, while for rate sticks the radius, not the diameter, is used. 124

6.1 This figure shows two time snapshots of an accelerating shock wave with velocity, D , and acceleration, a , as a function of space. The grey line shows the shock wave Δt before the blue line. 131

6.2 Gauge data for shock to detonation transition for an idealized explosive, with a Mach 3 ignition shock. The units are dimensionless. . . 137

6.3 Gauge data for shock to detonation transition for an idealized nondimensionalised explosive, with a Mach 3.25 ignition shock. Each line corresponds to a particular gauge. 137

List of Figures

6.4	Reaction rate data extracted from simulated gauge output for an ideal explosive is compared with the known rate law used to generate the data.	138
6.5	Data extracted from experimental data from shock to detonation transition experiments of PBX 9502.[8, 49, 129]	142
6.6	Simulation results for shock to detonation transition are compared with experimental data from Gustavsen et al. [49]. Only one degree of freedom was used for optimization, and yet the calibrated rate law fits the experimental data over a range of impact pressures. The vertical red lines correspond to individual simulations.	143
6.7	The plot shows the time taken for a piece of material to evolve from the initial condition of $\lambda = 1$ following the passing of a ZND wave. The red markers represent the experimental results from Seitz et al. [111].	146
6.8	Pop-plot using the reaction rate parameters for the best fit to the data in Figure 6.5. The lower and upper red lines indicate transition to detonation defined as the point where the wave velocity first exceeds 90% and 95% of the CJ velocity respectively. The vertical red lines correspond to specific simulations.	147
6.9	Predictions for the velocity of detonation in PBX 9502 rate sticks and slabs. The graph plots the velocity against the inverse radius, R , for rate sticks, and thickness, T , for slabs. The square markers represent individual simulations, while the lines are Eyring fits [27] through the simulation results. The circular markers represent experimental data from Jackson and Short [63].	148

List of Tables

3.1	Atomic abundances in moles/kg used to evaluate the equation of state of the detonation products in <i>IDeX</i>	51
3.2	Parameters for the product EoS models for PBX 9502 and EM120D. The proposed reference curves are shown in Figures 3.2 and 3.3. The first four rows of parameters correspond to the pressure and energy reference curves, while the next four (with subscript T) correspond to the temperature reference curve (3.32).	54
3.3	Parameters for the reactant EoS models for PBX 9502 and EM120D.	65
5.1	Initial conditions for Riemann tests in units of kgm^{-3} , Pa, m and s. .	105
5.2	Parameters for the shock Mie-Grüneisen EoS for modelled confinement.	114
5.3	Parameters for the reaction rate model for EM120D. See equation (5.54).	121
5.4	Parameters for the fits of the radial dependence of the VoD with rate stick radius for EM120D, with ideal VoD $D_{CJ} = 6.3895 \text{ kms}^{-1}$	122
5.5	Parameters for the fits of the radial dependence or thickness dependence of the VoD of PBX 9502, with $D_{CJ} = 7.755 \text{ kms}^{-1}$	124
6.1	Parameters for ignition to detonation of an idealized explosive. . . .	137
6.2	Reaction rate values for PBX 9502 as calculated from shock to detonation transition experiments using the methodology presented in this chapter. The thermodynamic values correspond to the state immediately following the shock wave and are calculated using the experimental post-shock flow velocity, u_H , and the previously calibrated equation of state for the reactants (Chapter 3). The final two columns of data are obtained from analysis of the experimental gauge data and are used to calculate the reaction rate, $\frac{D\lambda}{Dt}$, using the method presented in this chapter.	141
6.3	Parameters for the calibrated rate law of PBX 9502.	145

Nomenclature

Acronyms / Abbreviations

AMR	Adaptive mesh refinement
CJ	Chapman-Jouguet theory [29, 65]
DDZ	Detonation driving zone
DNS	Direct numerical simulation
DSD	Detonation shock dynamics
EM120D	Emulsion explosive developed by Orica, made with ammonium nitrate, water, fuel and emulsifier and sensitised with glass micro-balloons
EoS	Equation of state
HLLC	Harten-Lax-van Leer-contact solver introduced by Toro [126]
HMX	High-melting explosive
Hydrocode	A software package for modelling the evolution of continuous media by explicit integration of hyperbolic partial differential equations
JWL	Jones-Wilkins-Lee equation of state
MiNi16	Mathematical formulation developed by Michael and Nikiforakis [91]
MUSCL	Monotonic Upwind Scheme for Conservation Laws [76]
PBX	Plastic bonded explosive
PBX 9502	PBX explosive manufactured with 95% TATB and 5% Kel-F 800 plastic by weight
PDE	Partial differential equation

PETN	Pentaerythritol tetranitrate
SDT	Shock to detonation transition
SMG	Shock Mie-Grüneisen equation of state
TATB	2,4,6-triamino-1,3,5-trinitrobenzene
VoD	Velocity of detonation
WSD	Wescott, Stewart and Davis explosive model [129]
ZND	Zeldovich, von Neumann, Döring theory of detonations [38, 94, 134]

Symbols

ρ	Density
E	Specific energy
e	Specific internal energy
H	Hugoniot
p	Pressure
s	Specific entropy
u	Flow velocity

1 Introduction

1.1 Background

The phenomenon of detonation is of great interest for a wide variety of industrial and military applications. There are many examples of numerical studies conducted with the aim of expanding our understanding of the phenomenon. These studies have the potential to contribute to the design of efficient, safe, commercial explosives for mining applications.

One dimensional detonation waves are described by the ZND theory, which was developed during the second world war by Zeldovich [134], von Neumann [94] and Döring [38] independently. A detonation wave consists of a leading shock wave and a reaction zone. The shock wave raises the pressure and density in accordance with the Rankine-Hugoniot conditions. The state immediately behind the shock wave is known as the von Neumann spike. This is the point of maximum pressure and density. Pressures at the von Neumann spike will typically range from 10GPa to 40GPa, of order 10^5 times atmospheric pressure. The density, on the other hand will typically only be of order twice the density of the unshocked explosive. The detonation wave will typically propagate into the unburned explosive at speeds of order 1000ms^{-1} .

The increased temperature following the initial shock causes the explosive to begin to burn. The state after the burning process is complete is known as the Chapman-Jouguet (CJ) state [29, 65]. The region in between the von Neumann spike and the CJ state is called the reaction zone. The temperatures in this region can be of order 1000K.

1 Introduction

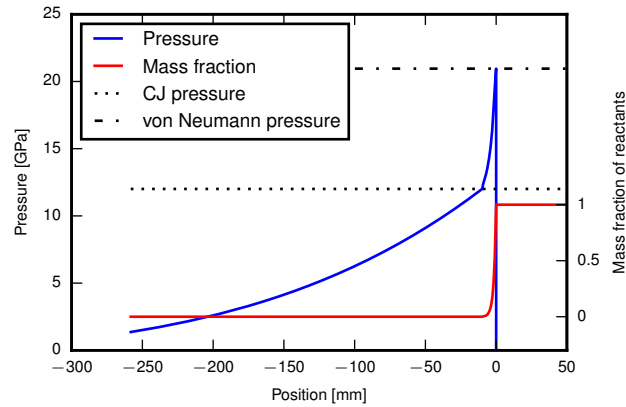


Figure 1.1: The pressure in a ZND wave propagating through the domain to the right is shown. The red curve shows the portion by mass of the explosive consisting of reactants, i.e. the portion which is not yet burned. The values of the pressure and reaction zone width are representative of the ammonium nitrate based emulsion explosive EM120D.

A schematic diagram of a one dimensional ZND wave is shown in Figure 1.1. This Figure shows a ZND wave for EM120D with a reaction zone length of approximately 5mm.

The reaction zone is of special interest because in this region the reactants and products co-exist. Much of the uncertainty surrounding the behaviour of explosives is associated with the extreme conditions in the reaction zone. There are many possible chemical reactions which can occur during very short time periods of order of 10ns to 100ns. The extremely short duration makes experimental investigations into what is occurring in the reaction zone difficult. Even measuring the temperature presents a significant challenge.

In multi-dimensional geometries, on the other hand, the phenomenon is more complex. Subsequent developments in the field have therefore relied on the use of computational simulations to make predictions and to compare models with experimental data.

In this thesis the focus will be specifically on condensed phase explosives, for which detonation waves are typically stable. In gaseous explosives, however, instabilities can lead to complex cellular structures in detonation phenomena [44, 75].

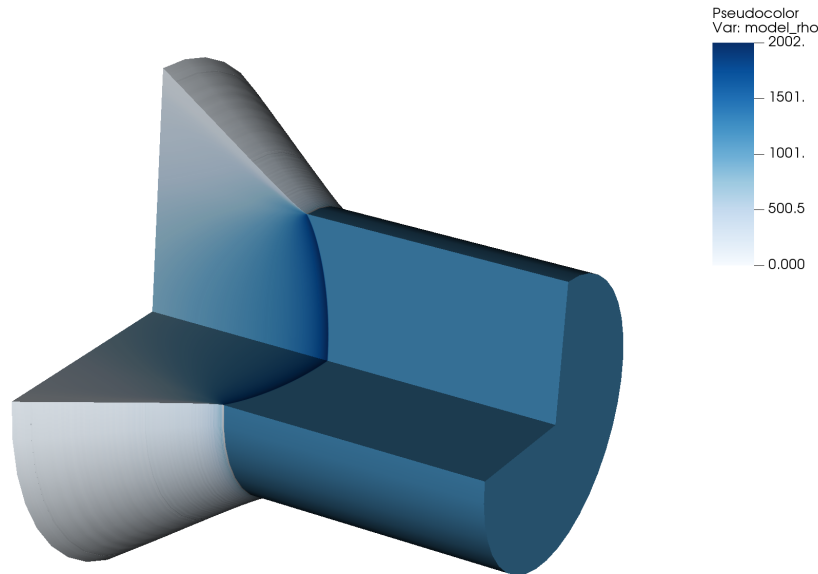


Figure 1.2: This image shows the density field for a cut out of a rate stick. The confining material (air) is not shown. The cylindrical shape of the unburned rate stick is visible on the right. The shock wave is identifiable as the area with the highest density. The gaseous products expand to low density behind the shock wave.

An important mechanism by which the dynamics of multi-dimensional detonation waves deviate from the ZND model arises due to the non-instantaneous burning of the explosive; this occurs when the reaction zone is of non-zero width. If the partially burnt explosive interacts with the surroundings, the state following the reaction will no longer be the CJ state, and the properties of the wave will deviate from those predicted by the ZND model [9, 16, 17, 67, 93].

Figure 1.2 shows a detonating cylindrical rate stick confined by air. Behind the detonation wave the product gases expand and do mechanical work as they push the confiner away. Due to the interaction of the detonation wave with the surrounding air, the shock front is curved, and propagates slower than the theoretical ZND detonation velocity.

Explosives are characterised as high explosives if they will detonate, even with weak confinement, while low explosives will instead deflagrate in many circum-

1 Introduction

stances. Explosives may be further characterised as sensitive or insensitive in reference to the impetus required to induce a detonation.

An explosive is considered ideal if the reaction rate is fast, and so the ZND model offers a good first approximation to the detonation wave. The mining industry, in particular, is concerned with the use of so-called non-ideal explosives, which exhibit a long reaction zone of the order of several mm. In this case, the nature of the confining material and the geometry of the charge must be taken into account if the detonation velocity is to be predicted accurately [61, 62]. Strong confinement (offered by a confining material with large acoustic impedance) will absorb less energy and cause the detonation to behave more ideally.

The effect of confinement is dependent on both the properties of the confining material and the geometry of the explosive charge. Charges are often cylindrically shaped, in which case the confinement effect will depend on the radius of the charge. For charges of small radius, the surface area is larger in comparison to the volume and energy content of the charge. The confinement therefore has a more pronounced effect on small radius cylinders. In the limit of small radius, the effect of confinement goes to infinity. For sufficiently small charge radius, even high explosives will fail to detonate. This occurs at the failure radius, defined to be the critical radius below which detonation waves will slow down and eventually dissipate. The failure radius is in general dependent on the acoustic impedance of the confining material. Experiments can be done to evaluate the failure radius of an explosive for a particular confiner [96, 97, 101].

In this thesis we focus on two specific condensed phase high explosives. EM120D is an ammonium nitrate based emulsion manufactured by Orica. It is a mixture of ammonium nitrate, water, oil and emulsifier. The emulsion is sensitised through the addition of glass micro-balloons. The micro-balloons make the explosive porous and serve to reduce the density [108]. EM120D is a non-ideal explosive – detonation waves with velocity as slow as 60% of the CJ velocity have been measured [39]. The reaction zone length is approximately 5mm.

We also study the insensitive high explosive PBX 9502, which is 95 wt. % TATB (triamino-trinitrobenzene) powder and 5 wt. % Kel-F 800 plastic. The porosity has been measured to be 2.6% [37], although this depends on the exact manufacturing

procedure. The name PBX stands for plastic-bonded explosive. When the explosive is exposed to shock pressures greater than 7GPa, a shock to detonation transition will occur. This is insensitive in comparison to conventional explosives such as HMX, TNT and PETN with typical ignition shock pressure thresholds of around 1GPa [55]. PBX 9502 is also comparatively ideal when compared with EM120D, with a much shorter reaction zone length of approximately 1mm.

Further experiments which can be used to test the validity of computational models include those measuring the dynamics of ignition. Ignition can occur in many regimes, ranging from low energy, long timescale ignition mechanisms to high energy, fast mechanisms [55]. At one end of the spectrum there is cook-off, where the explosive is heated up thermally, eventually causing a thermal explosion which may develop into a detonation. Cook-off can occur over a time period of hours and is difficult to model, since the physics describing the thermal heating occurs over a time scale very much longer than that associated with the detonation itself.

An intermediate regime is deflagration to detonation transition (DDT). A deflagration wave is a subsonic combustion wave, which propagates as a result of heat transfer. In contrast, the mechanism by which detonation waves propagate is via a shock wave.

At the opposite end of the spectrum is the regime of shock to detonation transition (SDT). A shock wave is created in the explosive, usually by firing a projectile at the sample. The shock wave propagates into the explosive for a distance on the order of mm and a time on the order of μs before transitioning to a detonation wave. If the explosive sample is set up appropriately, the ignition is approximately a one dimensional phenomenon. It must be borne in mind that it is impossible to completely eliminate the influence of three dimensional diffraction effects in experiments. Nevertheless, confinement effects have comparatively reduced influence on the results, which make SDT a convenient phenomenon with which to test explosive models.

The distance covered by the shock wave before transitioning to detonation can be measured as a function of the shock wave pressure in order to characterise the

1 Introduction

explosive. These measurements typically lie on a straight line when plotted on a log-log plot, which is known as a pop-plots in reference to Popolato [46].

The dynamics of the shock to detonation transition are an important characteristic of explosives. Two distinct types of behaviour were observed by Campbell et al. [25, 26]. For liquid and homogeneous explosives, thermal runaway occurs at the interface between the impacting projectile and the explosive. The detonation wave develops at the interface some time interval after the shock wave passes. It propagates faster than the shock wave and eventually overtakes it. For heterogeneous explosives, on the other hand, the shock wave gradually increases in strength as it propagates through the explosive before transitioning to detonation [55, 83]. The two types of behaviour can be distinguished, since in the first case two distinct waves can be observed before the overtake. The distinction and possible mechanisms behind it will be discussed further in this thesis.

A common type of experiment for studying shock to detonation transition uses embedded gauges placed in the explosive. Manganin gauges can be used to measure pressure [3]. Placing the experimental setup in a magnetic field means electromagnetic gauges can be used to measure the flow velocity. The gauges allow us to observe the dynamics of the shock prior to the development of a detonation wave, and also to measure the time and position at which this occurs. These experiments are also useful since they allow us to measure the shock Hugoniot of the unreacted explosive [48, 50, 116, 117]. Note that for sufficiently strong shocks the immediate onset of chemical reactions limits our capacity to make direct measurements of the unreacted Hugoniot.

Similar experiments also allow further properties of the explosive to be measured, and thus offer further opportunities to test our models. For example the dependence of the dynamics on the initial temperature [8] and the dependence on the explosive porosity [53]. Furthermore the explosive can be shocked multiple times [10, 11]. Short shocks can be used to observe how a release wave alters the dynamics [49]. These variations of the experiment are important since they allow us to explore parts of the state space away from the single-shock Hugoniot of the explosive in ambient conditions.

Other types of experiment include the study of detonation waves propagating towards the point of a conically shaped charge [43, 102]. As discussed previously, a detonation wave will only propagate along a cylindrical charge if the radius is larger than some critical failure radius. A detonation wave will therefore stop before reaching the end of a cone [102]. In more complex geometries, such as corner turning geometries, desensitization is an additional phenomenon which must be considered when building explosive models [36]. This is where an initial weak shock is observed to desensitize the explosive. The subsequent passing of a stronger shock does not cause the explosive to ignite as would otherwise be expected.

The first computational models employed “programmed burn”. With this approach, the energy release associated with the exothermic reaction is programmed to happen at a specific time, chosen in accordance with a previously determined detonation velocity. This enables predictions of how the energy released will interact with the surrounding environment. However it cannot be used to predict the detonation velocity itself [55].

Detonation shock dynamics is a simulation approach which relies on the use of a D_n - κ relationship. This is an empirical relationship between the normal velocity of a wave, D_n , and the curvature of the wave surface, κ . This approach can be used to calculate the effect of confinement and geometry on the propagation of a detonation wave [6, 63, 119]. The implementation is reliant on shock polar analysis to describe the interface between the explosive and the inert confining material [9]. It is therefore non-trivial to extend the approach to more complex geometries.

Neither of the above approaches explicitly resolve the conversion from reactants to products in time, or the reaction zone in space. As a result they cannot be used to model ignition.

In order to resolve the reaction zone explicitly, the explosive may be modelled directly using reactive fluid dynamics. This means that the energy release associated with the exothermic reaction is controlled by a state-dependent rate law, while the evolution of the state is described by hydrodynamics. This approach to modelling does not require the explicit inclusion of a pre-determined detonation velocity (like programmed-burn) or a D_n - κ relationship. Direct computational modelling of the fluid dynamics and thermodynamics which govern the behaviour of explosives thus

1 Introduction

allows us to predict the dynamics of the more complex phenomena which we have introduced above: the deviation of the detonation velocity from the ZND prediction due to interaction with the confiner, and shock to detonation transition.

On the one hand, this approach is more computationally intensive; the reaction zone must be resolved with sufficient numerical resolution [112]. On the other hand, deviations from the ZND theory are captured automatically, both those dependent on the geometry of the explosive and those dependent on the material properties of the inert confiner. Furthermore, the approach is suitable for modelling ignition. The properties of the explosive are incorporated into the simulation via the equation of state and the reaction rate model. The equation of state for the explosive is typically constructed using two independent equations of state: one for the condensed phase reactants and one for the gaseous phase products. The conversion of mass from reactants to products is calculated using the reaction rate model. These two equations of state and the reaction rate model control the properties of the explosive and can collectively be termed the explosive model.

In this thesis I will present an encompassing methodology to build a computational model using experimental data from the types of experiments which have been introduced above.

1.2 Outline

Chapter 2 reviews the literature upon which the work presented in this thesis is built. This chapter examines the advantages and disadvantages of a range of explosive models which have been presented in the literature. All of the models discussed here are viewed from the perspective of computational physics. This means the focus is on models which have been designed with the intention of being implemented in a numerical software package which explicitly integrates the governing set of partial differential equations (a hydrocode). For example, the equations of state considered in this thesis are all in mechanical form, expressed without explicit use of entropy. This is the most convenient approach for implementation in a hydrocode where entropy is cumbersome to evaluate. Similarly, the reaction rate models considered in this thesis are all relatively simple empirical forms. More

advanced models of chemical reaction have been developed in the field of chemical kinetics, however these are overly complex for the present application. Given the degree of uncertainty surrounding variables such as the temperature, a full chemical kinetics model involving explicit chemical species would offer little improvement in predictive capability and yet would dramatically increase simulation running times. Chapter 2 also clarifies the novel contributions of this thesis in the context of the state of the art.

In Chapter 3, the equation of state models are discussed in more detail. Novel equations of state are presented with the aim of improving the robustness of the explosive model. Particular attention is paid to the mixture rules of pressure equilibrium and temperature equilibrium and the applicability of the equations of state in this context. Furthermore, a methodology is presented with which the equation of state parameters for a specific explosive can be determined. The content of this chapter has been published previously [132].

Chapter 4 presents the ZND theory of one dimensional detonations and an approach to calculate the structure of the ZND wave, including the reaction zone, given an explosive model. This approach is applicable even in the case where the reactants and products are each described using separate equations of state of Mie-Grüneisen form. The analysis is thus more general than the ZND theory as it is generally presented in the literature. This chapter follows the chapter on equations of state since the specific equations of state developed in the previous chapter are employed to calculate the structure of ZND waves for the explosives at hand.

Having calibrated equations of state for both reactants and products, a reaction rate model with calibrated parameters is still required in order to complete the explosive model. Two approaches are used in this thesis. The most typical approach [8, 129] is to apply an optimization algorithm to determine parameters with which simulations using the explosive model can reproduce experimental data. This approach is taken in Chapter 5.

Chapter 5 introduces the numerical methods used to solve the set of partial differential equations required to run a simulation. The numerical methods are validated. The equations of state are also validated by comparing the ZND wave structure from simulation of a detonation wave with the wave structures calculated

1 Introduction

in Chapter 4. Experimental data is used along with an optimization algorithm to determine suitable reaction rate parameters. Finally, predictions obtained using the calibrated rate law are presented and compared favourably with experimental data. This chapter serves to demonstrate the validity, robustness and accuracy of the equation of state models which are presented in chapter 3.

Chapter 6 presents a novel approach to calibrating the reaction rate model, which avoids an expensive optimization procedure involving many executions of the hydrocode. The results presented in this chapter rely on the equations of state which are introduced in this thesis. It is shown that values for the reaction rate can be calculated via direct analysis of experimental data from embedded gauges in shock to detonation transition experiments. The predictive capability of the resulting model is then tested by comparing simulation results with experimental data.

1.3 Novel Contributions of this Thesis

The novel contributions of this thesis include

- Developed a robust, temperature capable equation of state for porous explosive **reactants**, along with a methodology to systematically determine parameter values using experimental data.
- Developed a simple and robust temperature capable equation of state for the explosive **products** based on the use of a thermochemical code.
- Developed and implemented a method to directly calculate reaction rate values from experimental measurements of shock to detonation transition.

1.4 Publications

- S. D. Wilkinson, M. Braithwaite, N. Nikiforakis, and L. Michael. “A complete equation of state for non-ideal condensed phase explosives”. *Journal of Applied Physics* 122.22 (2017), p. 225112 based on the results of Chapters 3 to 5.
- S. D. Wilkinson, N. Nikiforakis, and L. Michael. “Calibration of Rate Laws for Hydrocode Modeling of Explosives” (*in preparation*) comprising the content of Chapter 6.

Furthermore, work pertaining to this thesis has been presented at

- 16th International Conference on Numerical Combustion, Orlando, FL, 2017,
- 16th International Detonation Symposium, Cambridge, MD, 2018.

2 Literature Review

2.1 Equations of State

2.1.1 Fundamentals

The evolution of an inviscid, compressible fluid in d dimensions is described by the Euler equations [73],

$$\frac{\partial \rho}{\partial t} + \nabla \cdot \rho \mathbf{u} = 0 \quad (2.1)$$

$$\frac{\partial \rho \mathbf{u}_k}{\partial t} + \nabla \cdot \rho \mathbf{u}_k \mathbf{u} = -(\nabla p)_k \quad \text{for } k \in \{1, \dots, d\} \quad (2.2)$$

$$\frac{\partial \rho E}{\partial t} + \nabla \cdot \rho E \mathbf{u} = -\nabla \cdot p \mathbf{u}. \quad (2.3)$$

The equations corresponds to conservation laws for mass, the components of the momentum and energy respectively. They are expressed using the density, ρ , the flow velocity, \mathbf{u} , and the specific energy, E . The left hand side of the equations describes the advection of the material with the flow. The right hand side corresponds to the physical forces of relevance to the physical system at hand. For this application it is only necessary to consider the force corresponding to gradients of the pressure field, since this force is very much stronger than contributions arising from gravity or viscosity for example [44]. It is apparent that to solve the Euler equations, an equation of state with which to calculate the pressure field is required.

The most convenient variables with which to construct the equation of state are density and energy. Equations of state for use in this context are therefore often of ‘mechanical’ form and define the pressure, p , as a function of specific volume, v , and specific internal energy, e ,

$$p = p(v, e), \quad (2.4)$$

2 Literature Review

where the specific internal energy is obtained by subtracting the kinetic component from the specific energy,

$$e = E - \frac{1}{2} \|\mathbf{u}\|^2, \quad (2.5)$$

and the specific volume is defined as $v = 1/\rho$.

From the perspective of thermodynamics, on the other hand, the starting point from which to construct an equation of state is the first law of thermodynamics [18],

$$de = T dS - p dv, \quad (2.6)$$

which describes a change in specific internal energy, e , in terms of the change in specific entropy, S , and specific volume, v . In the context of this thesis, it is convenient to express the law in terms of intensive variables, as opposed to the more common extensive form. The temperature, T , and pressure, p , correspond to the first derivatives of the energy,

$$T := \left(\frac{\partial e}{\partial S} \right)_v, \quad p := \left(\frac{\partial e}{\partial v} \right)_S. \quad (2.7)$$

A complete equation of state must therefore be a function of either the entropy or temperature. Such an equation of state is described as ‘complete’ in contrast to incomplete, mechanical equations of state.

Use of complete equations of state can be cumbersome in the context of fluid dynamics simulations since evaluation of the entropy and temperature is non-trivial. As is discussed in [34], a hydrodynamics code calls the equation of state $\mathcal{O}(N^{d+1})$ times for a d -dimensional simulation where N is a measure of the resolution. It is therefore of great importance that the equation of state allow for the pressure to be calculated as an explicit function of volume and energy.

Mechanical equations of state are therefore more convenient to use in practice, but their construction necessarily includes some simplification with regard to the thermodynamics of the material. In this thesis we use equations of state of linear Mie-Grüneisen form [85]. The assumption in this case is that the Grüneisen gamma, Γ , is a function of volume only, and is independent of entropy.

An equation of state is a function of two variables, and can be thought of as a surface in three dimensional space. The Mie-Grüneisen equation of state is constructed

using reference functions, $p_{\text{REF}}(v)$ and $e_{\text{REF}}(v)$, which define a one dimensional line on the surface. This implies that

$$p(v, e_{\text{REF}}(v)) = p_{\text{REF}}(v). \quad (2.8)$$

States away from this one dimensional line can then be expressed using a Taylor expansion in the change in specific internal energy,

$$p(v, e) = p(v, e_{\text{REF}}(v)) + \left(\frac{\partial p}{\partial e} \right)_v (e - e_{\text{REF}}(v)) + \frac{1}{2} \left(\frac{\partial^2 p}{\partial e^2} \right)_v (e - e_{\text{REF}}(v))^2 + \dots \quad (2.9)$$

The Grüneisen gamma is defined in terms of the mixed second derivative of the energy,

$$\Gamma(v, S) = -\frac{v}{T} \frac{\partial^2 e}{\partial S \partial v}. \quad (2.10)$$

The derivatives in (2.9) are dependent on the Grüneisen gamma, since we can write

$$\Gamma(v, S) = -v \frac{\partial S}{\partial e} \frac{\partial^2 e}{\partial S \partial v} = v \left(\frac{\partial p}{\partial e} \right)_v. \quad (2.11)$$

The Grüneisen gamma is in general a function of both volume and entropy, and therefore indirectly a function of specific internal energy. However, by making the assumption that the Grüneisen gamma is a function of volume only, the higher order terms of the Taylor expansion (2.9) go to zero. We can then construct the mechanical linear Mie-Grüneisen equation of state,

$$p(v, e) = p_{\text{REF}}(v) + \frac{\Gamma(v)}{v} (e - e_{\text{REF}}(v)), \quad (2.12)$$

henceforth simply referred to as the Mie-Grüneisen equation of state. A similar construction is presented by Menikoff among many others [81].

This assumption is valid provided the state sampled by the equation of state remains sufficiently close to the reference curve. This could be for example an isentrope, an isotherm or a Hugoniot locus. The physics of the material being modelled is encoded in the definition of the reference functions and $\Gamma(v)$. These functions can be arbitrarily complex, nonlinear functions, and the equation of state remains invertible. That is to say that the equation can be rearranged to express the specific internal energy as an explicit function of volume and pressure,

$$e(v, p) = e_{\text{REF}}(v) + \frac{v}{\Gamma(v)} (p - p_{\text{REF}}(v)). \quad (2.13)$$

2 Literature Review

This is an important consideration if the equation of state is to be implemented efficiently in a hydrodynamic code.

The modelling of explosives creates an additional complication in that we must model mixtures of materials. As discussed in the introduction, accurate modelling of detonation waves requires resolution of the reaction zone, where burned (products) and unburned (reactants) explosive coexist. The combustion is exothermic, and for condensed phase explosives, the combustion is also associated with a phase change from condensed phase to a dense gas.

The first attempt to construct a complete physical description of multiphase reactive fluids was developed by Baer and Nunziato (BN) in 1986 [12]. The BN model has a complete set of Euler equations for each phase present in the simulation. Source terms allow for the exchange of momentum and energy between the various phases and correspond to physical effects such as drag (due to velocity disequilibrium) and compression/expansion (due to pressure disequilibrium). Source terms in the volume fraction account for the influence of compaction - the change in the volume fraction arising from the compression of a mixture, the constituents of which have differing compressibilities.

The complete model is generally considered too complex and computationally intensive for use in numerical simulations. Furthermore it is not trivial to scale the model up to an arbitrary number of phases; even three phases creates significant complications as compared to a two phase system.

The full two phase BN model consists of seven equations: three for each phase and an additional equation for the compaction dynamics. Kapila et al. [66] justify simplifications to the BN model by approximating the time- and length-scales across which mechanical equilibrium occurs. This occurs via two mechanisms: the exchange of momentum due to drag forces means the flow velocities will tend towards each other, while the expansion and compression due to variations in pressure lead to pressure equilibrium.

The time scale associated with velocity equilibrium can be estimated with reference to experimental measurements of permeability such as that presented by Shepherd and Begeal [118]. Kapila et al. [66] concluded that for condensed phase

explosives the time scale is of order $0.1\mu s$. The length-scale of velocity equilibrium is found to be of the same order as the grains size or mean free path of the fluid, motivating a unique velocity field. The number of equations is thus reduced to six.

Furthermore, the time scale of pressure equilibration between the phases due to volume exchange is found to be shorter than a microsecond, depending on factors such as the sound speed of the fluid. If the dynamics of the problem under investigation occur over longer time-scales, a single-pressure, single-velocity five equation model is justified.

Thermal equilibration on the other hand, is estimated to occur significantly more slowly with timescales on the order of 10ms. In any case, thermal equilibration cannot be incorporated into the model, or the system would be reduced to the single phase model.

Saurel et al. [106] report on the difficulties associated with Kapila's five equation model. They offer an improvement to the model by relaxing the problematic pressure equilibrium condition. In particular the problem is separated into a hyperbolic part without the pressure equilibrium condition, and a separate relaxation step. The model was further developed by Petitpas et al. [98]. It was calibrated for the explosive EM120D and shown to have predictive capability by Schoch et al. [108].

While the reduced model is both mechanically and thermodynamically consistent, the equations cannot be expressed in conservative form. As a result a regularization scheme is required to fully specify the system in the presence of shock waves. This is of particular relevance to this work, since we aim to model both ignition and detonation. In a detonation wave, there is a single strong shock wave, across which the regularization scheme can be applied. However in ignition phenomena, a shock wave develops dynamically. A pressure wave develops, and the pressure gradient increases gradually. Eventually the pressure gradient is steep enough for the wave to be considered a shock wave, but the exact point at which the transition is considered to have occurred is somewhat arbitrary. In hydrodynamic simulations shock waves are never completely sharp, they will diffuse over a space of 3 to 5 cells. It is therefore difficult to distinguish between a shock wave and a pressure

2 Literature Review

wave algorithmically, thus making the implementation of a regularization scheme tricky in practice.

Further problems can arise from the fact that the speed of sound in the multiphase fluid does not change monotonically. Moreover, the pressure equilibrium condition can lead to robustness issues relating to the positivity of the volume fraction.

An alternative approach to model mixtures is to do so implicitly – two independent equations of state are constructed, and are then combined with the help of mixture rules and closure rules. The equations then constitute a system of non-linear equations. From the perspective of the system of partial differential equations, this approach is equivalent to using a single equation of state for the mixture with the addition of a mass fraction parameter, λ , to represent the degree to which the explosive is burned. The mass fraction parameter is then advected with the flow of the fluid, and serves as an additional parameter for the equation of state.

$$p = p(v, e, \lambda) \tag{2.14}$$

This approach avoids complications associated with a regularization scheme; the same algorithm is applied to every cell. The algorithm can therefore be applied to both ignition and detonation without modification.

The difficulty in the construction of a combined equation of state lies in the construction of the mixture rules. This is related to the ambiguity over the subdivision of space and energy in the explosive between reactants and products. Even in the case where the density of the explosive is known, the densities of the constituents may vary, and the density of the reactants need not equal that of the products. Moreover the internal energy may be arbitrarily distributed between reactants and products. As a result, the construction of an equation of state for the mixture introduces two additional degrees of freedom [137].

A commonly used closure rule is that of pressure equilibrium. Any differences in pressure are neglected on the assumption that they will equilibrate on a sufficiently fast time scale [66]. In the limit of long time scales, the second closure condition is that of temperature equilibrium. The temperature equilibrium condition has been applied successfully in many studies [8, 91, 129]. However the time scales associated with detonation mean that application of a temperature equilibrium condition is

not physically motivated. An alternative assumption, based on the limit of short time scales, is that no heat transfer occurs between the reactants and products [51, 120]. This is a thermal isolation closure condition and has been termed the ISE (Isentropic Solid Equation) mixture rule [55]. Following Zukas and Walters [137], the physical case will be somewhere between these two extreme assumptions; some heat will transfer between reactants and products, but there will not be sufficient time for the materials to reach thermal equilibrium.

Stewart et al. [121] discuss various closure models for modelling of the reaction zone of detonation waves. A third possible closure rule assumes that the ratio of specific volumes of the reactants and products remains constant throughout the burning process. The value of this constant must be chosen carefully using the thermal properties of each of the reactants and products.

Implementation of a temperature equilibrium condition naturally requires temperature capable equations of state. In the context of equations of state of Mie-Grüneisen form, this can be accomplished by adding an additional reference function for temperature, T_{REF} , to go along with the reference functions for pressure and energy.

From equation (2.10), the Grüneisen gamma can be expressed in terms of temperature and volume,

$$\Gamma(v) = -\frac{v}{T} \left(\frac{\partial T}{\partial v} \right)_S = -v \left(\frac{\partial \ln(T)}{\partial v} \right)_S. \quad (2.15)$$

In the case where the reference curve is an isentrope, the temperature reference function, T_{REF} , is therefore related to the Grüneisen gamma by

$$T_{\text{REF}}(v) = T_0 \exp \left(- \int_{v_0}^v \frac{\Gamma(\tilde{v})}{\tilde{v}} d\tilde{v} \right), \quad (2.16)$$

where $T_0 = T_{\text{REF}}(v_0)$ is the temperature at some reference specific volume, v_0 . On the one hand, this means that any values for the Grüneisen gamma which are available can be used to calculate the reference temperature function. On the other hand, if temperature data for the material in question is available, this can be used to calculate the Grüneisen gamma. This is the fundamental idea at the heart of the equations of state for detonation modelling developed by Davis [34, 35]. It was also used by Baudin [15] to extend the JWL (Jones-Wilkins-Lee) equation of state, which is discussed further in Section 2.1.3.

2 Literature Review

For states which are displaced from the reference curve the temperature may be evaluated using a constant volume integral from the reference curve and an expression for the specific heat capacity at constant volume,

$$c_v = \left(\frac{\partial e}{\partial T} \right)_v \quad (2.17)$$

$$e(v, T) = e_{\text{REF}}(v) + \int_{T_{\text{REF}}(v)}^T c_v(\tilde{T}) d\tilde{T}. \quad (2.18)$$

This is analogous to using the Grüneisen gamma for evaluating the pressure or energy away from the reference curve.

An expression for the heat capacity can also be used to evaluate the entropy,

$$c_v(S) = \left(\frac{\partial e}{\partial T} \right)_v = T \left(\frac{\partial S}{\partial T} \right)_v \quad (2.19)$$

$$S(v, T) = S_{\text{REF}}(v) + \int_{T_{\text{REF}}(v)}^T \frac{c_v(\tilde{T})}{\tilde{T}} d\tilde{T}. \quad (2.20)$$

In the case where the reference curve is an isentrope, S_{REF} will of course be independent of volume. Evaluating an actual value for the entropy is not always feasible, however this method can still be used to evaluate the change in entropy.

To use these equations, the heat capacity can be defined as a function of temperature or entropy. However, the central assumption used by equations of state of Mie-Grüneisen form is that the Grüneisen gamma is independent of entropy, and this is equivalent to the assumption that the heat capacity is independent of volume. So a volume dependent expression for the heat capacity would lead to thermodynamic inconsistencies. This can be demonstrated by considering a third derivative of the energy,

$$\frac{\partial}{\partial S} \frac{\partial^2 e}{\partial S \partial v} = \frac{\partial}{\partial v} \frac{\partial^2 e}{\partial S^2} \quad (2.21)$$

$$\frac{\partial}{\partial S} \left(-\frac{\Gamma T}{v} \right) = \frac{\partial}{\partial v} \frac{T}{c_v} \quad (2.22)$$

$$-\frac{\partial \Gamma}{\partial S} \frac{T}{v} - \frac{\Gamma}{v} \frac{\partial T}{\partial S} = \frac{1}{c_v} \frac{\partial T}{\partial v} - \frac{T}{c_v^2} \frac{\partial c_v}{\partial v} \quad (2.23)$$

$$-\frac{\partial \Gamma}{\partial S} \frac{T}{v} - \frac{\Gamma T}{vc_v} = -\frac{\Gamma T}{vc_v} - \frac{T}{c_v^2} \frac{\partial c_v}{\partial v}. \quad (2.24)$$

Therefore

$$\frac{\partial \Gamma}{\partial S} = 0 \iff \frac{\partial c_v}{\partial v} = 0. \quad (2.25)$$

The extension of an equation of state of Mie-Grüneisen form to include temperature using this method effectively completes the equation of state; it is now possible to calculate temperature and entropy. Note however that we have not sidestepped the need to make an assumption about the thermodynamics of the material. The assumption that the Grüneisen gamma is independent of entropy is still necessary. Likewise the convenience provided by the mechanical part of the equation of state (2.12) can still be exploited for efficiency in hydrodynamic simulations.

2.1.2 Reactants

Following the ZND model, detonation waves consist of a shock wave which is followed by the reaction zone. This occurs because the timescale associated with the shock wave itself is much shorter than the timescale of the reaction. This means that the properties of the shock wave are described by the normal (inert) Rankine-Hugoniot conditions along with the equation of state for unreacted explosive. Accurate modelling of the shock wave therefore necessitates an accurate Hugoniot locus for the reactants equation of state. This motivates the choice of the Hugoniot curve as the reference curve.

The shock Mie-Grüneisen equation of state [115, 131] uses the Hugoniot curve as the reference curve, so that the state will remain on or close to the reference curve when the material is shocked. It is one of the most commonly used equations of state for modelling the reactants.

As a shock wave propagates past a piece of material, the flow velocity of the material is increased. The shock Mie-Grüneisen equation of state is developed based on the relationship between this change in flow velocity and the velocity of the shock wave itself. The relation between the shock speed and the flow velocity behind the shock can be investigated experimentally. An impact between the material under investigation and a projectile will initiate a shock wave. The speed of propagation of the shock wave can be measured using gauges placed in the material. The post-shock flow velocity in the sample is just the speed of the interface after the impact.

The form of the shock Mie-Grüneisen equation of state is based on the assumption that the shock propagation velocity, D , is linearly related to the flow velocity behind

2 Literature Review

the shock, u , such that

$$D = a + bu, \quad (2.26)$$

for two empirically determined constants, a and b . The value of a is just the ambient speed of sound, since in the limit of small pressure differences, shock waves are simply sound waves. This linear approximation fits experimental data well for most solids. It cannot however be applied universally, and can be problematic for example in the presence of multiple shocks [81]. If a linear relationship is found to not match the experimental data with sufficient accuracy, a quadratic relationship may also be used. This approach is presented by Asay and Shahinpoor [5].

Equation (2.26) leads to the following expressions for the Hugoniot pressure and specific internal energy as a function of volume,

$$p_{\text{REF}}(v) = \frac{\rho_0 \chi a^2}{(1 - b\chi)^2} \quad (2.27)$$

$$e_{\text{REF}}(v) = \frac{1}{2}(v_0 - v)p_{\text{REF}}(v), \quad (2.28)$$

$$\text{where } \chi = 1 - \frac{v}{v_0}. \quad (2.29)$$

The energy reference curve is related to the pressure reference curve via the Hugoniot equation,

$$e - e_0 = \frac{1}{2}(p + p_0)(v_0 - v). \quad (2.30)$$

These expressions are then used as reference functions for an equation of state of Mie-Grüneisen form. The derivation of these expressions is given in Appendix A.

In the absence of data, Davis [35] assumes that the Grüneisen gamma, Γ , satisfies

$$\frac{\Gamma}{v} = \frac{\Gamma_0}{v_0} \quad (2.31)$$

where Γ_0 is the value at ambient specific volume, v_0 . This is a crude approximation, and thus the equation of state is of limited use for modelling phenomena where the state deviates significantly from the reference curve. The principal problem with this choice of reference curve is that it does not lend itself to calculating temperatures. The temperature on the Hugoniot curve cannot be derived directly, and is not easy to measure experimentally.

Davis [35] presented an equation of state for the reactants using the same basic assumption (2.26) but using an isentrope as a reference curve. Following the

derivation in Appendix B, this leads to the following expression

$$p_{\text{REF}}(v) = \frac{\rho_0 a^2}{4b} [\exp(4b(1 - v/v_0)) - 1] \quad (2.32)$$

$$e_{\text{REF}}(v) = \left(\frac{a}{4b}\right)^2 (\exp(4b(1 - v/v_0)) - 1) + \frac{\rho_0 a^2}{4b} (v - v_0). \quad (2.33)$$

In this case the reference curves are related to each other via the thermodynamic definition for pressure as a derivative at constant entropy,

$$p = - \left(\frac{\partial e}{\partial v} \right)_S. \quad (2.34)$$

Davis [35] defines the Grüneisen gamma using the expression

$$\frac{\Gamma(v)}{v} = \frac{\Gamma_0}{v_0} \left(\frac{v}{v_0} \right)^N, \quad (2.35)$$

where Γ_0 is the Grüneisen gamma in ambient conditions, and v_0 is the initial specific volume. Note that for $N = 0$, this expression reduces to the same expression as is typically used with the shock Mie-Grüneisen equation of state (2.31). The Hugoniot curve for this equation of state is dependent on N , and so a suitable value for N can be determined using Hugoniot data.

The motivation for using an isentrope in place of the Hugoniot as a reference curve comes from the relationship between the Grüneisen gamma and temperature,

$$\frac{\Gamma(v)}{v} = \left(\frac{\partial p}{\partial e} \right)_v = -\frac{1}{T} \left(\frac{\partial T}{\partial v} \right)_S = - \left(\frac{\partial \ln(T)}{\partial v} \right)_S. \quad (2.36)$$

This relationship permits us to define the temperature on the reference curve in terms of the Grüneisen gamma. Since the relationship involves a derivative at constant entropy, application of this equation to find an expression for T_{REF} relies on the fact that the reference curve is itself an isentrope. The resulting expression for the temperature on the reference curve is

$$\int_{T_0}^{T_{\text{REF}}} \frac{dT}{T} = - \int_{v_0}^v \frac{\Gamma(\tilde{v})}{\tilde{v}} d\tilde{v} \quad (2.37)$$

$$T_{\text{REF}}(v) = T_0 \exp \left(-\frac{\Gamma_0}{N+1} \left[\left(\frac{v}{v_0} \right)^{N+1} - 1 \right] \right), \quad (2.38)$$

where T_0 is the temperature under ambient conditions, on the reference curve at specific volume v_0 .

2 Literature Review

Nevertheless, data for the heat capacity is required to determine temperature values on the Hugoniot. This is because the reference curve is an isentrope at entropy corresponding to the initial conditions, while states on the Hugoniot curve are at higher entropy. As such, the predicted temperature for shocked explosive is also dependent on the expression for the heat capacity. Davis uses a linear function of the entropy,

$$c_v = c_{v_0} + \alpha(S - S_0). \quad (2.39)$$

Using equation (2.19), this is equivalent to

$$c_v = c_{v_0} \left(\frac{T}{T_0} \right)^\alpha. \quad (2.40)$$

The linear dependence of the heat capacity on the change in entropy is controlled by the free parameter α , while c_{v_0} is the heat capacity on the reference curve. The value of α can only be determined if a temperature at a state off the isentropic reference curve is known.

One method to obtain temperature values in the shocked explosive applies a thermal model based on a vibrational spectrum obtained via Raman scattering [82]. Kittell and Yarrington [68], on the other hand, derive an expression for post-shock temperatures using a multi-term Einstein oscillator model for the specific heat capacity. Alternatively the relationship between temperature and the Stokes/anti-Stokes ratio in Raman spectroscopy can be used to directly measure the temperature in shocked explosives [80]. However temperature data such as this is only available for a limited selection of explosives. The references given above all relate to PBX 9502, an explosive which has been the subject of many experimental and numerical studies. In this thesis we develop a methodology which can also be applied to explosives for which no direct information for temperature in the shocked explosive is available, such as EM120D. In the absence of data, some information regarding the temperature can be inferred from measurements of the Hugoniot locus. A methodology to do this will be presented in this work.

The Davis equation of state has been developed further and implemented in various studies [7, 8, 129]. The so-called WSD model [129] uses an extension of the Davis equation of state designed to accommodate a nonlinear D, u relationship. This form is derived from a truncated Taylor expansion of the exponential function

in (2.32),

$$p_{\text{REF}}(v) = \frac{\rho_0 a^2}{4b} \left[\sum_{j=1}^3 \frac{(4b\chi)^j}{j!} + C \frac{(4b\chi)^4}{4!} + \frac{\chi^2}{(1-\chi)^4} \right], \quad (2.41)$$

$$\text{where } \chi = 1 - \frac{v}{v_0}. \quad (2.42)$$

This expression introduces a new parameter for the calibration of the Hugoniot, C , which affects the predicted pressures for strong shocks. The final term has the effect of ensuring the correct behaviour of the reference function in the limit of small volumes. The result of these alterations is that the predicted D,u relationship is no longer restricted to being a straight line. The parameter C can be adjusted to permit a closer fit to the experimental data.

In particular for the explosive PBX 9502, the D,u relationship has been observed experimentally to be nonlinear. As such the extra free parameter, C , facilitates a closer fit to the data than would otherwise be possible.

The WSD model also employs an alternative form for the Grüneisen gamma,

$$\Gamma(\chi) = \Gamma_0 + \frac{\Gamma_{\text{sc}} - \Gamma_0}{\chi_{\text{max}}} \chi, \quad (2.43)$$

where Γ_{sc} and χ_{max} are determined with reference to the equation of state of the products. Its value is chosen specifically to ensure that the Hugoniot of the reactants does not intersect the Crussard curve, the behaviour of which is determined by the equation of state of the products at small volumes.

The Hugoniot curve is defined as the locus of possible states following a shock wave, on the assumption that no chemical reactions occur, while the Crussard curve is the locus of states following a shock and the completion of all energetically favourable chemical reactions. Since the pressure is expected to decrease, and the volume increase as the shocked condensed phase reactants combust to form a gas, it is expected that the Hugoniot and Crussard curves will not cross.

Aslam [7] further refines the calibration methodology by using isobaric thermal expansion data, as well as values for the specific heat from Menikoff [82] to calibrate an entropy dependent expression for the heat capacity. Additional adjustments are introduced by Aslam with the specific aim of ensuring that the equation of

2 Literature Review

state remains robust in the expansion regime (for volumes larger than the initial conditions). While the equation of state in this regime is not expected to play a role in the simulation of detonation waves, it is nevertheless necessary to ensure that the thermodynamic behaviour is correct to ensure that the governing set of partial differential equations can be solved robustly in wide-ranging conditions.

A further issue to be considered with regards to the equation of state of the reactants is porosity. Porosity plays an important role in the dynamics of shock waves [135]. The pressure-volume relationship as well as the temperature-pressure relationship of the Hugoniot curve will be different for a porous explosive than for a homogeneous explosive of the same density. The importance of porosity in explosive modelling is discussed by Handley et al. [53, 55].

2.1.3 Products

Returning to the ZND model, following the leading inert shock wave and the reaction zone is a rarefaction (or Taylor) wave. In this region the products expand adiabatically. While the timescale associated with the chemical reaction is much longer than that of the shock wave, the timescale of the rarefaction is much longer again.

If the detonation is ideal (fast reaction rate) the state at the end of the reaction zone is the CJ state. This state is on the Crussard curve – the Hugoniot curve corresponding to the passing of a shock wave and subsequent complete combustion of the explosive.

It should be noted that it is the equation of state of the products along with the initial conditions and heat of combustion which determine the CJ state and the CJ detonation velocity [44, 75]. If the CJ state is measured experimentally, then this information can be used in the process of determining equation of state parameters. More details can be found in Chapter 4.

The isentrope corresponding to the subsequent rarefaction wave is known as the principal isentrope, and is the isentrope intersecting the CJ state. Accurately reproducing the path of the isentrope in pressure volume space is important if models

are to correctly predict the effect of a detonation wave on the surrounding material. The natural choice of reference curve for the reaction products is therefore the principal isentrope. The mechanical JWL (Jones-Wilkins-Lee) equation of state [84, 115] for the detonation products uses this choice of reference curve.

Information about the principal isentrope may be measured using cylinder tests [60]. The data is obtained by measuring the wall velocity of the cylinder using a streak camera or Doppler velocimetry. Information about the pressure within the cylinder can then be inferred via a numerical calculation. This method captures the post reaction expansion of the detonation products and can measure the path of the isentrope in pressure volume space. The time scale is too short to measure temperatures.

The isentrope pressure is fitted to the data using the sum of a power law and one or more exponential terms depending on the accuracy which is required, and the quality of fit which can be achieved with a single exponential term [84, 103]. The reference energy can then be derived from the reference pressure using the standard thermodynamic relation

$$p = - \left(\frac{\partial e}{\partial v} \right)_S. \quad (2.44)$$

$$p_S(v) = A \exp(-R_1 v) + B \exp(-R_2 v) + C v^{-(\Gamma+1)} \quad (2.45)$$

$$e_S(v) = \frac{A}{R_1} \exp(-R_1 v) + \frac{B}{R_2} \exp(-R_2 v) - \frac{C v^{-\Gamma}}{\Gamma} - Q \quad (2.46)$$

The free parameter Q is the integration constant. In these equations e is the specific internal energy and v is the specific volume. The integration constant corresponds to the ‘zero’ energy of the material. It is the energy of the material in the limit of large volume. Its value is irrelevant to the properties of the products when considered in isolation. However a convenient method of encoding the release of energy which occurs in the transfer of mass from reactants to products is to set Q to a positive value for the products, while the zero energy of the reactants is set to zero. The value of Q is thus the energy per unit mass which is released by the chemical reaction. The other free parameters are A , R_1 , B , R_2 , C and Γ . The choice of symbol of Γ is natural since this corresponds to the Grüneisen gamma. This is because for an ideal gas equation of state with fixed Grüneisen gamma, isentropes have the form corresponding to the power law in equation (2.45).

2 Literature Review

As a result, the parameter C does not play a role. Its value corresponds to the entropy of the CJ state, but it does not influence the evaluation of the pressure for a given volume and energy. This is evident, in that the parameter cancels out when substituting p_S and e_S as reference curves in the Mie-Grüneisen equation of state, with fixed Grüneisen gamma, Γ ,

$$p(v, e) = p_S + \frac{\Gamma}{v}(e - e_S) \quad (2.47)$$

$$= A \left(1 - \frac{\Gamma}{R_1 v}\right) \exp(-R_1 v) + B \left(1 - \frac{\Gamma}{R_2 v}\right) \exp(-R_2 v) + \frac{\Gamma(e + Q)}{v} \quad (2.48)$$

As a consequence, the reference functions for the JWL equation of state are usually quoted as

$$p_{\text{REF}}(v) = A \exp(-R_1 v) + B \exp(-R_2 v) \quad (2.49)$$

$$e_{\text{REF}}(v) = \frac{A}{R_1} \exp(-R_1 v) + \frac{B}{R_2} \exp(-R_2 v) - Q \quad (2.50)$$

$$\Gamma(v) = \Gamma_0, \quad (2.51)$$

with a fixed value for the Grüneisen gamma, Γ_0 .

The principal isentrope serves as an appropriate choice for the reference curve. For the purposes of modelling however, we must include a method to evaluate states with a differing entropy. This method must also be accurate if the equation of state is to correctly model non-ideal detonation waves as well as ideal. For non-ideal detonation waves, the state following the reaction zone will be at lower entropy than the CJ state. The following rarefaction wave will consequently occur at lower entropy than that corresponding to the principal isentrope. We therefore need an accurate value for the Grüneisen gamma.

For many explosives, no experimental data is available for states away from the isentrope which can inform a suitable choice of the Grüneisen gamma. The JWL equation of state therefore assumes a constant value for the Grüneisen gamma. This is not strictly valid but is the best approximation that can be made if cylinder test data is to be used [33, 120].

Byers Brown et al. [23, 24] developed a complete equation of state for detonation products called the Williamsburg equation of state. This was used for the first

analysis of the ZND model for detonation waves which incorporated temperature and entropy. In particular this allowed for an investigation into the relative merits of temperature equilibrium and heat isolation closure rules for the mixture of reactants and products in the reaction zone.

The Williamsburg equation of state [24] can be expressed as

$$e = \frac{pv}{g(v, \sigma) - 1} \quad (2.52)$$

$$g(v, \sigma) = 1 + \sum_{j=1}^M \left(\alpha_j + \frac{1}{1 + \beta_j v \sigma^{\alpha_j}} \right) \gamma_j \quad (2.53)$$

$$\sigma = \exp \left(\frac{S - S_0}{nR} \right), \quad (2.54)$$

where σ is a reduced entropy factor. The parameters α_j , β_j , γ_j and δ_j are chosen such as to fit the calibration data as provided by a thermochemical code. Unlike many other equations of state used for modelling explosives, the Williamsburg defines the energy as a function of volume and entropy, and is thus a complete equation of state. Various alternative fitting forms have been applied for the function g , which corresponds to the adiabatic gamma. The fitting forms given here are informed by statistical mechanics considerations. However for practical purposes simpler forms may be used, including

$$g(v) = 1 + \frac{A(v)}{B(v)} \quad (2.55)$$

for polynomials in the volume A and B . This form was successfully applied by Schoch et al. [108] to model the products of EM120D. However in this reduced form, the ability to calculate temperatures is no longer available.

The calibration of the Williamsburg equation of state uses the output from a thermochemical ideal detonation code. There is some approximation in the use of an ideal detonation code, since strictly the results only apply to a system in chemical equilibrium. A non-ideal detonation will inevitably depart from this to some degree.

Nevertheless this leverages more data than is typically used for JWL including temperature and entropy values, thus enabling the calibration of a complete equation of state for detonation products. Test cylinder data, on the other hand, only allows for the calibration of an incomplete equation of state such as JWL.

2 Literature Review

Braithwaite and Sharpe [22] discuss motivation for the development of the Williamsburg equation of state in relation to further limitations of the JWL equation of state. The Williamsburg equation of state is formulated such as to have the correct asymptotic behaviour in the extreme thermodynamic limits. While such states may not be expected to be sampled in the running of a simulation, anomalous behaviour extreme regimes can cause robustness issues. Well behaved, smooth derivatives are also essential for calculation of properties such as the sound speed which are required for the simulation. Their results show that the Grüneisen gamma is dependent on volume, and the constant gamma approximation used by JWL is invalid. This is of particular importance for non-ideal detonations since states are expected to be significantly removed from the reference curve.

An additional advantage to the Williamsburg equation of state is that its use is not dependent on the availability of experimental data for each explosive which is to be investigated. In some cases cylinder tests are not a viable option, such as when the critical detonation failure diameter is large. The Williamsburg equation of state has been shown to produce results as accurate as the JWL equation of state despite not using experimental data for determining the parameters [40].

The WSD model [129] employs an equation of state of Mie-Grüneisen form for the products which is extended to facilitate calculation of the temperature following the same approach as was used for the reactants. This form was first introduced by Davis [34] and was also used by Aslam [8]. The forms chosen for the reference functions are

$$p_{\text{REF}}(v) = p_c \frac{\left[\frac{1}{2} \left(\frac{v}{v_c} \right)^n + \frac{1}{2} \left(\frac{v}{v_c} \right)^{-n} \right]^{a/n}}{(v/v_c)^{k+a}} \frac{k-1+F(v)}{k-1+a} \quad (2.56)$$

$$F(v) = \frac{2a(v/v_c)^{-n}}{(v/v_c)^n + (v/v_c)^{-n}} \quad (2.57)$$

$$e_{\text{REF}}(v) = \frac{p_c v_c}{k-1+a} \frac{\left[\frac{1}{2} \left(\frac{v}{v_c} \right)^n + \frac{1}{2} \left(\frac{v}{v_c} \right)^{-n} \right]^{a/n}}{(v/v_c)^{k-1+a}} \quad (2.58)$$

$$\Gamma(v) = k-1 + (1-b)F(v) \quad (2.59)$$

with free parameters k , b , a , n , v_c and p_c . The value of k corresponds to the adiabatic gamma of the equation of state in the large volume limit. The parameters

values are chosen such as to ensure that the equation of state correctly reproduces the CJ state and the accompanying principal isentrope. Furthermore the integral corresponding to the work done by the explosive products as they expand, must correctly reproduce the amount of work which is the explosive is observed to do experimentally.

The parameter, b , which affects the Grüneisen gamma is fixed using experimental data for the Crussard curve which is obtained by measuring overdriven detonations. Overdriven detonations are detonation waves which are supported by a piston causing the detonation wave to travel faster than a wave supported solely by the energy content of the explosive. The state following such a wave is at a higher pressure than the CJ state but nevertheless lies on the Crussard curve, which is related to the equation of state of the products.

2.2 Reaction Rate Models

2.2.1 Construction and Calibration of Reaction Rate Models

Construction and calibration of equations of state is a critical step in the endeavour to simulate explosives accurately. However it is only sufficient to recover accurate results in the case of one dimensional ZND detonation waves. A key effect which comes into play in the case of multi-dimensional detonations is the loss of energy to the surroundings of the partially burnt explosive. This energy is lost in the form of shock waves which propagate into the inert confining material at a direction not parallel with the propagation vector of the detonation wave itself. It is therefore not observed in the context of a one dimensional setup. This process and the chemical reaction are coupled since any loss of energy contributes to a reduction of temperature and pressure in the reaction zone.

The calibration process has thus far relied on the independent characterisation of the reactants and products, and we have as yet not considered the reaction rate model. The CJ model is built on the assumption that the reaction rate is fast, and thus the reaction zone can be neglected. While this approximation is inconsequential as regards the propagation of a wave in one dimension, it does play

2 Literature Review

a role in multidimensional detonation waves. The degree to which the wave deviates from the ZND model is strongly dependent on the width of the reaction zone, which in turn is a function of the reaction rate. See Chapter 4 for more details.

A wide reaction zone permits the loss of energy from the explosive to a yielding confiner. As a result of this energy loss, the detonation wave propagates at sub-CJ velocities. This is to be expected given the dependence of the CJ velocity on the heat of combustion of the explosive. This sub-CJ wave will furthermore exhibit lower pressures and temperatures which may in turn leads to a further decrease of the reaction rate. By this mechanism, a detonation wave may decelerate further and eventually stop (detonation failure) in the right circumstances.

Faithful simulation of detonation failure therefore necessitates accurate thermodynamic dependence of the reaction rate. Similarly ignition phenomena rely on the thermodynamic dependence of the reaction rate. For steady detonation waves, on the other hand, the reaction rate only affects the behaviour of the wave via the profile of the reaction zone. This, combined with the difficulties discussed previously in establishing what the pressures and temperatures in the reaction zone actually are, makes it difficult in practice to establish what thermodynamic dependency is appropriate. Furthermore this relationship implies that it may be possible to use multiple choices of parameters to run accurate simulations in practice.

A comprehensive review of the reaction rate models which have been proposed was published by the NIMIC shock modelling group in 2002 [99]. This review emphasises the variety of reaction models which have been employed over the preceding thirty years. The review by Handley et al. [55] provides a more recent comprehensive overview. In general, reaction rate models describe the time derivative of the mass fraction variable, λ , (used to represent the portion by mass of the explosive which is unreacted) in the generic form

$$\frac{D\lambda}{Dt} = f(T, p)g(\lambda), \quad (2.60)$$

where the material derivative of the mass fraction variable is dependent on one or more thermodynamic variables as well as λ which also serves as a reaction progress variable.

Some recent models also employ so-called ‘shock state’ variables to express the reaction rate as a function of the shock strength for a specific piece of material. The shock state variable is set as the shock wave passes, and is subsequently advected with the material. An example of this is the model presented by Aslam [8].

The rate of a chemical reaction can be modelled using an expression of Arrhenius form,

$$\frac{D\lambda}{Dt} = \lambda A \exp\left(-\frac{T_A}{T}\right). \quad (2.61)$$

This form is motivated by thermodynamics. Using the Maxwell-Boltzmann distribution, the reaction rate can be related to the portion of collisions between particles in a gas for which the energy associated with the collision exceeds some activation energy which is related to the activation temperature, T_A . In the context of explosives this form is at best an empirical relationship. Firstly, the chemical reaction is unlikely to occur in a single step, but will instead involve intermediary species. Secondly, the large variations in pressure and density which occur during the reaction of an explosive can influence the pathway of the reaction as well as the chemistry of the product gases. Thirdly, especially for condensed phase explosives, heterogeneity of the reactants, will create non-uniform pressure and temperature fields in the explosive following the shock wave. The average reaction rate over a heterogeneous domain will not match the reaction rate for a homogeneous material with the same average temperature.

Historically, pressure dependent rate laws have also been favoured due to their comparative ease of implementation, and the fact that pressures within the reaction zone are more easily measured experimentally than temperatures. Furthermore, an equation of state with which to calculate pressures is already necessitated by the need to calculate the gradient of the pressure field and is therefore already possible in all explosive models. Whereas temperatures are not available in the context of some models.

Nevertheless some models describe the rate as a function of temperature. See for example Menikoff and Shaw [88] for nitromethane and Aslam [8] for PBX 9502. Many others use pressure dependence, for example the ignition and growth model [74] and WSD model [129]. A third option is to use entropy dependence like the CREST model [51].

2 Literature Review

One of the first attempts to calibrate a reaction rate model which could be used to reproduce a wide range of experimental data was the ignition and growth model presented by Lee and Tarver [74]. This model describes the rate as being a function of the pressure and the reaction progress variable. The rate law is constructed using a sum of separately contributing terms, each of which corresponds to a different physical phenomenon. Many variations of the model have been used by many different authors, however, following Lee and Tarver [74], a generalised form can be expressed as

$$\frac{D\lambda}{Dt} = I(1 - \lambda)^x \eta^r + G(1 - \lambda)^x \lambda^y p^z, \quad (2.62)$$

where $\eta = v_0/v_1 - 1$,

where I, x, y, r, G, z are constants. The specific volumes v_0 and v_1 correspond to the initial specific volume of the explosive and the present specific volume of the unreacted explosive respectively.

The first term corresponds to the ignition part of the ignition and growth model. It is designed to capture the contribution of hot spots which are generated by the passing shock wave. The term η represents the relative compression of the unreacted explosive by the shock wave. The second term on the other hand, is dependent on the pressure, and describes the subsequent growth of the reaction. The constant G corresponds to a surface area to volume ratio. The exponent z means that the pressure may serve as a proxy for other thermodynamic variables which may vary nonlinearly with pressure, such as temperature.

A variation of the ignition and growth model is used in the WSD model [129]. In this case the rate law is expressed as

$$\frac{D\lambda}{Dt} = r_I S_I(\lambda) + r_G S_G(\lambda) + [1 - S_G(\lambda)] r_B. \quad (2.63)$$

In this case, r_I corresponds to the ignition part, while r_G represents the growth part of the model. The ignition term is

$$r_I = k_I \left(\frac{\rho}{\rho_0} - 1 - a \right)^7 (1 - \lambda)^{2/3} H \left(\frac{\rho}{\rho_0} - 1 - a \right). \quad (2.64)$$

The form of $S_I(\lambda)$ is chosen such that r_I dominates for $\lambda > 0.975$, in other words almost completely unburned explosive. The form of r_I is such that the explosive

will ignite or not, as a function of the compression and the free parameter, a , due to the use of the Heaviside function, $H(x)$. The compression is expressed in terms of the density, ρ , and the initial density ρ_0 . This term thus also serves to represent the shock sensitivity of the explosive that is observed empirically. The bulk of the reaction is controlled by the growth term, which is itself constructed out of two sub-terms, one of which is chosen to match ignition experiments, r_{IG} , while the other is calibrated to match detonation velocities, r_{DG} . The switching function, $W(\rho_{SH})$, compares the post-shock density, ρ_{SH} , to some threshold density ρ_c , which will be superseded only by strong shocks as found in detonation waves,

$$r_G = r_{IG}W(\rho_{SH}) + r_{DG}(1 - W(\rho_{SH})) \quad (2.65)$$

$$r_{IG} = k_{IG} \left(\frac{p}{p_{CJ}} \right)^{4.5} \lambda^{1/3}(1 - \lambda) \quad (2.66)$$

$$r_{DG} = k_{DG} \left(\frac{p}{p_{CJ}} \right)^2 \lambda^{1/3}(1 - \lambda) \quad (2.67)$$

where p_{CJ} is the pressure at the CJ state.

An additional term, r_B is used to capture the reaction rate at the back of the reaction zone, and has been designed to reproduce the specific properties of PBX 9502. This serves to capture the effect of coagulation of solid carbon products which corresponds to energy released on a time scale of order 5 times longer than the principle sources of energy release. The form of $S_G(\lambda)$ is chosen such that this term only affects the rate for $\lambda < 0.1$, where the explosive is almost completely burnt.

$$r_B = k_B \left(\frac{p}{p_{CJ}} \right) (1 - \lambda)^{1/2} \quad (2.68)$$

The free parameters of this model are ρ_c , k_I , k_{IG} , k_{DG} , k_B , a , and there are other degrees of freedom associated with the exponents and the form of the model itself. The switching functions, $S_I(\lambda)$, $S_G(\lambda)$ and $W(\rho_{SH})$ are expressed using the hyperbolic tangent functions, such that the overall reaction rate changes smoothly from one regime to the next.

By setting each of the parameters in accordance with the data from various experiments, it is possible to reproduce a wide range of data with a single parameter set. While ignition and growth is still one of the most used models [13, 59], it is often

2 Literature Review

cited as a model lacking predictive capability [8, 55, 130] – the inclusion of new experimental data frequently requires a retrospective adjustment of the parameters. The large number of parameters means that the successful calibration of the model to fit a set of data does not necessarily justify the specifics of the various terms in the model. This also implies that the underlying physics has not been captured correctly. This is especially relevant when the parameter values are chosen based on a global optimization of the simulation results with respect to experimental data.

A second criticism of the ignition and growth model arises from its use of pressure dependency. On the one hand, pressure dependent models are commonly implemented, due to the limited availability of experimental data relating to other thermodynamic properties of the explosive such as temperature. They can be implemented using standard mechanical equations of state, while the implementation of alternative temperature or entropy dependent models requires suitable equation of state models. Furthermore, pressure dependent models have proven to be robust and predictive in practice [108, 129]. The correlation of pressure with other thermodynamic variables, in particular temperature, can be used as physical justification for pressure dependence. However, this correlation only applies for a limited subset of possible experiments. For certain experiments it has been demonstrated that pressure dependence is inappropriate [10]. Temperature dependence, on the other hand, is motivated by chemical kinetics models, which can be applied much more generally. The issue with temperature dependent models is that its success relies on the homogeneity of the temperature field. This will be discussed further in section 2.2.2.

Most experiments are carried out in ambient conditions – the explosive is subject to a single shock wave before undergoing a chemical reaction. In this case the state in the unburned explosive is a state on the Hugoniot curve of the ambient state. On this curve, there is a one to one relationship between pressure and temperature. The experiments presented by Aslam et al. [10] deliberately avoid this one to one relationship by subjecting the explosive to a pair of shocks. The state in the explosive is thus no longer on the single-shock Hugoniot. The results show that in this case it is no longer appropriate to describe the rate as a function of pressure only. Aslam [8] has also presented experiments carried out using explosive at a range of initial temperatures, and the results support this conclusion. The

experiments sample multiple states of equal pressure and demonstrate that the states do not correspond to a single value for the reaction rate. These experiments motivate the use of either temperature or entropy to distinguish between these states.

A recent experimental method has been presented by Aslam et al. [11], with which temperature dependent and entropy dependent models may be compared. In this experimental set up, an initial shock wave is followed by a release wave. The release wave affects the temperature in the explosive, but leaves the entropy unchanged. The predictions of an entropy dependent model will therefore be different to those of a temperature dependent model in this case.

2.2.2 Homogeneous and Heterogeneous Explosives

The discussion above makes an implicit assumption about the homogeneity of explosives. The equations of state are such that the explosive is described as having a single uniform temperature on the length scale of computational cells, and thus the explosive is also assumed to burn homogeneously.

Experiments have shown that the properties of explosives are affected by physics which occurs on the length scale of micrometre heterogeneities in the explosive. This has been observed for granular explosives [25, 26]. The properties of homogeneous explosives such as nitromethane can also be altered through the introduction of artificial heterogeneities such as glass micro-balloons. The effects arising from the presence of cavities in explosives have been studied extensively [19, 20, 92, 100].

The size of these cavities is on the scale of micrometres. The computational power of modern technology means that it is generally prohibitively expensive to resolve the cavities directly in the context of a simulation of an explosive. Recently, however, research has been carried out which takes this approach [89].

Much research has been done with the aim of indirectly including these effects in hydrodynamic simulations [55]. The exact mechanism by which the collapse of cavities affects the reaction of the explosive is still not fully understood. The most important mechanism is likely the development of hot spots at which the reaction

2 Literature Review

rate is much faster than the in the surrounding comparatively cold bulk material [92]. However there may be an additional contribution to the overall rate resulting from the compression of the bulk material which occurs as the hot spots burn [55]. The contribution of temperature diffusion may also be significant.

Analysis on the effect of pores on the macroscopic reaction rate has been carried out by Levesque et al. [77, 78]. Saurel et al. [105], on the other hand evaluate the macroscopic reaction rate directly, based on analysis of the evolution of spherical hot spots. These approaches necessarily lead to the introduction of free parameters associated with physical unknowns such as the thermal diffusivity. Furthermore there are unknowns related to the size distribution of the pores. Menikoff has also discussed the influence of heterogeneities in the explosive via shock waves which are reflected off impurities [88]. A recent approach relies on the use of a stochastic reaction rate model [69].

The heterogeneity of explosives has also been used as an argument against reaction rate models which are a function of temperature only. This is because of the heterogeneous temperature field arising from cavity collapse in the explosive following a shock wave. A nonlinear Arrhenius temperature dependence means a heterogeneous temperature field will have a faster average reaction rate than what would be predicted by applying the same Arrhenius rate law to the average temperature. As such a heterogeneous explosive is expected to have a faster rate following a shock wave, than following an isentropic raise in temperature. This dependency can be accounted for in an empirical rate law through the inclusion of a pressure or entropy dependent term [83, 87].

Alternatively, this can be handled through the use of shock state dependent reaction rate models [8, 129]. With this approach the reaction rate for a piece of material of the explosive is determined using the strength of the shock which passed that piece of material. In other words, a variable is set as the shock wave passes. This variable is then advected with the flow, and does not change according to the subsequent thermodynamic evolution of the material. This method has been argued for by James and Lambourn [64]. Their analysis of experimental data yielded a correlation between local shock strength and the subsequent reaction rate.

In the case of the WSD model [129], the shock state is used merely as a switch to distinguish between the ignition regime and the detonation regime. However the value may also be used as a quantitative variable. An early example of this approach is the DAGMAR rate form [3], which is a modified Arrhenius rate law,

$$\frac{D\lambda}{Dt} = \lambda Z_0 p_{SH}^n \exp\left(-\frac{T_A}{T}\right), \quad (2.69)$$

with calibration parameters Z_0 , n and T_A . The value of p_{SH} is determined using the pressure at the time when the explosive begins to burn, after which it is kept fixed. It is a separate variable to the thermodynamic pressure, which continues to evolve with the flow. The inclusion of this term allows for the construction of a model which is strongly dependent on the shock strength, with a comparatively weak dependence on the subsequent evolution of the state. This can therefore go some way to capturing the increased reaction rate which occurs on account of the heterogeneity of the temperature field following a strong shock wave.

A more recent example of this approach is the reaction rate model for PBX 9502 presented by Aslam [8]. In this work, the reaction rate is a product of a pressure dependent expression and an Arrhenius-like expression,

$$\frac{D\lambda}{Dt} = F_p(F_1 + F_2)F_\lambda, \quad (2.70)$$

$$F_p = \begin{cases} \exp(-(p_0/p)^{n_p}), & \text{if } p > p_\zeta \\ 0 & \text{otherwise} \end{cases} \quad (2.71)$$

$$F_1 = k_1 \exp(-T_1/T_{SH})(\lambda + a_1 F_p)(1 - \lambda)^{b_1} \quad (2.72)$$

$$F_2 = k_2 \exp(-T_2/T_{SH})(1 - \lambda)^{b_2} \quad (2.73)$$

$$F_\lambda = f_s + \frac{1}{2}(1 - f_s) \left(1 - \tanh\left(\frac{\lambda_c - \lambda}{\delta_\lambda}\right)\right) \quad (2.74)$$

Here p_ζ serves to limit the sensitivity of the explosive to weak shock waves. In this case the dependence on the temperature is kept fixed after the initial shock; T_{SH} is determined as the shock passes, and then kept fixed. The pressure, p , on the other hand, corresponds to the thermodynamic variable and continues to vary. The free parameters in this case are k_1 , k_2 , b_1 , b_2 , a_1 . The expression for F_λ is chosen such that its value will be close to unity for $\lambda > \lambda_c$ and reduce to f_s for the final stage of the reaction. Once again, this behaviour is specifically designed to reproduce the empirically observed properties of PBX 9502 and is analogous to a

2 Literature Review

similar term used in the WSD model. The two terms F_1 and F_2 permit the model to be calibrated for both ignition and detonation.

The limitations of pressure dependent models has also been used as motivation for the development of the entropy dependent CREST model (Computational Reaction Evolution on entropy (S) and Time) [51, 54, 130]. Entropy dependence offers a solution to two of the problems discussed above. On the one hand, pure pressure dependent models are not capable of reproducing experiments which sample states off the single-shock Hugoniot. On the other hand, the heterogeneity of granular condensed phase explosives motivates a dependence on the strength of the shock wave. Entropy dependence addresses both of these issues. Firstly, the entropy dependence can account for the difference between a single shock and a pair of shocks. Secondly, CREST does not require explicit shock state dependence. This is because CREST is usually implemented in models with an ISE (Isentropic Solid Equation) closure law for the mixture of reactants and products. This closure law means that no heat will transfer between reactants and products, and so the entropy of the unburned reactants will not change as the explosive begins to burn (unless the explosive is subject to a second shock wave). The entropy of the explosive thus serves implicitly as a shock-state variable.

The rate law is expressed as expressed as a weighted sum of fast and slow components of the reaction rate [51],

$$\frac{D\lambda}{Dt} = m_1 \frac{D\lambda_1}{Dt} + m_2 \frac{D\lambda_2}{Dt} \quad (2.75)$$

$$\frac{D\lambda_1}{Dt} = b_1 t (1 - \lambda_1) \quad (2.76)$$

$$\frac{D\lambda_2}{Dt} = b_2 t \lambda_1 (1 - \lambda_2) \quad (2.77)$$

$$b_1 = c_0 Z_S^{c_1} \quad (2.78)$$

$$b_2 = c_3 Z_S^{c_3} \quad (2.79)$$

where Z_S is a function of entropy obtained by integrating the heat capacity from an isentropic reference curve. The form of m_1 and m_2 is chosen such as to match experimental data.

Handley and James [52] have used CREST with the aim of capturing desensitization effects directly, without the inclusion of a specifically designed term as has been used with pressure dependent models [36].

2.3 Discussion

The current state of the art in explosive modelling makes use of empirical reaction rate forms which can be dependent on a number of thermodynamic variables. On the one hand, pressure dependent models are often convenient to use and produce accurate results. On the other hand, more complex experiments have revealed the limited capability of pressure dependency to fully describe the properties of the explosive. Furthermore, experiments have shown that these issues cannot necessarily be resolved by simply using temperature in the place of pressure, for example when heterogeneities are present in the explosive.

The typical approach taken to determine suitable parameter values for these reaction rate models involves application of an optimization algorithm. This limits our ability to quantify the correctness of a model. Firstly, the propagation of a detonation wave is a function of the structure of the reaction zone, and thus only indirectly a function of the reaction rate model. Secondly, thermodynamic properties are strongly correlated with each other within the reaction zone. A global optimization algorithm can therefore find parameters which work well in practice even if the ideas motivating the original rate law were flawed.

The question of the reaction rate model is naturally strongly dependent on the equations of state. To address these issues, accurate, reliable temperature-capable equations of state are essential. An assessment of the effectiveness of a temperature dependent rate law relies on the accuracy of the temperature values that are used. In particular, the equations of state should only rely on calibration data which is available for a wide range of explosives, such that the method presented in this thesis is widely applicable without significant alteration for each explosive of interest.

The most commonly applied equation of state for the reactants is the shock Mie-Grüneisen equation of state, however it cannot be extended to incorporate temper-

2 Literature Review

atures, since it uses the Hugoniot curve directly as a reference curve rather than an isentrope. The approach introduced by Davis, on the other hand, successfully incorporates temperatures into the model. However, the original form of the reference curves has been shown to only be robust over a narrow range of specific volumes. Furthermore a porosity model must be used if the equation of state is to be applied to explosives such as EM120D. The modifications introduced in the WSD model for PBX 9502, on the other hand, introduce more parameters than can be justified to model explosives for which less experimental data is available.

In the case of the products, the JWL equation of state is very popular, and has the advantage of using simple empirical functional forms for the reference functions. The Davis equation of state for the detonation products, is much more complex. This is in part because of the difficulty associated with inferring temperatures for the products using experimental data for the Crussard curve. The Williamsburg equation of state, on the other hand, was developed with the aim of using data made available by a thermochemical code. The form of the Williamsburg equation of state is motivated by statistical mechanics, however this form is unnecessarily complex for implementation in a hydrocode, where efficient evaluation of the state is paramount.

Chapter 3 of this thesis is focused on developing equations of state with which temperatures in the reaction zone can be evaluated. The equations of state presented are shown to be appropriate for modelling both ideal and non-ideal explosives, and are only reliant on a limited experimental dataset, thus making them applicable to a wide variety of condensed-phase explosives. There are four key issues which must be addressed.

Firstly, an equation of state is introduced for the reactants. This extends the equation of state of Davis [35] with a porosity model. An important distinction between this method and other work is that it relies only on experimental data which is generally available. The data used includes only the thermodynamic properties of the explosive in ambient conditions, and single shock Hugoniot data. While additional data does exist for some explosives [80], this method is applicable to other explosives for which such data is unavailable. The method includes a porosity model, and it is demonstrated that this is necessary for accurate predictions.

Secondly, a modified JWL equation of state is introduced. The equation of state is amended to include a temperature reference curve and a volume dependent expression for the Grüneisen gamma. It is designed with the intention of using a thermochemical equilibrium code to determine suitable parameters for the equation of state of the products. This not only allows for temperatures to be calculated, but furthermore renders the equation of state more accurate for states where the entropy deviates from that of the principal isentrope, as is expected in non-ideal detonation waves. The reference curves are however expressed using the same simple form as is used in the standard JWL equation of state.

The third issue is that of implementing closure laws in the reaction zone. The equations of state presented in Chapter 3 have been developed while keeping the need to implement pressure and temperature equilibrium laws in mind. To do so robustly requires equations of state which are well behaved, and so the mathematical form for the reference curves must be chosen carefully. In this thesis we present mathematical forms for the reference curves and demonstrate that these can be used robustly in practice.

Finally, the validity of temperature equilibrium itself must be considered. Any heat transfer between reactants and products will affect the temperature of the reactants and thus will have a knock-on effect on the reaction rate. This is discussed in Chapter 4. A method is presented with which the amount of heat transfer expected in the reaction zone of a ZND wave can be directly evaluated. This permits a direct comparison between the predictions of the model when using temperature equilibrium and those of a model employing heat isolation, where no heat transfers between the reactants and products.

To establish the accuracy of the equations of state, we must make some predictions which can be compared with experimental data. To do this, an empirical reaction rate is calibrated for simulating the detonation of compliantly confined rate sticks. The calibration is done via global optimization of the rate law parameters, and thus given the arguments presented above, does not necessarily justify the rate forms which were chosen. Nevertheless, this does allow for a rigorous test of the equations of state. If the rate law calibrated in this way can then be used to predict detonation velocities in other contexts such as different geometries or different confiners, then

2 Literature Review

it demonstrates that the material properties of the explosive are being reproduced accurately in the simulations.

The general applicability of the calibration methods and equation of state forms is demonstrated by applying the same method to two explosives with very different characteristics. Once the accuracy, and validity of the equations of state has been established, these can be used to address the question of thermodynamic dependence of the reaction rate model.

A systematic approach is required to quantitatively establish the thermodynamic dependence of the reaction rate. The Arrhenius form is not necessarily suitable in the case of heterogeneous explosives, where a shock wave may create a heterogeneous temperature field. On the other hand, pressure dependent models have been shown to fail in the contexts of some types of experiment. This suggests that when pressure dependent models do work, it is as a result of the correlation between pressure and other thermodynamic variables. This has led to the development of shock state models, which effectively introduces a history-dependence on the reaction rate by advecting additional variables with the flow. The entropy dependent CREST model is to some degree equivalent to this since the entropy can be used to determine the strength of the shock wave incident on the material.

Chapter 6 introduces a mechanism with which experimental data from shock to detonation transition experiments can be interpreted. This mechanism permits direct evaluation of the reaction rate immediately following a shock wave which induces a reaction in the explosive. This approach avoids the computationally expensive optimization procedure which is otherwise necessary to determine the rate law parameters. The resulting data can be used to quantitatively assess how the reaction rate depends on the various thermodynamics properties of the shocked explosive. For example, the reaction rate can be evaluated following a 1GPa shock wave. An equivalent evaluation can be carried out for a pair of shock waves with an equal final pressure of 1GPa. If the reaction rates do not match, then this provides a quantitative justification for the inclusion of other thermodynamic properties besides the pressure in the rate form.

3 Equations of State

3.1 Introduction

The objective of the work presented in this chapter is to improve the robustness and accuracy of numerical simulations of condensed phase explosives by developing temperature capable mechanical equations of state (EoS models) for reactants and products. We aim to develop EoS models applicable to both ideal and non-ideal explosives. In order to evaluate the velocity of non-ideal detonations, the intention is to implement the EoS models in a direct numerical simulation which resolves the mixture of reactants and products in the reaction zone via the implementation of a temperature equilibrium condition. The EoS models must therefore be suitable for calculating the temperature.

In addition, for non-ideal detonations, the EoS of the products must be valid even for states at lower entropy than the CJ or principal isentrope. This is achieved using a thermochemical equilibrium code (also called an ideal detonation code) *IDeX* [21], with which properties of the equation of state can be calculated that are difficult to measure experimentally. In particular, temperature and the Grüneisen gamma can be evaluated, and used to calibrate an equation of state. Accurate values for the Grüneisen gamma ensure that the EoS is valid for states farther from the reference curve than the JWL EoS which assumes a constant value for the Grüneisen gamma.

Furthermore an equation of state for the reactants which permits estimation of the temperature is required. A calibration methodology is developed which uses readily available experimental data. As such the methodology can be applied to a wide range of explosives.

3 Equations of State

The EoS models were calibrated for two explosives. The plastic bonded explosive PBX 9502 is chosen since it is the subject of many experimental and numerical studies [8, 63, 129]. The method is also applied to the ANFO based emulsion EM120D as an example of a non-ideal explosive; the detonation velocity in narrow rate sticks can deviate from the Chapman Jouguet (CJ) velocity by as much as 35% (compare with the 5% deviation observed in PBX 9502). EM120D has also been the subject of a previous numerical study [108].

The EoS model for the reactants is extended with a porosity model. EM120D is porous (14% by volume) and as such a porosity model is necessary to accurately predict post-shock temperatures. To a lesser degree, PBX 9502 is also porous. We demonstrate that the nonlinear D,u relationship which has been measured for PBX 9502 [49] can be successfully reproduced through application of the porosity model.

For both reactants and products a fitting form for the temperature reference curve consisting of a power law and an exponential term is used. Note that for an ideal gas at constant entropy the temperature and pressure can be expressed as a power law in the volume. So for large volumes, for which the exponential term is negligible, the power law dominates and the material behaves like an ideal gas, with constant adiabatic gamma and Grüneisen gamma. This fitting form has the desirable property that the Grüneisen gamma is well-behaved for all volumes: it remains positive everywhere and does not diverge. As a result, the implementation of the thermal equilibrium condition is much more robust.

3.2 Mie-Grüneisen

All the equations of state in this work are presented in Mie-Grüneisen form,

$$p - p_{\text{REF}}(v) = \frac{\Gamma(v)}{v}(e - e_{\text{REF}}(v)). \quad (3.1)$$

The Mie-Grüneisen form uses reference functions to constrain the equation of state such that if one of the pressure or energy are on the reference curve for the current density then the other property will also be on its respective reference curves. The reference curves specify a one dimensional path through the equation of state (which has two degrees of freedom).

These equations can be used in lieu of a complete equation of state since knowledge of the Grüneisen gamma (3.2) allows for states away from the reference curves to be approximated too. It is assumed that the Grüneisen gamma can be expressed as a function of specific volume only.

$$\Gamma = v \left(\frac{\partial p}{\partial e} \right)_v \quad (3.2)$$

If the reference curve is chosen to be an isentrope, then the EoS can be supplemented with a reference function for temperature, T_{REF} . This is because the Grüneisen gamma can be expressed in terms of the derivative of temperature with respect to volume at constant entropy

$$\Gamma = v \left(\frac{\partial p}{\partial S} \right)_v \left(\frac{\partial S}{\partial e} \right)_v = -\frac{v}{T} \left(\frac{\partial T}{\partial v} \right)_S \quad (3.3)$$

where use has been made of one of Maxwell's relations.

$$\frac{\partial^2 e}{\partial S \partial v} = - \left(\frac{\partial p}{\partial S} \right)_v = \left(\frac{\partial T}{\partial v} \right)_S \quad (3.4)$$

Note that the Grüneisen gamma is analogous to the adiabatic gamma γ which can be defined as

$$\gamma = -\frac{v}{p} \left(\frac{\partial p}{\partial v} \right)_S. \quad (3.5)$$

Furthermore if the reference curve is an isentrope then the reference energy and pressure functions can be related (although the integration constant may be an additional degree of freedom)

$$de|_S = -p dv. \quad (3.6)$$

Finally a value for the specific heat capacity at constant volume, c_v , can be used to evaluate temperatures for states off the reference curve. In this thesis, a constant value for the heat capacity is assumed. This choice ensures that the temperature can be expressed as an explicit function of volume and energy. Since this function must be evaluated for each iteration of the temperature equilibrium root finding algorithm, this has a significant bearing on the overall performance of the algorithm.

3 Equations of State

The equation of state is thus fully constrained with just two reference functions: one of p_{REF} and e_{REF} and one of Γ and T_{REF} .

$$\begin{aligned}
 p - p_{\text{REF}}(v) &= \frac{\Gamma(v)}{v}(e - e_{\text{REF}}(v)) & (3.7) \\
 T - T_{\text{REF}}(v) &= \frac{e - e_{\text{REF}}(v)}{c_v} \\
 p_{\text{REF}}(v) &= -\frac{de_{\text{REF}}(v)}{dv} \\
 \frac{\Gamma(v)}{v} &= -\frac{1}{T_{\text{REF}}(v)}\frac{dT_{\text{REF}}(v)}{dv}
 \end{aligned}$$

The methodology above defines an EoS with temperature without having to explicitly calculate any entropies. The fundamental assumption being made here is that any changes in entropy (at constant volume) can be modelled using entropy independent values for the Grüneisen gamma and specific heat capacities.

The frozen speed of sound in a material modelled by such an equation of state can be calculated using

$$c^2 = \left(\frac{\partial p}{\partial \rho}\right)_S = -v^2 \left(\frac{\partial p}{\partial v}\right)_S \quad (3.8)$$

$$= -v^2 \left[\left(\frac{\partial p}{\partial v}\right)_e + \left(\frac{\partial p}{\partial e}\right)_v \left(\frac{\partial e}{\partial v}\right)_S \right] \quad (3.9)$$

$$= -v^2 \left[\left(\frac{\partial p}{\partial v}\right)_e - \frac{\Gamma}{v}p \right] \quad (3.10)$$

where, from (3.7),

$$\left(\frac{\partial p}{\partial v}\right)_e = \frac{\partial p_{\text{REF}}}{\partial v} + \frac{\partial \rho \Gamma}{\partial v}(e - e_{\text{REF}}) - \rho \Gamma \frac{\partial e_{\text{REF}}}{\partial v}. \quad (3.11)$$

If this equation gives a negative value for the square of the sound speed, this indicates that the functions chosen for the reference curves are unphysical.

While the entropy is usually not used explicitly as a variable, it is nevertheless possible to calculate isentropic paths on the equation of state and changes in entropy. To calculate the specific internal energy, e , at volume, v , such that the entropy matches that of a reference state with volume and energy, v_0 and e_0 , we can simply solve the ordinary differential equation

$$\frac{de}{dv} = -p(v, e), \quad (3.12)$$

using the reference state as initial conditions. This can always be evaluated numerically using an ODE algorithm such as a Runge-Kutta method. However, if the reference curve itself corresponds to an isentrope, as is often the case in this thesis, the expression can be simplified. This is done by defining a reduced pressure and energy,

$$\hat{p} := p - p_{\text{REF}} \quad (3.13)$$

$$\hat{e} := e - e_{\text{REF}} \quad (3.14)$$

If the reference curve is isentropic,

$$\frac{de_{\text{REF}}}{dv} = -p_{\text{REF}} \quad \Rightarrow \quad \left(\frac{\partial \hat{e}}{\partial v} \right)_S = -\hat{p}. \quad (3.15)$$

We can then derive an explicit expression for the energy on the isentrope,

$$\frac{\partial \hat{e}}{\partial v} = -\hat{p} = -\rho \Gamma \hat{e} \quad (3.16)$$

$$\ln \left(\frac{\hat{e}}{\hat{e}_0} \right) = \int_{v_0}^v -\frac{\Gamma(\tilde{v})}{\tilde{v}} d\tilde{v} \quad (3.17)$$

$$e(v, S(v_0, e_0)) = e_{\text{REF}}(v) + (e_0 - e_{\text{REF}}(v_0)) \exp \left(- \int_{v_0}^v \frac{\Gamma(\tilde{v})}{\tilde{v}} d\tilde{v} \right). \quad (3.18)$$

This expression can be further simplified using the relationship between the Grüneisen gamma and temperature,

$$T_{\text{REF}}(v) = T_{\text{REF}}(v_0) \exp \left(- \int_{v_0}^v \frac{\Gamma(\tilde{v})}{\tilde{v}} d\tilde{v} \right) \quad (3.19)$$

$$\Rightarrow \quad e(v, S(v_0, e_0)) = e_{\text{REF}}(v) + (e_0 - e_{\text{REF}}(v_0)) \frac{T_{\text{REF}}(v)}{T_{\text{REF}}(v_0)}. \quad (3.20)$$

The difference in entropy between two states, (v_0, e_0) and (v_1, e_1) can be evaluated by first calculating the energy of an intermediate state with the volume of one state, v_1 , and the entropy of the other, $S(v_0, e_0)$, using equation (3.20). The change in entropy can now be expressed as an integral at constant volume with respect to temperature,

$$\Delta S = \int_{T^*}^{T_1} \frac{c_v}{T} dT, \quad (3.21)$$

where T^* is the temperature of the intermediate state and T_1 is the temperature corresponding to (v_1, e_1) .

$$T^* = T(v_1, e(v_1, S(v_0, e_0))) \quad (3.22)$$

$$T_1 = T(v_1, e_1) \quad (3.23)$$

3 Equations of State

In the case where the heat capacity is independent of temperature,

$$\Delta S = c_v \ln \left(\frac{T_1}{T^*} \right). \quad (3.24)$$

3.3 Products

Cylinder test experiments only provide data for the pressure and energy reference curves of the EoS. Hence, data must be leveraged from elsewhere if a complimentary reference function for the temperature is to be constructed. An ideal detonation code (*IDeX*) such as that presented by Braithwaite et al. [21] can be used for this purpose.

An ideal detonation code is a stand-alone program for evaluating the equation of state of a material composed of atoms of various elements in a specific distribution. Given the chemical composition of the reactants, we know the relative abundance of carbon, nitrogen, oxygen and hydrogen and potentially other elements – and we know that the number of atoms of each element will be conserved during the chemical reaction. The ideal detonation code then uses equations of state for each of the chemicals which may form during the reaction. The relative amount of each chemical product is determined using an optimization algorithm which distributes the atoms among the chemical products such as to minimize the total Helmholtz free energy for a given volume and temperature. This minimization is done on the assumption that the reaction products are in chemical equilibrium. This assumption is reliant on the hypothesis that the chemical reaction occurs at sufficiently high temperatures to break all chemical bonds, thus allowing the energetically optimal combination of chemicals to form in the products.

The energy for any given combination of chemicals is evaluated using empirical equations of state for each product along with empirical mixing rules which account for the entropy of mixing. *IDeX* code uses fluid EoS based on an intermolecular Buckingham alpha exponential 6 potential.

The atomic abundances for EM120D and PBX 9502 are presented in Table 3.1. The chemical products considered were CH₄, CO, CO₂, H₂, NH₃, H₂O, N₂, NO, O₂.

	EM120D	PBX 9502
C	2.955260000	22.753076846
H	2.475539268	22.248408665
N	9.490254873	22.080185938
O	8.920408921	22.080185938
Si	0.208055925	
Cl		1.177559088

Table 3.1: Atomic abundances in moles/kg used to evaluate the equation of state of the detonation products in *IDeX*.

With the addition of SiO_2 for EM120D, and HCl , Cl_2 and C (diamond) for PBX 9502.

Once the equation of state, $F(v, T)$, of the burnt products can be evaluated, it is then straightforward to evaluate the Crussard curve – the locus of states in the explosive following a shock and complete reaction. This is achieved by finding for a fixed specific volume, v , the temperature, T , such that the specific internal energy defined as

$$e(v, T) = F(v, T) - TS(v, T) \quad (3.25)$$

satisfies the Hugoniot equation,

$$e(v, T) - e_0 = \frac{1}{2}(p(v, T) + p_0)(v_0 - v), \quad (3.26)$$

where

$$S(v, T) = - \left(\frac{\partial F}{\partial T} \right)_v \quad \text{and} \quad p(v, T) = - \left(\frac{\partial F}{\partial v} \right)_T \quad (3.27)$$

and e_0 is the mechanical and chemical energy content of the unreacted explosive with initial pressure and specific volume p_0 and v_0 respectively. The Crussard curve, denoted with the subscript C , is thus a function of one variable, conventionally chosen to be volume. The Crussard pressure can thus be expressed as $p_C(v)$.

The CJ state of the explosive is found by determining the CJ volume, v_{CJ} , such that the Crussard curve is tangent to the Rayleigh line in pressure volume space,

$$p'_C(v_{CJ}) = \frac{p_0 - p_C(v_{CJ})}{v_0 - v_{CJ}}. \quad (3.28)$$

More details on the derivation of these equations is presented in Chapter 4.

3 Equations of State

Finally, data for the principal isentrope which intersects the CJ state can be found by using the equation of state to integrate the ordinary differential equation

$$\left(\frac{\partial e(v, T)}{\partial v}\right)_S = -p. \quad (3.29)$$

This also requires knowledge of the energy content of the explosive. If in practice the energy content is not known accurately, it can be reverse engineered using an experimental value for the ideal detonation velocity. Using empirical EoS models for each of the product chemicals and mixture rules, an EoS for the product mixture can be constructed. However, it is cumbersome to use such an EoS directly in hydrocodes. So instead the code is used to output pressure, energy and temperature data for the principal isentrope, which is used to calibrate numerical expressions for the reference functions.

Reference functions of the following form

$$p(v)|_{S_{CJ}} = av^b + c \exp(-dv) \quad (3.30)$$

$$e(v)|_{S_{CJ}} = -\frac{a}{b+1}v^{b+1} + \frac{c}{d} \exp(-dv) - Q \quad (3.31)$$

$$T(v)|_{S_{CJ}} = a_T v^{b_T} + c_T \exp(-d_T v), \quad (3.32)$$

where S_{CJ} represents the entropy of the CJ state which lies on the principal isentrope are then fit to the data. The energy reference function is obtained by integrating the pressure reference function, with integration constant Q representing the specific energy in the large volume limit. The value of the constant is arbitrary, but is by convention chosen to be the specific energy release associated with the conversion of material from reactants to products. The specific energy of the reactants in the large volume limit is set to zero. The energy release associated with the reaction from reactants to products is thus accounted for directly in the EoS.

The fitting process is done by fitting the high volume data to a power law first, and then adding the exponential term as a correction such as to also fit the low volume data and to satisfy the CJ criterion. In the large volume limit, where the exponential term goes to zero, the presence of the power law means that the isentrope approximately takes on the properties of an ideal gas and is well behaved even at volumes far larger than the volume range of the data used for the fitting.

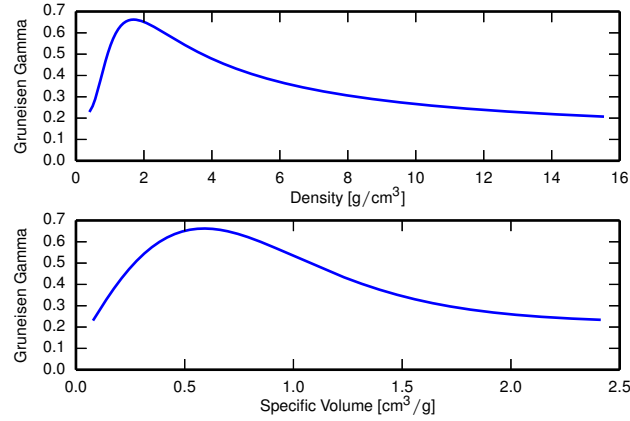


Figure 3.1: The form chosen for $T_{S_{CJ}}$ ensures that the Grüneisen gamma is bounded and well behaved in both the limit of large volume and the limit of large density. The values plotted here are for the EoS of the products of PBX 9502, the parameters of which are presented in Table 3.2.

In order to accurately reproduce the CJ pressure and ideal detonation velocity it is important that the value and the derivative of the pressure reference function are exactly reproduced at the CJ state [44, 75]. To this end, the parameters c and d are fixed in terms of a and b using

$$\left. \begin{aligned} p_{CJ} &= av_{CJ}^b + c \exp(-dv_{CJ}) \\ \frac{\partial p}{\partial v} \Big|_{S,v=v_{CJ}} &= abv_{CJ}^{b-1} - cd \exp(-dv_{CJ}) \end{aligned} \right\} \Rightarrow \begin{cases} d = \frac{abv_{CJ}^{b-1} - \frac{\partial p}{\partial v} \Big|_{S,v=v_{CJ}}}{p_{CJ} - av_{CJ}^b} \\ c = \exp(dv_{CJ}) (p_{CJ} - av_{CJ}^b) \end{cases} \quad (3.33)$$

The form of the function for the Grüneisen gamma is derived from (3.3) and (3.32). The chosen form for $T|_{S_{CJ}}$ is shown to be suitable in Figure 3.1 which demonstrates that for the products of PBX 9502 the Grüneisen gamma is well behaved across the whole range of volumes – it never diverges, nor does it go negative or close to zero. This takes the form:

$$\Gamma(v) = -v \frac{a_T b_T v^{b_T-1} - c_T d_T \exp(-d_T v)}{a_T v^{b_T} + c_T \exp(-d_T v)}. \quad (3.34)$$

The physical interpretation of the parameters is discussed further in the following section since the same form is used for the reactants.

Parameters for the product EoS were determined for the two explosives PBX 9502 and EM120D. The parameters are presented in Table 3.2. Note that for

3 Equations of State

	PBX 9502	EM120D
a	0.2865	17.47
b	-3.219	-2.712
c	2.233×10^{11} Pa	2.109×10^{11} Pa
d	10700 kgm^{-3}	6571 kgm^{-3}
a_T	264.8	107.5
b_T	-0.2195	-0.3861
c_T	3188 K	1171 K
d_T	3053 kgm^{-3}	2025 kgm^{-3}
Q	2.953 MJkg^{-1}	2.446 MJkg^{-1}
c_V	$2500 \text{ JK}^{-1}\text{kg}^{-1}$	$2500 \text{ JK}^{-1}\text{kg}^{-1}$
v_{CJ}	$1/2450.2 \text{ m}^3\text{kg}^{-1}$	$1/1598.4 \text{ m}^3\text{kg}^{-1}$
p_{CJ}	26.12 GPa	12.00 GPa
D_{CJ}	7755.0 ms^{-1}	6389.5 ms^{-1}

Table 3.2: Parameters for the product EoS models for PBX 9502 and EM120D. The proposed reference curves are shown in Figures 3.2 and 3.3. The first four rows of parameters correspond to the pressure and energy reference curves, while the next four (with subscript T) correspond to the temperature reference curve (3.32).

PBX 9502, the ideal detonation velocity of 7755 ms^{-1} from Jackson and Short [63] was used to calibrate the heat of reaction, since *IDeX* predicts a slightly higher ideal detonation velocity of 7933 ms^{-1} . This may be a reflection of the limited applicability of the chemical equilibrium assumption, and suggests that in this case not all of the theoretically available chemical energy is released and is available to sustain the propagation of the detonation wave.

For EM120D, on the other hand, the ideal detonation velocity is taken to be the one which is predicted by *IDeX*, as this is found to be in close agreement with what is expected experimentally. Figures 3.2 and 3.3 show the reference curves along with the constituent exponential and power law terms. This is to show that the presented fitting parameters are such that the power law is the dominant term, especially in the large volume limit.

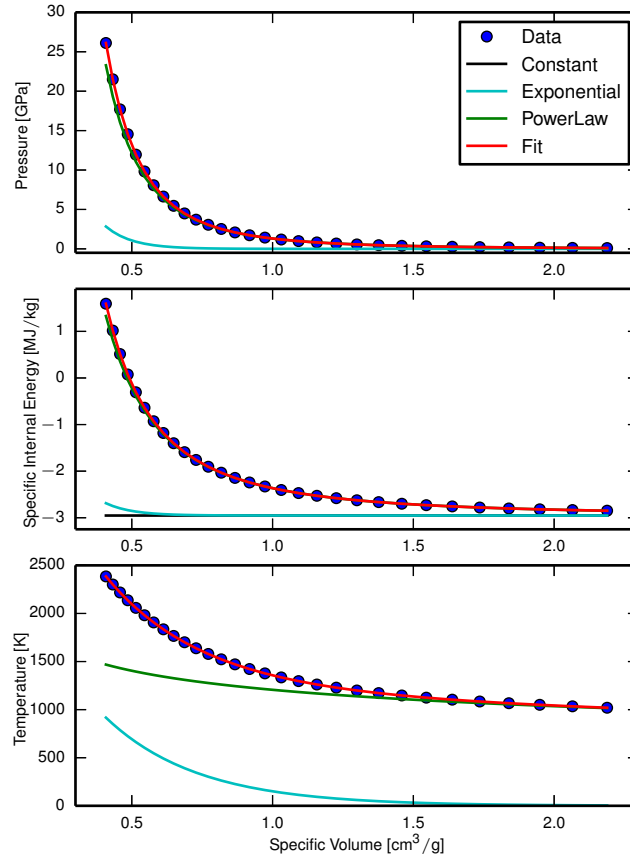


Figure 3.2: A fit to the principal isentrope from *IDeX* for PBX 9502. The principal isentrope data are given as blue dots. The fit (red) is the sum of the power law (cyan) and the exponential curve (green). The energy reference curve also includes a non-zero constant, Q , corresponding to the energy content of the explosive. Note how the fitting parameters are chosen such that the exponential term only plays a role in the small volume regime.

3 Equations of State

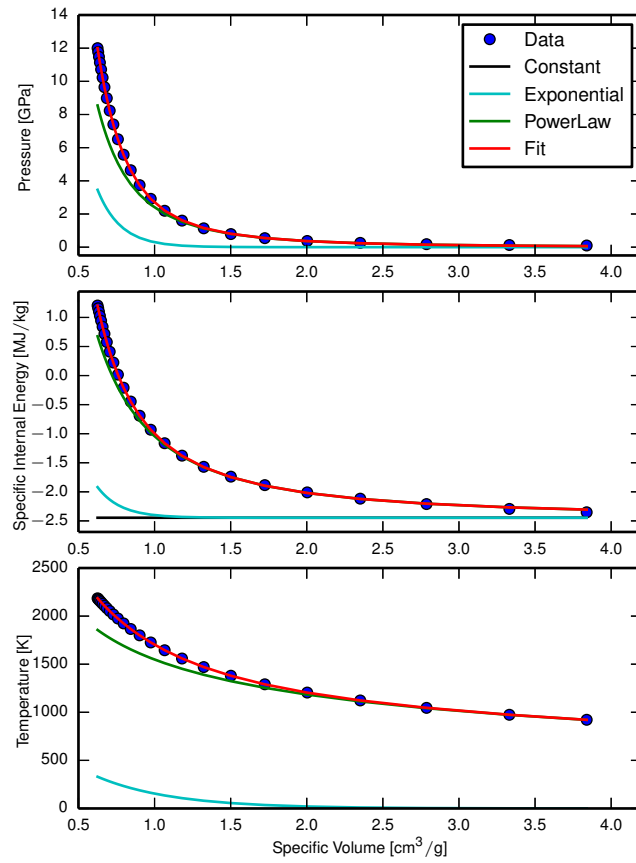


Figure 3.3: A fit to the principal isentrope from *IDeX* for EM120D.

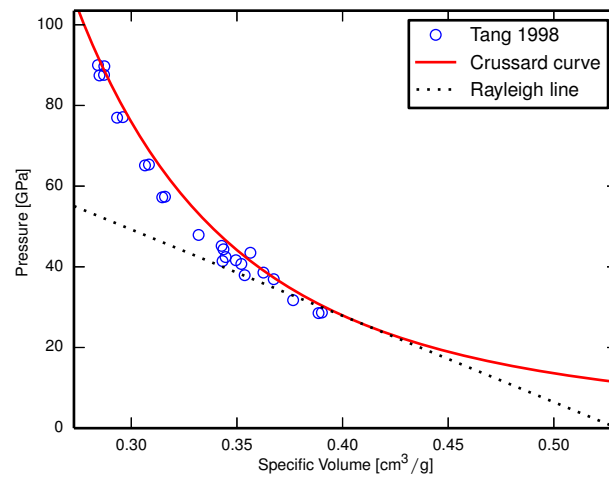


Figure 3.4: The EoS calibrated using the ideal detonation code data is used to calculate the Crussard curve for PBX 9502. It matches the experimental data from Tang et al. [123] reasonably well. The CJ state is at the intersection of the Crussard curve with the Rayleigh line.

Having calibrated the EoS to fit the principal isentrope, it cannot be assumed that the EoS will accurately reproduce the Hugoniot curve for the products (also called the Crussard curve) for overdriven detonations. These states are at higher entropy than the principal isentrope, and thus rely on accurate values for the Grüneisen gamma, as well as an accurate isentrope. Figure 3.4 shows that the EoS for PBX 9502 nevertheless matches the overdriven detonation data from Tang et al. [123] reasonably well. This serves to validate the calibration.

3.4 Reactants

A methodology presented by Davis [35] can be used to construct an EoS for explosive reactants using an isentropic reference curve. An equation for the isentrope pressure is derived using the assumption of a linear D,u relationship (2.26) as is used in the

3 Equations of State

shock Mie-Grüneisen EoS

$$D = a + bu \quad (3.35)$$

$$p_{\text{REF}}(v) = \frac{\rho_0 a^2}{4b} [\exp(4b(1 - v/v_0)) - 1] \quad (3.36)$$

$$e_{\text{REF}}(v) = \left(\frac{a}{4b}\right)^2 (\exp(4b(1 - v/v_0)) - 1) + \frac{\rho_0 a^2}{4b} (v - v_0). \quad (3.37)$$

Note that these expressions for the pressure and energy reference curves do not diverge in the limit of small volumes, but grow sufficiently quickly to avoid potential practical issues. The derivation is reproduced in Appendix B.

Data for the volume and pressure on the Hugoniot curve can be used to calibrate the Grüneisen gamma, Γ . Across a shock wave the entropy increases, and thus states on the Hugoniot curve lie above the reference curve which is an isentrope. This is demonstrated mathematically in Chapter 4. The expression for the Hugoniot curve (4.9),

$$p_H(v) = \frac{\frac{p_{\text{REF}}(v)}{\rho^\Gamma} - e_{\text{REF}}(v) + e_0 + \frac{1}{2}p_0(v_0 - v)}{\frac{1}{\rho^\Gamma} - \frac{1}{2}(v_0 - v)}, \quad (3.38)$$

is justified in Chapter 4. Note, that in practice this calibration process is somewhat ill-conditioned. Small relative errors in pressure measurements for Hugoniot states become more significant when the isentrope pressure is subtracted from it. The fitting process must therefore be carried out with care.

Figure 3.5 shows the isentrope which is used as a reference curve for PBX 9502, and compares it with the Hugoniot curve. The data for the Hugoniot curve informs the choice of parameters for the Grüneisen gamma, since the difference between the curves is a function of the Grüneisen gamma.

The Grüneisen gamma must not diverge or go negative for a thermodynamically stable EoS [110]. To ensure that this is the case, we fit it with the same form that was used for the products EoS,

$$\Gamma(v) = -v \frac{a_T b_T v^{b_T - 1} - c_T d_T \exp(-d_T v)}{a_T v^{b_T} + c_T \exp(-d_T v)}, \quad (3.39)$$

constructed such that the reference temperature is

$$T_{\text{REF}}(v) = a_T v^{b_T} + c_T \exp(-d_T v). \quad (3.40)$$

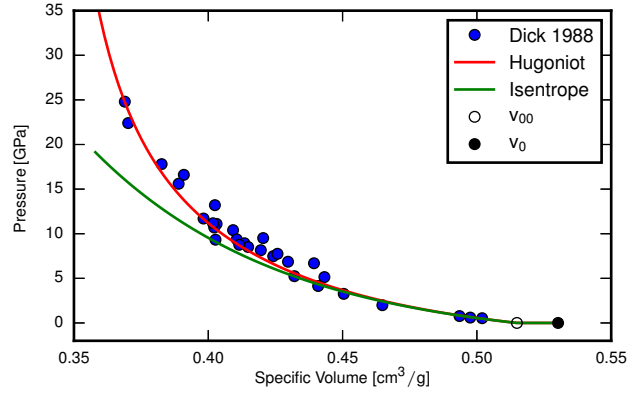


Figure 3.5: The isentrope through the initial state is shown in green. The empty marker indicates the neat specific volume. The porosity model means that the isentrope is flat in between the initial the specific volume and the neat specific volume. For smaller volumes, the difference in pressure between an isentropic compression and following a shock wave is evident.

The fitting procedure restricts the values of the parameters such as to ensure that the EoS behaves normally: a_T , c_T and d_T are set to be positive, while b_T must be negative. The values of the parameters can be further constrained by observing that $-b_T$ is the Grüneisen gamma in the limit of large volumes, where the EoS begins to behave like an ideal gas. As such we expect $-b_T$ to have a value close to the ambient Grüneisen gamma, Γ_0 ,

$$\Gamma_0 = \frac{\beta c^2}{c_p}, \quad (3.41)$$

where β is the ambient coefficient of thermal expansion, c is the ambient frozen sound speed and c_p is the ambient specific heat capacity at constant pressure. Furthermore we choose initial values for the fitting process such that the power law is the dominant term. As a result, the EoS will approach ideal gas-like behaviour in the large volume limit.

3.5 Porosity Model

For porous materials of total specific volume, v_0 , we define the crushing specific volume, v_{00} , to be the specific volume of the matrix material - the material excluding

3 Equations of State

the pores. Compression of the material at low densities requires little work, since it principally leads to closing of the pores, while the density of the matrix material remains largely unchanged. Compression at higher density, on the other hand, leads to compression of the matrix material and requires more work.

The leading shock at the front of a detonation wave compresses the material to volumes significantly smaller than the crushing volume. As such it is adequate to adapt the reference curves of the reactant EoS following the snow plow model [54, 136]. The compressibility of the material at volumes larger than the crushing specific volume is taken to be infinity. In other words, it is assumed that the integral of pressure with respect to volume, which represents the work done compressing the material, is entirely due to the work done for compression beyond the crushing volume. The reference pressure on the isentrope is thus taken to be zero for larger volumes.

It is possible to calibrate the EoS such as to match the volume-pressure experimental data for the Hugoniot curve even without employing any porosity model. However the temperature and D,u relationship is significantly affected by the explosive porosity. Figure 3.6 shows how the temperature of the Hugoniot path is increased if the porosity of the reactants is captured using the method presented here. The explosive modelled is PBX 9502 with an initial density of 1886 kgm^{-3} . The density corresponding to the crushing specific volume [37] is taken to be 1942 kgm^{-3} .

Note that when using the porosity model, the parameters representing the EoS of the solid are chosen such that the EoS of the porous solid is in agreement with the experimental data. In other words as an intermediate result we recover the EoS of the non-porous solid. This equation of state could therefore be used to predict the behaviour of the explosive with a different amount of porosity to that present in the experimental data. However, no data is available with which to validate a predictions made in this way. A similar methodology was applied in order to construct a model for TNT with varying initial density by Erkman and Edwards [41].

It has been noted before that the D,u relationship for PBX 9502 is not linear across all shock velocities [115]. Figure 3.7 shows however that an EoS constructed using a linear fit for the D,u relationship and extended with a porosity model will

3.6 Temperature of Reactants in the Expansion Regime

match the experimental data for moderate as well as strong shocks. Use of the porosity model here means a simple linear fit of the D,u data in the strong shock regime is sufficient to model a wide range of shock strengths. The WSD model [129], on the other hand, uses a nonlinear fit to the D,u data.

Modelling porosity in this way can be problematic in the weak shock regime. The speed of sound in the porous reactants under ambient conditions is unphysical. This is because the compressibility of the porous material is of course finite, but we have assumed it to be infinite. Furthermore the predicted shock velocity is unphysical for weak shocks. Figure 3.7 shows that the Hugoniot curve in the D,u space curves towards zero in the limit of small u . As such the snow plow model must be improved upon if for example ignition is to be modelled.

More complex models of porous materials, such as the $P-\alpha$ model capture the effect of porosity for weak shocks much more accurately [1, 28, 57, 86].

The curved shape of the D,u Hugoniot arising from the snow plow model matches that presented by Lambourn and Handley [72], Menikoff [81], and Schoch [107, Appendix G] where the porosity is modelled explicitly using a multiphase model. In the multiphase model, the matrix material is represented by the shock Mie-Grüneisen EoS which is calibrated using data for the non-porous explosive. The pores are modelled using the ideal gas EoS.

3.6 Temperature of Reactants in the Expansion Regime

The modelling of explosive reactants poses difficulties when states in the expansion regime occur [110]. The data available for calibration relate exclusively to states under compression – which is the regime of interest for modelling shock waves. However states in the expansion regime can occur in the context of direct numerical simulation of detonation waves. The usual location of these states is far behind the detonation wave where the detonation products have rarefied and depressurised to ambient conditions. If the loss of pressure is fast, the explosive may stop burning while a small amount of reactants is still present. The pressure in these cells must be found by applying the usual pressure and temperature closure conditions. The EoS

3 Equations of State

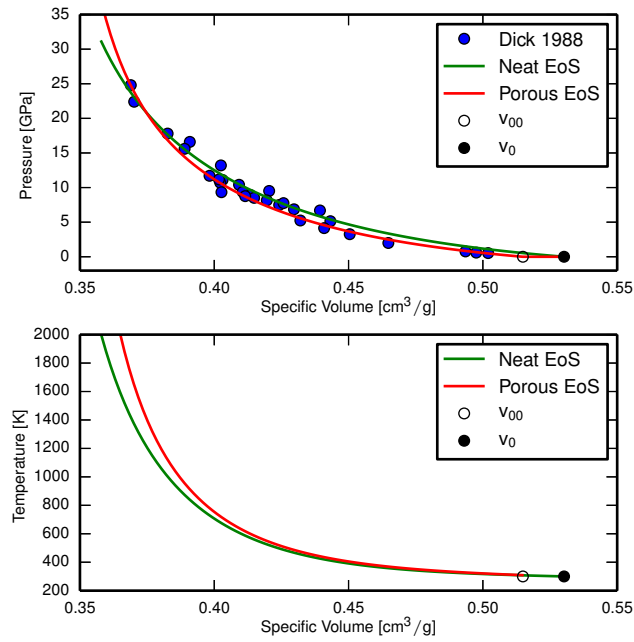


Figure 3.6: Comparison of Hugoniot curves when using the porosity model, and when using the standard EoS for neat materials. The EoS models are compared with experimental data for PBX 9502 [37, 49]. Both EoS models are calibrated using the same volume-pressure Hugoniot data. The predicted temperatures at each volume increase as a result of using the porosity model.

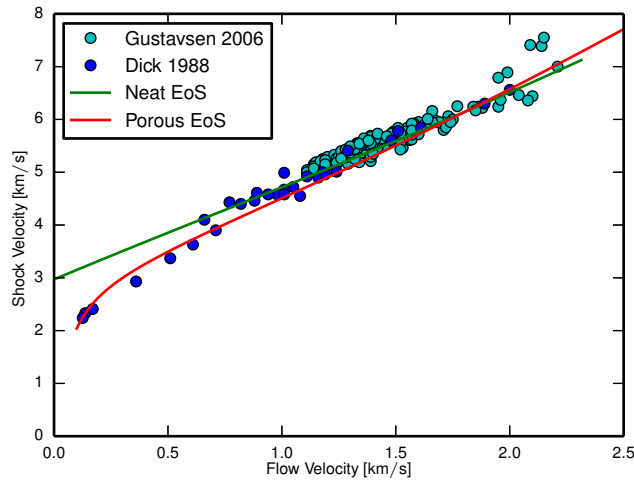


Figure 3.7: The relationship between shock velocity and flow velocity is affected by the porosity model. The linear relationship curves towards zero for weak shocks. In the limit of small shocks, this is clearly not valid, however for moderate shocks this curve fits the data well [37, 49].

3.6 Temperature of Reactants in the Expansion Regime

models must therefore be suitable for finding pressure equilibrium and temperature equilibrium under these conditions, even though the state has much less energy than typical cells in the reaction zone.

Other authors have also encountered this problem. Arienti et al. [4] developed an approach for dealing with large volume states when using the shock Mie-Grüneisen EoS. Menikoff [82] also introduces a work-around specifically for the expansion regime. Since states in the expansion regime will only occur far from the front of the detonation wave, outside the detonation driving zone, the handling of these states will not influence the predicted detonation velocity. It is only required to ensure that the model can be applied robustly across the entire domain of the simulation.

Given the porosity model discussed above, the pressure reference curve is chosen to be exactly zero for volumes above v_{00} . It is clearly not isentropic in this regime, as such an additional term (which increases with volume) must be added to the temperature reference curve for large volumes. This ensures that the coefficient of thermal expansion,

$$\beta = \frac{1}{v} \left(\frac{\partial v}{\partial T} \right)_p, \quad (3.42)$$

is positive for all volumes, including the expansion regime. This is essential for robust solution of the thermal equilibrium equations.

The form of this additional term required by the temperature reference curve in the expansion regime is calculated by considering the difference between the new p_{REF} which has been set to zero for the purpose of modelling the porosity and the original form, \tilde{p}_{REF} ,

$$p_{\text{REF}} - \tilde{p}_{\text{REF}} = \rho \Gamma(v) \frac{T_{\text{REF}} - \tilde{T}_{\text{REF}}}{c_V}. \quad (3.43)$$

3 Equations of State

The summarized equations for the reactant EoS are

$$\tilde{p}_{\text{REF}}(v) = \frac{\rho_0 a^2}{4b} [\exp(4b(1 - v/v_{00})) - 1] \quad (3.44)$$

$$\tilde{e}_{\text{REF}}(v) = \left(\frac{a}{4b}\right)^2 [\exp(4b(1 - v/v_{00})) - 1] + \frac{\rho_0 a^2}{4b}(v - v_{00}) \quad (3.45)$$

$$\tilde{T}_{\text{REF}}(v) = a_T v^{b_T} + c_T \exp(-d_T v) \quad (3.46)$$

$$\Gamma(v) = -v \frac{a_T b_T v^{b_T-1} - c_T d_T \exp(-d_T v)}{a_T v^{b_T} + c_T \exp(-d_T v)} \quad (3.47)$$

$$\text{for } v < v_{00} \begin{cases} p_{\text{REF}}(v) = \tilde{p}_{\text{REF}}(v) \\ e_{\text{REF}}(v) = \tilde{e}_{\text{REF}}(v) \\ T_{\text{REF}}(v) = \tilde{T}_{\text{REF}}(v) \end{cases} \quad (3.48)$$

$$\text{for } v \geq v_{00} \begin{cases} p_{\text{REF}}(v) = 0 \\ e_{\text{REF}}(v) = 0 \\ T_{\text{REF}}(v) = \tilde{T}_{\text{REF}}(v) - \frac{\tilde{p}_{\text{REF}}}{\rho \Gamma(v) c_V} \end{cases} \quad (3.49)$$

The equation for the Grüneisen gamma is the same as for the products EoS (3.34).

Note that volume-pressure data for the Hugoniot curve are required to calibrate for the temperature reference curve of the EoS above. For the emulsion explosive EM120D, these data are not available. We therefore use the Hugoniot curve as calculated by Schoch [107], where the shock response of the porous material is modelled using a multiphase model. The parameters for the reactants of both explosives are presented in Table 3.3.

3.7 Closure Rules for Coexistence of Materials

Modelling of non-ideal detonation waves requires resolution of the DDZ (detonation driving zone) – only cells in this zone play a role in determining the velocity of detonation [44, 75]. This zone includes part of the reaction zone, where the explosive consists of both reactants and products. Since the reactants and products are modelled using independent EoS models, the coexistence of both materials in the reaction zone requires careful attention.

We aim to construct an equation of state of the form

$$p = p(v, e, \lambda) \quad (3.50)$$

	PBX 9502	EM120D
a	2970 ms ⁻¹	2170 ms ⁻¹
b	1.81	1.82
a_T	5.141	2.073
b_T	-0.5371	-0.6867
c_T	258020 K	22805 K
d_T	19960 kgm ⁻³	10660 kgm ⁻³
ρ_{00}	1942 kgm ⁻³	1400 kgm ⁻³
ρ_0	1886 kgm ⁻³	1210 kgm ⁻³
c_V	1000 JK ⁻¹ kg ⁻¹	1000 JK ⁻¹ kg ⁻¹

Table 3.3: Parameters for the reactant EoS models for PBX 9502 and EM120D.

with which to evaluate the pressure in the explosive. If the mass fraction variable, λ , is either zero or one, then this equation of state must yield the same results as would be obtained using the equation of state for the reactants or products respectively. In the case where the explosive is partially burnt, and both reactants and products coexist, the pressure must depend on both equations of state. It is also necessary to invert the equation of state, such that the energy can be evaluated for a known pressure.

Energy and volume are extensive variables and can be explicitly expressed in terms of the energy and volume of the constituents of the mixture. The mixing rules for the two-material mixture are presented here along with general equations of state of Mie-Grüneisen form

$$v = \lambda v_\alpha + (1 - \lambda)v_\beta \quad (3.51)$$

$$e = \lambda e_\alpha + (1 - \lambda)e_\beta \quad (3.52)$$

$$p_k - p_{k,\text{REF}}(v_k) = \rho_k \Gamma_k(v_k)(e_k - e_{k,\text{REF}}(v_k)) \quad \text{for } k \in \{\alpha, \beta\}. \quad (3.53)$$

The subscripts distinguish the reactants, α , from the products, β . Variables without a subscript refer to the properties of the two-material mixture, which is collectively referred to as the explosive. Equation (3.51) expresses the explosive specific volume, v , as a combination of the material specific volumes, v_α and v_β . This equation is an average weighted by the mass fraction, λ . The derivation of

3 Equations of State

this relation is explained fully in Appendix C. The specific internal energy of the mixture, e , of the three-material system (3.52) is defined using the sum of the specific internal energies contributions from each of the reactants and products, e_α and e_β , weighted by the mass fraction. Note that to calculate the specific internal energy from the total specific energy, E , we can simply use

$$e = E - \frac{1}{2}u^2, \quad (3.54)$$

on the assumption that the materials have equal flow velocity, u .

Coexisting materials will reach pressure equilibrium and temperature equilibrium given sufficient time. The time scale on which pressure equilibrium is reached is very fast, typically taken to be less than $1\mu s$. The assumption of pressure equilibrium is applied almost universally in the literature. The temperature equilibrium time scale, however, may be of order a thousand times as long and is not necessarily fast in comparison to the time scale associated with the detonation wave. Davis [137, chap. 3] and Stewart et al. [121] discuss the merits of various closure laws that could be used in place of temperature equilibrium. Matignon et al. [79] discuss various such laws and their effect on detonation shock dynamics.

The pressure equilibrium closure condition can be used with the energy mixture rule (3.52) and the equations of state to express the pressure, p , as

$$e = p \left(\frac{\lambda}{\rho_\alpha \Gamma_\alpha(v_\alpha)} + \frac{1-\lambda}{\rho_\beta \Gamma_\beta(v_\beta)} \right) + \lambda \text{REF}_\alpha + (1-\lambda) \text{REF}_\beta, \quad (3.55)$$

where

$$\text{REF}_k = \frac{-p_{k,\text{REF}}(v_k)}{\rho_k \Gamma_k(v_k)} + e_{k,\text{REF}}(v_k) \quad \text{for } k \in \{1, \alpha, \beta\}.$$

The unknowns in this equation are p , v_α and v_β . The mixture law (3.51) reduces the number of degrees of freedom to two. One additional closure condition is still required.

Implementation of a temperature equilibrium condition is achieved by using the difference in temperatures as an objective function for a nonlinear root-finding algorithm,

$$f(v_\alpha) = T_\alpha(p, v_\alpha) - T_\beta(p, v_\beta), \quad (3.56)$$

where

$$v_\beta = \frac{v - \lambda v_\alpha}{1 - \lambda}. \quad (3.57)$$

The temperatures are calculated using

$$T_k(v_k, p) = T_{k,\text{REF}}(v_k) + \frac{p - p_{k,\text{REF}}(v_k)}{\rho_k \Gamma_k(v_k) c_{v,k}}, \quad (3.58)$$

and the pressure is calculated using (3.55).

To invert the equation of state (3.50) and calculate the energy when the pressure is known, we can solve the temperature equilibrium equation (3.56) directly. Equation (3.55) is only required to calculate the energy once the root has been found.

If the mixture consists of mainly products ($\lambda < 0.5$) then v_α is taken as the independent variable, and v_β is calculated using (3.57), while for mixtures with mainly reactants ($\lambda > 0.5$), v_β is chosen as the independent variable. This is necessary because evaluating v_β using (3.57) is ill-conditioned for λ close to one, since it involves subtracting two numbers of almost equal magnitude.

An alternative to temperature equilibrium is the heat isolation condition, where it is assumed that no heat transfer occurs between the reactants and products. Usually this is implemented in practice by imposing a fixed entropy for the shocked reactants. Of course the entropy is expected to change as a result of passing shock waves. Implementing such a closure condition therefore requires special handling of the state in the presence of shock waves, or a set up in which it can be assumed that the explosive is not shocked once it has begun to react. The objective function can be defined as

$$f(v_\alpha) = p_\alpha(v_\alpha, e_\alpha(v_\alpha, S(v_0, e_0))) - p_\beta(v_\beta, e_\beta) \quad (3.59)$$

where v_β and e_β are defined by the mixture rules (3.51) and (3.52), and e_α is calculated using equation (3.18). The reference values v_0 and e_0 are used to determine the entropy of the reactants. For isentropic flow, these values can be advected with the flow. In the presence of shocks however, these values must be updated to reflect the change in entropy.

Inversion of an equation of state defined using this closure condition can be done by solving

$$f(v_\alpha) = p - p_\alpha(v_\alpha, e_\alpha(v_\alpha, S(v_0, e_0))), \quad (3.60)$$

3 Equations of State

where p_α represents the pressure as calculated using the equation of state of the reactants, while p is the known pressure. Finally the energy is calculated using equation (3.55).

3.8 Sound speed in the Mixture of Materials

A method is also required to evaluate the speed of sound in the mixture of materials. The form used for the speed of sound in a single material (3.10), is inconvenient to apply in this case. This is because the pressure is only known implicitly – we can evaluate the pressure, but cannot express the pressure explicitly.

It is more convenient to derive the speed of sound using the following expression for an infinitesimal change in energy on an isentrope.

$$de = \left(\frac{\partial e}{\partial p}\right)_v dp + \left(\frac{\partial e}{\partial v}\right)_p dv \quad (3.61)$$

$$-p = \left(\frac{\partial e}{\partial v}\right)_S = \left(\frac{\partial e}{\partial p}\right)_v \left(\frac{\partial p}{\partial v}\right)_S + \left(\frac{\partial e}{\partial v}\right)_p \quad (3.62)$$

$$\Rightarrow c^2 = -v^2 \left(\frac{\partial p}{\partial v}\right)_S = v^2 \frac{p + \left(\frac{\partial e}{\partial v}\right)_p}{\left(\frac{\partial e}{\partial p}\right)_v} \quad (3.63)$$

The derivatives of the specific internal energy can be evaluated using the mixture rule for the energy (3.52)

$$e = \lambda e_\alpha + (1 - \lambda)e_\beta \quad (3.64)$$

$$\left(\frac{\partial e}{\partial p}\right)_v = \lambda \frac{\partial e_\alpha}{\partial p} + (1 - \lambda) \frac{\partial e_\beta}{\partial p} \quad (3.65)$$

$$\left(\frac{\partial e}{\partial v}\right)_p = \lambda \frac{\partial e_\alpha}{\partial v_\alpha} \frac{\partial v_\alpha}{\partial v} + (1 - \lambda) \frac{\partial e_\beta}{\partial v_\beta} \frac{\partial v_\beta}{\partial v} \quad (3.66)$$

$$= \frac{\partial e_\alpha}{\partial v_\alpha} + \frac{\partial e_\beta}{\partial v_\beta} \quad (3.67)$$

3.9 Approach for robust solution of the root-finding problem

Solving nonlinear equations like those introduced here can be problematic given the limited applicability of the EoS models. It cannot be guaranteed in general that a solution will exist. Furthermore, care should be taken, in view of the fact that mathematical solutions may exist which are physically invalid. In particular the negative density domain may have mathematical solutions which are physically meaningless. Depending on the EoS models, regions of negative temperature or negative pressure can also cause the root-finding algorithm to fail.

The solution is found by applying a numerical nonlinear root-finding method. This is done using a modified version of Brent's method. Brent's method uses the secant method principally, but resorts to the bisection method under certain conditions, thus guaranteeing convergence provided a root exists. We modify Brent's method slightly in order to use the Newton-Raphson method in place of the secant method.

Initially a volume range is defined in which to search for the solution. The objective function is evaluated along with its derivative in order to carry out an iteration of the Newton-Raphson method,

$$x_{n+1} = x_n - \frac{f(x_n)}{f'(x_n)}. \quad (3.68)$$

If the new value for the independent variable, x_{n+1} , is not inside the search space, we instead resort to the bisection method. Note that if an iteration of the Newton-Raphson method is successful, the function evaluation is also used to update the search space, thereby continuing to use the bisection method in parallel. It is also possible to take advantage of thermodynamic understanding of the objective function. For example, when solving equation (3.56), we can deduce that in the limit of large v_α , we have $T_\alpha > T_\beta$ and therefore f will be large and positive. Similarly for small v_α , we expect f to be large and negative. As such, the derivative of the objective function is expected to be positive over the physically valid volume range. This information can be used to further improve the robustness of the root-finding algorithm.

3 Equations of State

In practice it was found that the great majority of the iterations of the method proceed according to the Newton-Raphson method. The computationally expensive evaluation of the derivative required by Newton-Raphson (which would not be necessary using standard Brent's method) is therefore worthwhile, given that the Newton-Raphson method converges quadratically. This is faster than the usual form of Brent's method which utilises inverse quadratic interpolation, the order of convergence of which is ≈ 1.839 .

Note that the computational cost of evaluating the derivative of equation (3.56) can be greatly reduced by evaluating the function and its derivative together, thus eliminating multiple superfluous evaluations of the various reference functions.

The first consideration when establishing a suitable search domain should be the requirement that the specific volume of each material must be positive. This restriction can be expressed as

$$\lambda v_\alpha < v \quad \text{or} \quad (1 - \lambda)v_\beta < v. \quad (3.69)$$

In other words the volume occupied by material α cannot be greater than the total volume occupied by the mixture. If v_α violates this restriction the corresponding value for v_β will be negative. This is easily understood when it is considered that equation (3.51) is an addition of volumes, each of which must necessarily be positive.

This is the fundamental reason that the set of equations is not guaranteed to have solutions. If equation (3.56) is considered on its own (assuming the pressure has some fixed value) without any restrictions on the specific volumes, then it is guaranteed to have solutions for well behaved EoS models.

As the density of a material approaches zero, the temperature will also approach zero. In doing so the density of the other material will increase, and its temperature will accordingly increase. At some point these temperature curves are bound to cross; this is the point of temperature equilibrium. However this crossing point may be in the region that has been excluded by the restrictions on density (3.69).

It is thus not realistic to guarantee that the problem will have solutions for an arbitrary state. We can however ensure that the equations will have a solution for all realizable states by ensuring the thermodynamically consistent behaviour of the EoS models in the limits of large and small volumes.

3.9 Approach for robust solution of the root-finding problem

Firstly, the Grüneisen gamma must be positive and bounded for all possible volumes accessed by the simulation. The form of the fitting function chosen for T_{REF} ensures that this is the case as shown in Figure 3.1 which demonstrates that the limiting behaviour of the Grüneisen gamma is appropriate for large volumes as well as large densities.

Secondly, the temperature must increase monotonically with volume at any fixed pressure. In other words the coefficient of thermal expansion

$$\beta = \left(\frac{\partial T}{\partial v} \right)_p \quad (3.70)$$

must be positive. This can be verified for given EoS parameters before running the simulation. For the product EoS the isobars were found to increase monotonically across all volumes, while for the reactants the isobars were found to have a minimum, but at sufficiently low volumes to play no role in the simulation. To ensure that anomalous roots at these unphysically small volumes do not appear, smaller volumes are explicitly excluded from the search domain.

In this work we (somewhat arbitrarily) restrict the domain for the specific volume using the state with a pressure of 1.5 times the von Neumann pressure and zero temperature. This is the volume, $v_{k,\text{min}}$, such that

$$0 = T_{k,\text{REF}}(v_{k,\text{min}}) + \frac{1.5p_{\text{vN}} - p_{k,\text{REF}}(v_{k,\text{min}})}{\rho_k \Gamma_k(v_{k,\text{min}}) c_{v,k}} \quad (3.71)$$

for $k \in \{\alpha, \beta\}$. This choice was found to eliminate any unphysical behaviour in the small volume limit, while ensuring that the physical solution was never wrongly excluded from the search domain. No further explicit limitation on the maximum volume is required, since this is already controlled by the physical limits imposed by (3.69). Furthermore the equations of state are designed such that in the limit of large volumes, the behaviour approaches that expected of an ideal gas.

Using a minimum volume for both equations of state also means that the physical limits do not have to be considered explicitly. The maximum volume allowed for v_α is such that material the specific volume for material β is $v_{\beta,\text{min}}$, in which case v_α must necessarily satisfy the physical maximum (3.69). The search domain is thus

$$v_{\alpha,\text{min}} \leq v_\alpha \leq \frac{v - (1 - \lambda)v_{\beta,\text{min}}}{\lambda}. \quad (3.72)$$

3 Equations of State

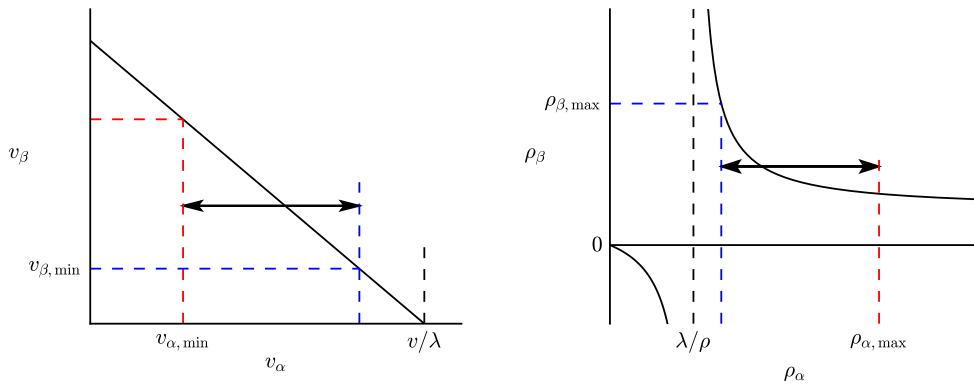


Figure 3.8: The dashed lines indicate where the restrictions on the domain are applied. The blue dashed lines indicate the limitation imposed by the equation of state for material β . The red dashed lines are the equivalent for material α . The black arrow indicates the region of the domain that will yield physical solutions. The left hand plot uses specific volumes while the right plot is in terms of density.

Figure 3.8 illustrates the search domain using both specific volume as well as density. The black dashed lines in figure 3.8 indicate the physical limit which will exist irrespective of the validity of the equations of state that are used. These restrictions on the search domain were consistently found to be sufficient to ensure that exactly one root of the thermal equilibrium existed within the domain to be searched.

3.10 Conclusions

In this chapter, equations of state have been developed for modelling the reactants and products of explosives. The focus throughout has been on ensuring that the resulting forms can be applied in practice to a wide range of explosives. This means the calibration process to determine parameters must only rely on readily available experimental data. This has been addressed, firstly, by adopting a method which infers information about the temperature in the shocked explosive directly from Hugoniot data. Explicit inclusion of a porosity model, means the method can also be applied to porous explosives. Secondly the equations of state must be suitable

for both ideal and non-ideal explosives. This is addressed through the use of the ideal detonation code to calibrate a modified JWL equation of state, which permits more accurate values for the Grüneisen gamma than is possible with the standard JWL form.

Finally, the mathematical forms are chosen with the aim of ensuring that a thermal equilibrium closure law can be implemented in a hydrocode and used to run simulations robustly in practice.

The reactant EoS was developed following Davis [35] and is calibrated using experimental data for the Hugoniot curve, thus reproducing the desired shock-response behaviour. The temperatures are derived solely from the Hugoniot data and the thermodynamics of the explosive in ambient conditions, since there is very limited thermal data available for explosive reactants. The EoS explicitly accounts for the influence of porosity on the post-shock temperatures using the snow plow model.

The product EoS is an adaptation of the JWL EoS which accommodates evaluation of the temperature. The reference curves are calibrated to data for the principal isentrope from the ideal detonation code *IDeX* [21]. The ideal detonation code requires the chemical composition of the explosive as well as the energy content of the explosive in comparison to the detonation products. Note that if the energy content is unknown, then an experimental measurement of the ideal velocity of detonation can be used instead.

Use of the ideal detonation code not only permits the calculation of temperatures but more accurate values for a volume-dependent Grüneisen gamma. This is important, since in non-ideal detonation waves the state of the products is expected to lie below the reference curve of the EoS. Away from the reference curve, the validity of the EoS relies on an accurate expression for the Grüneisen gamma.

4 ZND Waves

4.1 Introduction

In the previous chapter we discussed how to construct and calibrate equations of state suitable for faithful modelling of explosives. The rationale for this was based on the structure of ZND waves as predicted by the one dimensional ZND theory and the information which can be obtained from experimental measurements. In this chapter we will assume that the equations of state for both the reactants and products are known. We present a general methodology to calculate the structure of the ZND wave following Lee [75]. Furthermore, a method is presented to numerically calculate the structure of the reaction zone given a reaction rate model. The methods presented in this chapter will be applied to calculate the ZND structure of the explosives studied in this thesis directly. In Chapter 5 the numerical results will be compared to the results of this chapter in order to validate the numerical methods.

4.2 Inert Shock Waves

The ZND theory is an extension of the CJ theory, which in turn is derived through application of the Rankine-Hugoniot conditions. The Rankine-Hugoniot conditions are an expression of the fact that the conservation of mass, momentum and energy apply across a discontinuity in the flow.

It is assumed that the jump discontinuity (or shock) is steady, which is to say that the discontinuity propagates at a steady velocity, and the states before and after the discontinuity are constant. For each conservation law the flux flowing into

4 ZND Waves

the shock from the unshocked fluid must equal the flux leaving the shock on the other side.

Since only relative velocities are significant, the velocity of the unshocked fluid can be arbitrarily set to zero without loss of generality. The unshocked fluid is taken to have density ρ_0 and pressure p_0 . The density, velocity and pressure of the shocked fluid are labelled ρ , u and p . The speed of propagation of the shock itself is D and the specific internal energies for the unshocked and shocked fluid are e_0 and e respectively. The conservation of mass implies that

$$\rho(D - u) = \rho_0 D \quad (4.1)$$

since a mass of $\rho_0 D$ is passed by the shock per unit time. Momentum conservation leads to

$$p - p_0 = u \rho_0 D, \quad (4.2)$$

where we have equated the force across the shock wave (the pressure difference) with the momentum gained by the fluid through which the shock has passed. Finally the work done by the force in pushing the shock, pu , must equal the change in energy. As the shock passes, the fluid gains both kinetic and internal energy,

$$pu = \left(\frac{1}{2} u^2 + e - e_0 \right) \rho_0 D. \quad (4.3)$$

We wish to characterise the state behind the shock in terms of the initial state and the shock's propagation speed. Eliminating u from equations (4.1) and (4.2) gives the Rayleigh line:

$$p - p_0 = \rho_0^2 D^2 (v_0 - v) \quad (4.4)$$

where v_0 and v represent the specific volume before and after the shock respectively. When plotted in pressure volume space, the Rayleigh line is a straight line passing through the initial state p_0, v_0 and the final state p, v . The line has a gradient which is proportional to the shock velocity, D .

Eliminating D in place of u yields the hyperbola,

$$u^2 = (p - p_0)(v_0 - v), \quad (4.5)$$

which has a unique intersection with the Rayleigh line. In other words, D and u are sufficient to fully specify the state of the shocked fluid.

The position of the final state can be calculated as the intersection between the Rayleigh line and the Hugoniot curve, which is derived by eliminating D and u from equations (4.1) to (4.3),

$$pu^2 = \left(\frac{1}{2}u^2 + e - e_0\right)(p - p_0) \quad (4.6)$$

$$\Rightarrow e - e_0 = \frac{1}{2}(p + p_0)(v_0 - v). \quad (4.7)$$

Using an equation of state of Mie-Grüneisen form,

$$p - p_{\text{REF}}(v) = \rho\Gamma(e - e_{\text{REF}}(v)), \quad (4.8)$$

the post-shock pressure, p_H , can be expressed as a function of the post-shock specific volume,

$$p_H(v) = \frac{\frac{p_{\text{REF}}(v)}{\rho\Gamma} - e_{\text{REF}}(v) + e_0 + \frac{1}{2}p_0(v_0 - v)}{\frac{1}{\rho\Gamma} - \frac{1}{2}(v_0 - v)}. \quad (4.9)$$

Notice that the Rayleigh line is a representation of the path of the thermodynamic state as the shock passes, because it relates to the mechanical equilibrium of the fluid. The Hugoniot curve, on the other hand, uses the conservation of energy which is only expressed in terms of the initial and final states. As a result the Hugoniot curve does not represent the path, but the locus of all possible final states.

Weak shock waves, associated with a small change in specific volume, are nothing but isentropic sound waves. Stronger shock waves are associated with an increase in entropy and propagate faster than the speed of sound in the unshocked material in front of the shock. For shock waves with an associated decrease in the specific volume from v_0 to v , the increase in entropy across the shock front is $\mathcal{O}((v_0 - v)^3)$.

To demonstrate this we introduce a Taylor expansion of the pressure on an isentrope, around a reference state (v_0, p_0) ,

$$p_S(v) = p_0 + \left(\frac{\partial p}{\partial v}\right)_S (v - v_0) + \frac{1}{2} \left(\frac{\partial^2 p}{\partial v^2}\right)_S (v - v_0)^2 + \mathcal{O}((v - v_0)^3). \quad (4.10)$$

4 ZND Waves

Assuming that the energy at the reference state is e_0 , the energy on the isentrope is given by

$$\begin{aligned} e_S &= e_0 + \int_{v_0}^v -p \, dv \\ &= e_0 + p_0(v_0 - v) - \frac{1}{2} \left(\frac{\partial p}{\partial v} \right)_S (v_0 - v)^2 + \frac{1}{6} \left(\frac{\partial^2 p}{\partial v^2} \right)_S (v_0 - v)^3 + \mathcal{O}((v_0 - v)^4). \end{aligned} \quad (4.11)$$

On the other hand, using equation (4.7), the energy on the Hugoniot curve is related to pressure by

$$\begin{aligned} e_H &= e_0 + \frac{1}{2}(p_H + p_0)(v_0 - v) \\ &= e_0 + p_0(v_0 - v) - \frac{1}{2} \frac{\partial p_H}{\partial v} (v_0 - v)^2 + \frac{1}{4} \frac{\partial^2 p_H}{\partial v^2} (v_0 - v)^3 + \mathcal{O}((v_0 - v)^4). \end{aligned} \quad (4.12)$$

The quadratic terms in the expansions are equal in the limit as $v \rightarrow v_0$, since

$$\left(\frac{\partial p}{\partial v} \right)_S = \left(\frac{\partial p}{\partial v} \right)_e + \left(\frac{\partial p}{\partial e} \right)_v \left(\frac{\partial e}{\partial v} \right)_S \quad (4.13)$$

$$= \left(\frac{\partial p}{\partial v} \right)_e - \rho \Gamma p, \quad (4.14)$$

while, using equation (4.12),

$$\frac{\partial p_H}{\partial v} = \left(\frac{\partial p}{\partial v} \right)_e + \left(\frac{\partial p}{\partial e} \right)_v \frac{\partial e_H}{\partial v} \quad (4.15)$$

$$= \left(\frac{\partial p}{\partial v} \right)_e - \rho \Gamma p_0, \quad (4.16)$$

and at $v = v_0$, $p = p_0$ by definition. It follows that

$$e_H - e_S = \mathcal{O}((v_0 - v)^3). \quad (4.17)$$

Using the equation of state itself, this in turn implies that

$$p_H - p_S = \mathcal{O}((v_0 - v)^3) \quad (4.18)$$

$$\Rightarrow \left(\frac{\partial^2 p}{\partial v^2} \right)_S = \frac{\partial^2 p_H}{\partial v^2}. \quad (4.19)$$

Finally, subtracting equation (4.11) from equation (4.12), the increase in entropy can be quantified as

$$e_H - e_S = \frac{1}{12} \left(\frac{\partial^2 p}{\partial v^2} \right)_S (v_0 - v)^3 + \mathcal{O}((v_0 - v)^4), \quad (4.20)$$

from which it is apparent that the convexity of the isentrope is sufficient to guarantee that weak shock waves will be associated with an increase in entropy.

Furthermore, the speed of a shock wave can be expressed as

$$D^2 = v_0^2 \frac{p - p_0}{v_0 - v} \quad (4.21)$$

$$= v_0^2 \frac{p_0 + \left(\frac{\partial p}{\partial v}\right)_S (v_0 - v) - p_0}{v_0 - v} + \mathcal{O}(v_0 - v) \quad (4.22)$$

$$= c^2 + \mathcal{O}(v_0 - v), \quad (4.23)$$

where c is the sound speed at the reference state, (v_0, p_0) .

4.3 Reactive Shock Waves

In the case of a detonation wave, additional energy is released by the combustion of the explosive. The Hugoniot equation (4.7) must be adjusted to account for this additional energy. In practice this is done implicitly, by using independent equations of state to describe the state in the reactants and products. The equation of state of the products is used for the final state at the back of the wave. The initial internal energy, however, is calculated using the equation of state of the reactants. The Crussard curve is the name given to shock locus after the inclusion of the heat of combustion. This is the equivalent of the Hugoniot curve for inert shock waves. The Crussard curve is sometimes described as the Hugoniot curve of the products.

The Crussard curve is a function of the initial specific internal energy, $e_{\alpha,0}$, which is calculated using the equation of state of the reactants. However, since the initial specific internal energy is usually very small in comparison to that on the Crussard curve, this dependence is not very strong. The pressure on the Crussard curve, p_C , is primarily dependent on the equation of state of the products,

$$p_C(v) = \frac{\frac{p_{\beta,\text{REF}}(v)}{\rho_{\beta}\Gamma_{\beta}} - e_{\beta,\text{REF}}(v) + e_{\alpha,0} + \frac{1}{2}p_0(v_0 - v)}{\frac{1}{\rho_{\beta}\Gamma_{\beta}} - \frac{1}{2}(v_0 - v)}. \quad (4.24)$$

The reference functions of the products equation of state are those denoted with the subscript β . Faithful reproduction of the final state at the back of the ZND wave

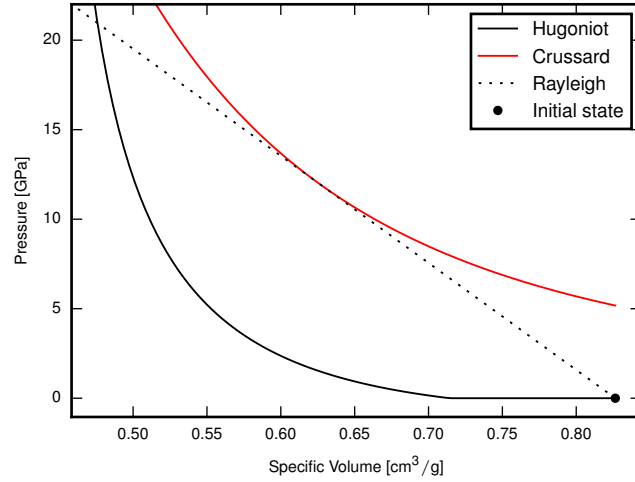


Figure 4.1: The Hugoniot curve and Crussard curve are shown in pressure volume space. The dotted line is the Rayleigh line, which is tangent to the Crussard curve. This corresponds to the slowest wave which intersects the Crussard curve. The intersection of the Rayleigh line with the Crussard curve is the CJ state. The von Neumann state is at the intersection of the Rayleigh line with the Hugoniot curve. This plot uses the equations of state for EM120D as presented in Chapter 3.

(also known as the CJ state) is thus primarily reliant on the products equation of state.

Just as the Hugoniot curve is a locus of possible final states following the passing of a shock wave, the Crussard curve is similarly a locus of possible final states following a detonation wave. Empirically, a self-sustaining detonation wave will propagate at the slowest velocity which is consistent with a final state on the Crussard curve. This is known as Chapman’s minimum velocity criterion. The justification for this choice was initially based on empirical observations. In the context of Figure 4.1, equation (4.4) tells us that the slowest wave is the wave with the shallowest gradient (negative gradient closest to zero) in pressure volume space. Chapman’s criterion is thus equivalent to the statement that the Rayleigh line corresponding to a self-sustaining detonation is a tangent to the Crussard curve. The intersection point is the point at the back of the detonation wave, known as the CJ state.

As an aside, note that in this chapter we are only concerned with ZND waves, which occur in ideal explosives or one dimensional geometries. Non-ideal detonations in multi-dimensional geometries, where energy is lost to the environment, will propagate at speeds slower than those predicted using the ZND model.

To calculate the CJ state, we apply a nonlinear root finding method to calculate the CJ volume, v_{CJ} , which satisfies an equation relating the gradient of the Crussard curve with the initial conditions,

$$\frac{\partial}{\partial v} p_C(v_{CJ}) = \frac{p_0 - p_C(v_{CJ})}{v_0 - v_{CJ}}. \quad (4.25)$$

The CJ state can be used to calculate the velocity of the detonation wave, D_{CJ} , using the equation of the Rayleigh line (4.4).

One possible justification for Chapman's criterion is the principle of minimum entropy [71]. The entropy increase associated with a shock wave is a strictly monotonically increasing function of the shock speed. The slowest wave is therefore the wave with the smallest associated increase in entropy. This implies that the Rayleigh line for a self-sustaining detonation is not only tangent to the Crussard curve, but also tangent to an isentrope at the same point.

Jouguet [65], on the other hand, proposed that the state at the back of the detonation must be a sonic point. This choice is motivated by the experimental observation that the dynamics of the flow downstream of the detonation wave does not have any effect on the detonation wave itself.

We demonstrate here, with reference to Fickett and Davis [44] that these choices are equivalent. We show that if an isentrope of the products is tangent to the Rayleigh line at the CJ state then this state is indeed a sonic point. To show that the CJ state is a sonic point we need to show that the velocity, u , plus the sound speed, c , is equal to the propagation velocity of the wave, D ,

$$u + c = D. \quad (4.26)$$

From the Rankine-Hugoniot conditions we have that

$$D^2 = -v_0^2 \frac{p - p_0}{v - v_0} \quad (4.27)$$

$$u^2 = -(p - p_0)(v - v_0) \quad (4.28)$$

4 ZND Waves

where v and p refer to the CJ state and v_0, p_0 refer to the initial conditions. Using the assumption that the isentrope is tangent to the Rayleigh line, the speed of sound can be related to the gradient of the Rayleigh line,

$$c^2 = \left(\frac{\partial p}{\partial \rho} \right)_S = -v^2 \left(\frac{\partial p}{\partial v} \right)_S = -v^2 \frac{p - p_0}{v - v_0}. \quad (4.29)$$

$$\Rightarrow (u + c)^2 = u^2 + c^2 + 2uc \quad (4.30)$$

$$\begin{aligned} &= -(p - p_0)(v - v_0) - v^2 \frac{p - p_0}{v - v_0} + 2\sqrt{v^2 \frac{p - p_0}{v - v_0} (p - p_0)(v - v_0)} \\ &= \frac{p - p_0}{v - v_0} [-(v - v_0)^2 - v^2 + 2v(v - v_0)] \\ &= -v_0^2 \frac{p - p_0}{v - v_0} \\ &= D^2 \end{aligned}$$

$$\Rightarrow u + c = D \quad (4.31)$$

Chapman's criterion of minimum velocity is thus equivalent to Jouguet's sonic criterion, which states that the state at the back of the detonation wave is a sonic point.

4.4 The Reaction Zone

Having established the pressure and volume at the CJ state at the back of the detonation wave, we also know the propagation speed of the wave. We can use this information to calculate the structure of the wave. The rise time of the shock wave propagating into the explosive is much shorter than the time scale of the combustion. The state immediately following the shock wave, but before the explosive has begun to burn is known as the von Neumann spike, and is the state with the highest pressure and density in the wave. This state is on the Hugoniot curve for the inert reactants, and can be determined using the shock wave speed, D_{CJ} , and the equation of state of the reactants. The specific volume at the von Neumann spike, v_{vN} , will be such that

$$\rho_0^2 D_{CJ}^2 = \frac{p_H(v_{vN}) - p_0}{v_0 - v_{vN}}, \quad (4.32)$$

where p_H is the Hugoniot curve of the inert reactants.

Between the von Neumann state and the CJ state is the reaction zone, where the explosive is partially burnt. Mechanical equilibrium implies that states in the reaction zone lie on the Rayleigh line in between the von Neumann spike and the CJ state. Furthermore, each state in the reaction zone will lie on a Hugoniot curve corresponding to the amount of energy which has been released by the chemical reaction up to that point. For each value of λ , there is a corresponding Hugoniot curve which lies between the Hugoniot of the inert reactants and the Crussard curve.

Using equations of state of Mie-Grüneisen form for the reactants (with subscript α) and the products (with subscript β), the specific internal energy for a mixture of reactants and products in pressure equilibrium is

$$e = \lambda e_\alpha(v_\alpha, p) + (1 - \lambda)e_\beta(v_\beta, p) \quad (4.33)$$

$$= \lambda \text{REF}_\alpha + (1 - \lambda) \text{REF}_\beta + p \left(\frac{\lambda}{\rho_\alpha \Gamma_\alpha(v_\alpha)} + \frac{1 - \lambda}{\rho_\beta \Gamma_\beta(v_\beta)} \right) \quad (4.34)$$

where

$$\text{REF}_k = \frac{-p_{k,\text{REF}}(v_k)}{\rho_k \Gamma_k(v_k)} + e_{k,\text{REF}}(v_k) \quad \text{for } k \in \{\alpha, \beta\}.$$

This can be substituted into the Hugoniot equation

$$e - e_0 = \frac{1}{2}(p + p_0)(v_0 - v), \quad (4.35)$$

to yield

$$p_H(v, \lambda) = \frac{e_0 - \lambda \text{REF}_\alpha - (1 - \lambda) \text{REF}_\beta + \frac{1}{2}p_0(v_0 - v)}{\frac{\lambda}{\rho_\alpha \Gamma_\alpha(v_\alpha)} + \frac{1 - \lambda}{\rho_\beta \Gamma_\beta(v_\beta)} - \frac{1}{2}(v_0 - v)}. \quad (4.36)$$

This is the Hugoniot curve corresponding to a partial burn of the explosive. For each specific volume, the pressure on this Hugoniot curve lies between the Hugoniot curve of the inert reactants and the Crussard curve corresponding to a complete reaction. Each of these Hugoniot curves will necessarily intersect the Rayleigh line somewhere in between the von Neumann state and the CJ state. The partial burn Hugoniot curves for EM120D are plotted in Figure 4.2.

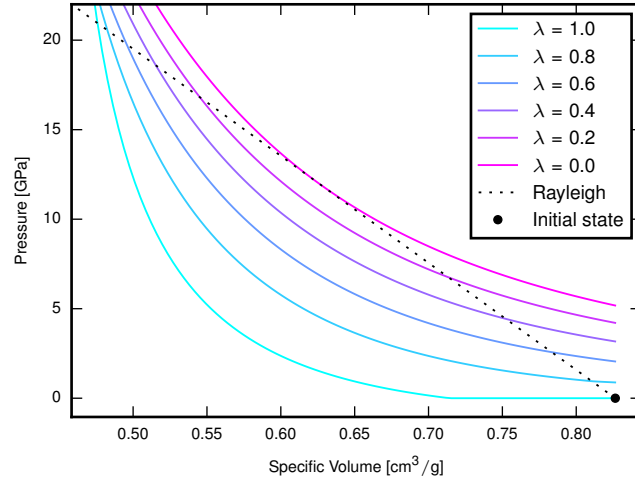


Figure 4.2: The partial burn Hugoniot curves for EM120D are plotted for several values of λ . Note that the curve for $\lambda = 1$ corresponds to the Hugoniot of the inert reactants, while the $\lambda = 0$ curve is the Crussard curve corresponding to a complete reaction.

Equation (4.36) has unknowns v_α , v_β , v and p , so must be solved along with the mixture rule and the temperature equilibrium condition,

$$v = \lambda v_\alpha + (1 - \lambda)v_\beta \quad (4.37)$$

$$T_\alpha(v_\alpha, p) = T_\beta(v_\beta, p). \quad (4.38)$$

This is done by a method analogous to that presented in Chapter 3 but with a different expression for the pressure. Either v_α or v_β is chosen as the independent variable. A nonlinear root finding method is used to find the value of the independent variable such that the temperature equilibrium condition (4.38) is satisfied, using the pressure as calculated by substituting (4.37) into (4.36).

We can thus evaluate the pressure as a function of specific volume for the partial burn Hugoniot corresponding to the given value of λ . The final step to evaluate states in the reaction zone is to apply a second root finding method to determine the specific volume such that the partial burn Hugoniot intersects the Rayleigh line corresponding to the CJ velocity,

$$\rho_0 D_{CJ} = \sqrt{\frac{p - p_0}{v_0 - v}}. \quad (4.39)$$

Now that we can evaluate states within the reaction zone as a function of λ only, it is possible to evaluate the time taken, Δt , for the detonation wave to traverse a piece of material. This is done using a reaction rate model, which defines the time derivative of λ for a specific piece of material as a function of thermodynamic variables and λ itself,

$$\frac{D\lambda}{Dt} = f(T, p)g(\lambda). \quad (4.40)$$

The time taken for the traversal of the detonation wave can be evaluated by integrating the material derivative of λ from the initial state of pure reactants ($\lambda = 1$), to the final state of pure products ($\lambda = 0$),

$$\Delta t = \int_1^0 1/\frac{D\lambda}{Dt} d\lambda. \quad (4.41)$$

Note that when using this definition of the reaction progress variable, the reaction rate as defined in (4.40) is negative.

The distance between points at which the reactant mass fraction is λ_1 and λ_2 , w is

$$w = \int_{\lambda_1}^{\lambda_2} \frac{\partial x}{\partial t} / \frac{D\lambda}{Dt} d\lambda, \quad (4.42)$$

where the derivative $\frac{\partial x}{\partial t}$ represents the speed of a element of material relative to the detonation wave. This is simply the difference between the wave speed, D_{CJ} , and the flow velocity,

$$u(\lambda) = \sqrt{(p(\lambda) - p_0)(v_0 - v(\lambda))}. \quad (4.43)$$

The width of the reaction zone is therefore

$$\Delta x = \int_1^0 \frac{D_{CJ} - u(\lambda)}{f(T(\lambda), p(\lambda))g(\lambda)} d\lambda. \quad (4.44)$$

Typical mathematical forms for the reaction rate are such that $g(0) = 0$. In this case, the above integral must be calculated with care. In particular if we define n such that

$$\lim_{\lambda \rightarrow 0} g(\lambda) \propto \lambda^n \quad (4.45)$$

then for $n \geq 1$ the integral in (4.44) diverges. In practice such a reaction rate model will not prevent the formation of a detonation wave with a finite reaction

4 ZND Waves

zone width, but the rarefaction of the detonation products will begin to be the dominant influencer of the flow already at some small, non-zero value of λ .

In the case where $0 < n < 1$, the integral is finite despite the divergence of the integrand. The integral over a range of λ close to zero can be evaluated numerically using integration by parts.

$$\begin{aligned} \int_0^\varepsilon f(x)x^{-n} dx &= \left[f(x) \frac{x^{1-n}}{1-n} \right]_0^\varepsilon - \int_0^\varepsilon \frac{x^{1-n}}{1-n} f'(x) dx \\ &= \frac{1}{1-n} \left[f(\varepsilon)\varepsilon^{1-n} - \int_0^\varepsilon x^{1-n} f'(x) dx \right] \\ &= \frac{\varepsilon^{1-n}}{1-n} [f(\varepsilon) + c\varepsilon + \mathcal{O}(\varepsilon^2)] \\ \text{where } c &\leq \frac{1}{2-n} \max_{\xi \in [0, \varepsilon]} |f'(\xi)| \end{aligned} \tag{4.46}$$

Calculation of states in the reaction zone of a ZND wave provides a direct method with which to evaluate the effect of temperature equilibrium in comparison to alternative closure conditions. The temperature equilibrium condition implies that heat transfers between reactants and products to the extent that the material temperatures equilibrate. As discussed in the literature review, a commonly applied alternative to temperature equilibrium, is ISE (isentropic solid equation), which assumes the opposite: that no heat transfer between reactants and products takes place.

The method presented in this chapter can be applied with the temperature equilibrium condition, and can be trivially modified to use a heat isolation closure condition. Solution of the equations to evaluate the thermodynamic state of the reactants and products in the reaction zone permits a direct comparison of the two closure conditions.

Figure 4.3 shows the ZND wave for PBX 9502 in pressure volume space. The blue line indicates the evolution of the state in the explosive as a whole, which follows the Rayleigh line as predicted by the ZND model. However in the reaction zone, the explosive consists of a mixture of reactants and products, the density of each of which will not be the same as the density of the explosive as a whole. The pressures on the other hand will always match, since we are using a pressure equilibrium closure condition. The figure shows the evolution of the reactants and products

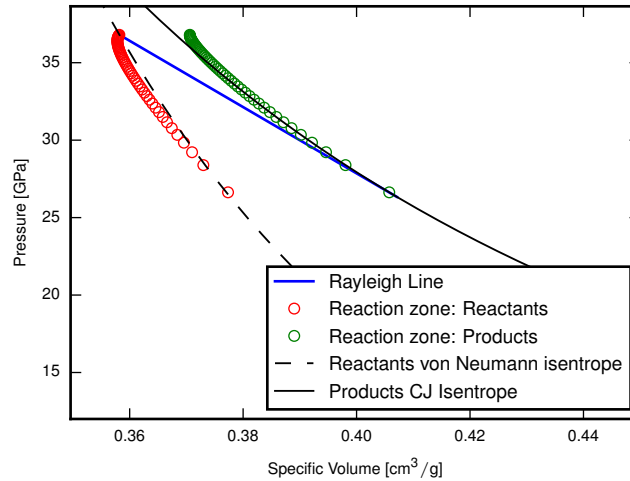


Figure 4.3: The markers indicate the evolution of the state in pressure-volume space across the reaction zone of a ZND wave in PBX 9502. The red and green markers represent the state of the reactants and products respectively. The black lines represent the paths expected for heat isolation, in which case the reactants and products evolve isentropically. The blue line represents the path of the explosive mixture, which follows the Rayleigh line.

separately using the markers. The isentropes are shown for comparison. Since heat transfer is equivalent to a change in entropy, the deviation of the path from the isentropes is representative of the amount of heat transfer which is required in order to satisfy the temperature equilibrium closure condition. Likewise the isentropes themselves are representative of the path which would be followed, were we to assume that no heat transfer takes place.

Note that the deviation of each material from its respective isentrope is not very substantial. This indicates that there is not much heat transfer between reactants and products in the reaction zone. The isentropic closure law could therefore be applied in place of temperature equilibrium and we would not expect the results to change considerably.

This is illustrated in Figure 4.4. The temperature in the reactants is at temperatures of order 100K greater when using the isentropic closure law as compared to the temperature equilibrium closure condition.

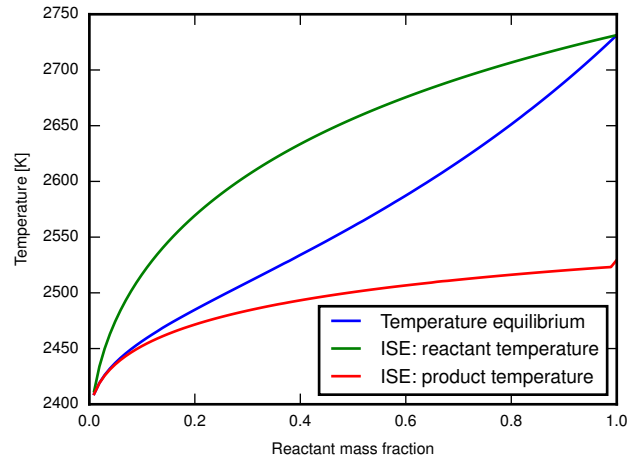


Figure 4.4: The temperature in the reaction zone as a function of the mass fraction of the explosive, λ , which consists of reactants. Note that as the reaction proceeds, the mass fraction goes from 1 to 0.

However, this is not true in general. Figure 4.5 shows the equivalent plot for the emulsion EM120D. The product density at the front of the reaction zone places the state above the principal isentrope. This shows that in the first stage of the burning the temperature equilibrium constraint causes heat to transfer from reactants to products, and the reactants compress to a higher density than the von Neumann density. Figure 4.6 shows that in this case the change in temperature is much larger - of order 500K. It is very unlikely that such a significant amount of heat transfer could occur on the timescale of a detonation wave.

The extent to which heat transfer between reactants and products occurs is dependent on the temperature at the von Neumann spike as predicted by the equation of state of the reactants, and how this temperature compares to the temperatures on the principal isentrope of the product equation of state. To illustrate this dependence, Figure 4.7 shows the ZND wave for the emulsion EM120D but with the specific heat capacity of the reactants arbitrarily increased from $1000 \text{ JK}^{-1}\text{kg}^{-1}$ to $1500 \text{ JK}^{-1}\text{kg}^{-1}$. This change reduces the von Neumann spike temperature in the reactants and alters the behaviour to be analogous to what is observed in PBX 9502. Depending on the heat capacities, and other parameters which are known with little precision, the difference between a thermal equilibrium condition and an

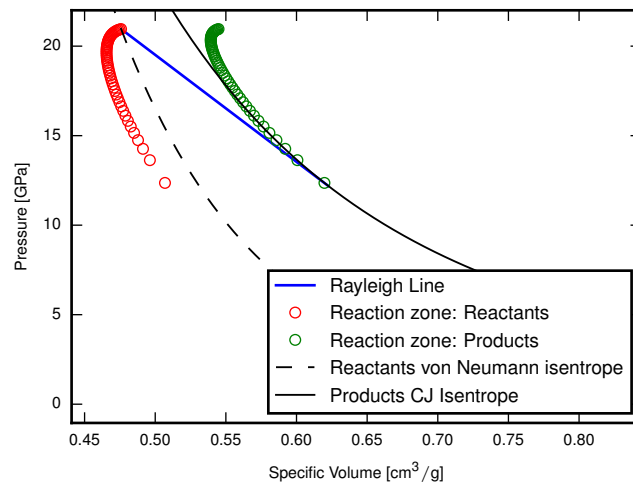


Figure 4.5: The one-dimensional ZND wave for EM120D is presented as for Figure 4.3. In this case the temperature equilibrium condition leads to more heat transfer between the reactants and products.

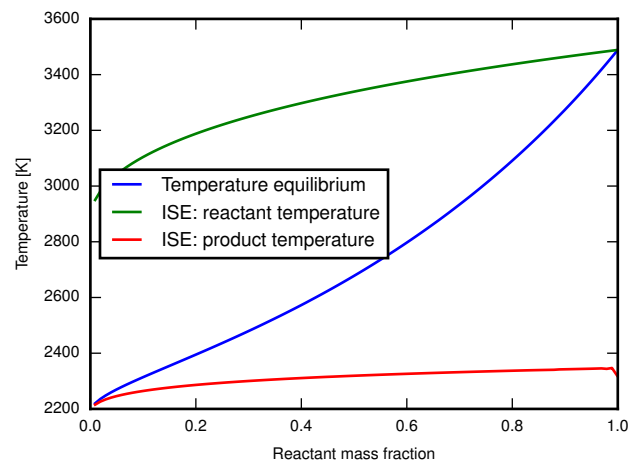


Figure 4.6: The temperatures in the reaction zone of EM120D are more disparate than what is predicted for PBX9502. In this case the temperature equilibrium condition leads to significantly lowered temperatures in the reactants than a heat isolation closure condition.

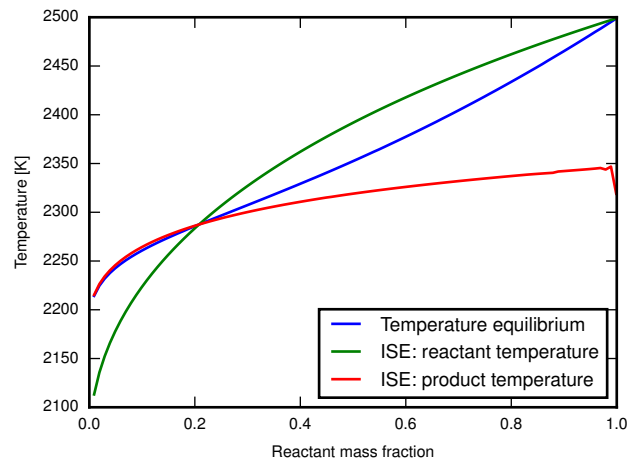


Figure 4.7: The temperatures in the reaction zone for EM120D are presented again, but this time with an increased heat capacity for the reactants. This has the effect of lowering the von Neumann spike temperature. In contrast to Figure 4.6, there is significantly less heat transfer in this case.

isentropic closure law may be of little significance. It is thus not possible to definitively conclude whether the thermal equilibrium condition is physically justified or otherwise.

4.5 Conclusions

An approach has been presented with which to calculate the structure of ZND waves for an explosive. This approach is suitable for explosives which are described by independent equations of state of Mie-Grüneisen form and closure conditions to fully constrain the mixture of materials in the reaction zone. This method can be used to validate numerical methods, by comparing the predicted ZND structure with the results of a simulated one dimensional detonation wave. Furthermore, the method presented here permits us to calculate the width of the reaction zone given a reaction rate model. This is helpful when determining the values of parameters for the reaction rate model, since it is expected that the deviation of a multi-dimensional detonation wave from the ZND wave is related to the width of the reaction zone.

This method can be used to quantitatively compare various closure conditions which may be suitable. For example, it allows us to directly evaluate the amount of heat transfer which is actually generated by a temperature equilibrium condition.

The results show that temperature equilibrium does not necessarily imply that a large amount of heat transfer must occur, and therefore the results may not be dissimilar to those from a heat isolation model. In addition, the results are also dependent on equation of state parameters, some of which are not known to a great degree of certainty. These results suggest that it is not possible to reach a meaningful conclusion as to which of the closure conditions will lead to the most accurate results for generic explosives.

From a physical perspective, large differences in temperature between the reactants and products suggest that some heat transfer is likely to take place, even on the short time scales associated with the ZND wave. On the other hand, large differences in temperature suggest that the temperatures are unlikely to fully equilibrate.

From a numerical perspective, the temperature equilibrium condition is more convenient, since it can be applied to every cell of the domain. Since the entropy of the explosive will change in the presence of shock waves, a heat isolation closure condition cannot be implemented by simply assuming that the entropy of the reactants is fixed.

5 Detonation Modelling

5.1 Formulations for multi-material fluid simulations

Detonation waves are not one dimensional phenomena; the observed detonation velocity depends on the geometry of the explosive charge as well as the properties of the confining material. Thus, numerically simulating detonation phenomena necessitates a mathematical formulation describing the evolution of the explosive and the confiner as well as the interface between the explosive and the confining material.

In previous chapters the discussion has addressed in detail the issue of modelling the material properties of the explosive. This is done through the introduction of a mass fraction parameter which indicates the portion of the explosive which is reacted and serves as a reaction progress variable. A pressure for the explosive material can then be calculated using the mass fraction parameter and independent equations of state for each of the reactants and products along with closure conditions.

This can be easily applied in the context of a hydrocode. The Euler equations are used to describe the properties of the flow of the explosive as a whole. The mass fraction parameter is simply advected with the flow,

$$\frac{\partial \rho \lambda}{\partial t} + \nabla \cdot \rho \lambda \mathbf{u} = K, \quad (5.1)$$

thus allowing us to model both reactants and products, even as the explosive moves with the flow field. The source term, K , represents the time derivative of λ corresponding to the chemical reaction. This approach can also be used to model the interface between the explosive and the confiner. This creates a formulation with two mass fraction parameters, and a root finding problem analogous to the one

introduced in chapter 3. However in this case it has two degrees of freedom. This is because the pressure equilibrium and temperature equilibrium conditions must now be applied to all three materials. This method is sometimes referred to as the Banks model [13, 14]. While it is possible to solve such a system numerically, it has been reported to not be robust [91]. Furthermore it cannot be extended to model more materials. In general such an approach will require the solution of a root finding problem of dimensionality $n - 1$ in order to simulate a system of n materials.

A contrasting approach to the numerical representation of fluids with multiple constituents is with so-called ‘multiphase’ models, as has been discussed previously in Chapter 2. However, for the purpose of modelling the explosive-confiner interface it is not necessary to use such a complex approach. Whereas the reactants and products of the explosive are a true mixture, the confiner and explosive are immiscible, with a well defined interface between the two. The nature of the relationship between the confiner and explosive is physically different, motivating an alternative numerical treatment. Numerical resolution of dynamically changing interfaces can be split into two broad categories: sharp interface methods (SIM) and diffuse interface methods (DIM) [106].

Examples of SIM include Lagrangian methods, where the mesh itself distorts to match the change in position of the material interface. However this is inconvenient to accommodate with an Eulerian numerical scheme, which captures shock waves more accurately. The volume of fluid (VOF) approach [58] uses a colour function to indicate the identity of the present fluid in each cell. The colour function is then advected with the fluid. This method is typically used for incompressible fluids [58, 106].

An alternative is the ghost fluid method [42]. With this method, an arbitrary function called the level set is defined such that the zero space of the function corresponds to the interface. The location of the interface is then calculated by interpolating the level set, and can thus be evaluated with greater precision than the resolution of the mesh. This method is well suited to the simulation of objects with rigid boundaries. Wescott et al. [129] use a level-set algorithm to model the explosive confiner interface in simulations of PBX 9502 [122].

5.1 Formulations for multi-material fluid simulations

In contrast to sharp interface methods, diffuse interface methods simplify the problem substantially by allowing the interface to spread out over several cells. While this leads to inaccuracies in the resolution of the interface itself, advantages include the fact that the same algorithm can be implemented for the entire domain. Furthermore, such algorithms are computationally less expensive than sharp interface methods. This is because sharp interface methods require special methods to update the cells which are intersected by the interface. For example, the ghost fluid method involves an interpolation of the level set to determine the precise location of the interface, followed by an extrapolation of the data across the interface to populate the ghost cells. Finally a suitable mixed Riemann solver is required. These complications can all be avoided through the use of a diffuse interface method.

Allaire et al. [2] developed a five equation model for simulating diffuse interfaces using equations based on multiphase models [104]. The interface is tracked using a parameter, z , representing the volume fraction of the materials which can take non-integer values between 0 and 1. The interface may spread out and become diffuse. This is not equivalent to the mass fraction parameter used in the Banks model since each phase is governed by its own separate mass conservation law:

$$\frac{\partial z \rho_1}{\partial t} + \nabla \cdot z \rho_1 \mathbf{u} = 0 \quad (5.2)$$

$$\frac{\partial (1-z) \rho_2}{\partial t} + \nabla \cdot (1-z) \rho_2 \mathbf{u} = 0 \quad (5.3)$$

$$\frac{\partial \rho \mathbf{u}_k}{\partial t} + \nabla \cdot \rho \mathbf{u}_k \mathbf{u} = -(\nabla p)_k \quad \text{for } k \in \{1, \dots, d\} \quad (5.4)$$

$$\frac{\partial \rho E}{\partial t} + \nabla \cdot \rho E \mathbf{u} = -\nabla \cdot p \mathbf{u}. \quad (5.5)$$

The densities of the two phases are ρ_1 and ρ_2 . This is a single-velocity, single-pressure model, and there is therefore just a single flow velocity, u , and specific energy, E , for the two phase fluid. The specific energy is the sum of the specific internal energy, e , and kinetic energy,

$$E = e + \frac{1}{2} \|\mathbf{u}\|^2. \quad (5.6)$$

The corresponding mixture rules are

$$\rho = z \rho_1 + (1-z) \rho_2 \quad (5.7)$$

$$\rho e = z \rho_1 e_1 + (1-z) \rho_2 e_2. \quad (5.8)$$

5 Detonation Modelling

The asymmetry between these mixture rules and those used in Chapter 3 is explained in Appendix C. Unlike the mass fraction, λ , the volume fraction, z , is not conserved. The volume fraction is not conserved – it is passively advected according to

$$\frac{\partial z}{\partial t} + \mathbf{u} \cdot \nabla z = 0. \quad (5.9)$$

In contrast to the Banks model [14], only one closure rule is required since the density of each of the individual phases is known explicitly. Both isobaric and isothermal closure conditions are investigated by Allaire et al. [2]. The resulting set of partial differential equations is shown to be hyperbolic in both cases. However the isobaric scheme is found to be favourable, since it allows for the interface between fluids to be simulated without spurious oscillations forming in the pressure profile.

An important difference between the Allaire model and the multiphase model by Kapila [66] is that the Allaire model neglects the compaction term, which accounts for variation in the compressibility of mixture constituents. The compaction term would normally manifest as a non-zero source term on the right hand side of equation (5.9). As a result the Allaire model is not suitable for modelling genuine mixtures, despite the successful handling of mixture cells which occur within the diffuse interface. In the Allaire model, the fluid mixture has a unique value for the compressibility, and each constituent of the mixture will compress at the same rate. Consequently the Allaire model does not accurately reproduce the behaviour of fluid mixtures without sharp interfaces. It is better suited to modelling situations where there is only a narrow intermediate zone in which the fluids are mixed, and most of the domain is occupied by only one constituent. As a result, it would not be possible to use the Allaire model to describe the reactant product mixture which constitutes the explosive.

The approach for modelling the two-material explosive presented in chapter 3 has been combined with the Allaire multiphase approach in the MiNi16 formulation introduced by Michael et al. [90, 91]. It uses a mass fraction, λ , to simulate the mixture of reactants and products using pressure equilibrium, temperature equilibrium and a single mass conservation equation. These materials collectively constitute the explosive. The explosive confiner interface, on the other hand, is

modelled using a volume fraction, z , pressure equilibrium and separate mass conservation equations. An attractive property of the MiNi16 formulation is that the same algorithm is applied to every cell of the simulation. No special handling of shock waves is required as in multiphase models of the type presented by Schoch et al. [108]. Furthermore the temperature equilibrium condition can be applied in every cell using the same algorithm, irrespective of the presence or absence of shock waves. In contrast, the isentropic solid equation (ISE) applied in CREST requires special handling of the shock wave, since the entropy of the reactants is expected to change across the shock wave, but not in the subsequent reaction zone [55].

These properties render the MiNi16 formulation very practical for modelling ignition. The same algorithm as is implemented for modelling detonation waves can be applied without additional work to simulations which exhibit partial burn, ignition and transition to detonation.

5.2 MiNi16 Formulation

The mathematical formulation employed in this thesis to model detonation and ignition of explosives is the MiNi16 formulation for a three-material fluid system [91]. The three materials correspond to the confiner (labelled 1), the reactants (α) and the products (β). In addition, the reactants and products collectively constitute the explosive, which is referred to as the second phase (labelled 2). Variables without subscript labels refer to the properties of the three-material mixture.

The governing equations consist of a mass conservation equation for each of phases 1 and 2. It is a single-velocity single-pressure model and so has just one equation for the conservation of each of momentum and energy. There is an equation which specifies the evolution of the volume fraction, z , of the first phase with respect to the two phase mixture. Finally the mass fraction of the reactants with respect to the explosive, λ , is advected with the fluid. Note that this is not the mass fraction

5 Detonation Modelling

with respect to the three-material mixture, but with respect to the second phase.

$$\frac{\partial z\rho_1}{\partial t} + \nabla \cdot z\rho_1\mathbf{u} = 0 \quad (5.10)$$

$$\frac{\partial(1-z)\rho_2}{\partial t} + \nabla \cdot (1-z)\rho_2\mathbf{u} = 0 \quad (5.11)$$

$$\frac{\partial\rho\mathbf{u}_k}{\partial t} + \nabla \cdot \rho\mathbf{u}_k\mathbf{u} = -(\nabla p)_k \quad \text{for } k \in \{1, \dots, d\} \quad (5.12)$$

$$\frac{\partial\rho E}{\partial t} + \nabla \cdot \rho E\mathbf{u} = -\nabla \cdot p\mathbf{u} \quad (5.13)$$

$$\frac{\partial z}{\partial t} + \mathbf{u} \cdot \nabla z = 0 \quad (5.14)$$

$$\frac{\partial\rho_2\lambda}{\partial t} + \nabla \cdot \rho_2\lambda\mathbf{u} = K \quad (5.15)$$

The mixture rules for the three-material mixture are

$$\rho = z\rho_1 + (1-z)\rho_2 \quad (5.16)$$

$$\frac{1}{\rho_2} = \frac{\lambda}{\rho_\alpha} + \frac{1-\lambda}{\rho_\beta} \quad (5.17)$$

$$\rho e = z\rho_1 e_1 + (1-z)\rho_2 e_2 \quad (5.18)$$

$$e_2 = \lambda e_\alpha + (1-\lambda)e_\beta. \quad (5.19)$$

Equation (5.16) expresses the overall density, ρ , in terms of the phase densities, ρ_1 and ρ_2 . The density of the second phase is itself a function of the reactant density, ρ_α , and the product density, ρ_β , (5.17). The total specific internal energy, e , of the three-material system is defined in (5.18), and is once again related to the specific energy E by

$$E = e + \frac{1}{2}\|\mathbf{u}\|^2. \quad (5.20)$$

The reaction rate is represented by K , a source term in the equation for the evolution of the mass fraction variable, λ . Note that there is no source term in the energy equation, because the energy source is handled implicitly by the equations of state for the reactants and products.

The three materials are each modelled with an EoS model of Mie-Grüneisen form

$$p_k - p_{k,\text{REF}}(v_k) = \rho_k \Gamma_k(v_k)(e_k - e_{k,\text{REF}}(v_k)) \quad \text{for } k \in \{1, \alpha, \beta\}. \quad (5.21)$$

Following MiNi16 [91], pressure equilibrium is assumed between phases 1 and 2. For the second phase, both pressure and temperature equilibrium are applied. Thus

pressure equilibrium applies to all three materials, while temperature equilibrium is applied between materials α and β .

Unfortunately the closure conditions of pressure and temperature equilibrium, which are introduced to remove the degrees of freedom associated with space and energy distribution, do not permit a closed form expression for the pressure. The new equation for the pressure is derived by substituting the component EoS models into the energy equation (5.18)

$$\begin{aligned} \rho e = p & \left(\frac{z}{\Gamma_1(v_1)} + \frac{(1-z)\rho_2\lambda}{\rho_\alpha\Gamma_\alpha(v_\alpha)} + \frac{(1-z)\rho_2(1-\lambda)}{\rho_\beta\Gamma_\beta(v_\beta)} \right) \\ & + z\rho_1 \text{REF}_1 + (1-z)\rho_2\lambda \text{REF}_\alpha + (1-z)\rho_2(1-\lambda) \text{REF}_\beta, \end{aligned} \quad (5.22)$$

where

$$\text{REF}_k = \frac{-p_{k,\text{REF}}(v_k)}{\rho_k\Gamma_k(v_k)} + e_{k,\text{REF}}(v_k) \quad \text{for } k \in \{1, \alpha, \beta\}.$$

This equation has two unknowns: the pressure and one or other of v_α and v_β (the other is fully constrained by (5.17)). The pressure equation is solved along with the equation for temperature equilibrium between the reactants and products,

$$T_\alpha = T_\beta. \quad (5.23)$$

The method used to solve this equation is described fully in Chapter 3.

The speed of sound in the three-material mixture is found in two steps. First the speed of sound of the explosive is calculated using partial derivatives of the mixture (see section 3.8), while the sound speed in the confiner is calculated according to (3.10).

Following [2], the sound speed in the multiphase system with densities ρ_i , and corresponding volume fractions z_i and mass fractions λ_i , is calculated using the standard relation

$$c^2 = \frac{h - \left(\frac{\partial \rho e}{\partial \rho}\right)_p}{\left(\frac{\partial \rho e}{\partial p}\right)_\rho}, \quad (5.24)$$

5 Detonation Modelling

where h is the enthalpy. Using (5.16) and (5.18), it follows that

$$h = \sum_i \lambda_i h_i \quad (5.25)$$

$$\left(\frac{\partial \rho e}{\partial \rho}\right)_p = \sum_i z_i \left(\frac{\partial \rho_i e_i}{\partial \rho_i}\right)_p \left(\frac{\partial \rho_i}{\partial \rho}\right)_p \quad (5.26)$$

$$\left(\frac{\partial \rho e}{\partial p}\right)_\rho = \sum_i z_i \left(\frac{\partial \rho_i e_i}{\partial p}\right)_{\rho_i}. \quad (5.27)$$

In the Allaire model, the compaction term is neglected. In other words the volume fraction does not change as a result of the addition of energy. It therefore follows that

$$\left(\frac{\partial \rho_i}{\partial \rho}\right)_p = \left(\frac{\partial \rho_i}{\partial \rho}\right)_{z_i, \lambda_i} = \frac{\lambda_i}{z_i}, \quad (5.28)$$

where we have used the general relationship

$$z_i = \frac{\lambda_i \rho}{\rho_i}, \quad (5.29)$$

which is derived in Appendix C.

Hence

$$c^2 = \frac{\sum_i \lambda_i \left(h_i - \left(\frac{\partial \rho_i e_i}{\partial \rho_i}\right)_p \right)}{\sum_i z_i \left(\frac{\partial \rho_i e_i}{\partial p}\right)_{\rho_i}}. \quad (5.30)$$

Introducing the thermodynamic quantity ξ

$$\xi = \left(\frac{\partial \rho e}{\partial p}\right)_\rho = \frac{1}{\Gamma} = \frac{1}{\gamma - 1} \quad (5.31)$$

which is the inverse of the Grüneisen gamma, we may express the speed of sound, c , in terms of the speed of sound of each phase, c_i , as

$$\left(\sum_i z_i \xi_i\right) c^2 = \sum_i \lambda_i \xi_i c_i^2. \quad (5.32)$$

Following MiNi16 [91], the value of ξ in the explosive is evaluated with reference the adiabatic gamma, which is found by taking a weighted average of the constituent adiabatic gamma values. The weighting is determined by the relative heat capacity which is the mass fraction, λ , multiplied by the specific heat capacity $c_{v,k}$,

$$\gamma = \frac{\lambda \gamma_\alpha c_{v,\alpha} + (1 - \lambda) \gamma_\beta c_{v,\beta}}{\lambda c_{v,\alpha} + (1 - \lambda) c_{v,\beta}}. \quad (5.33)$$

5.3 Numerical Methods

The equations of the MiNi16 formulation presented above comprise a system of hyperbolic partial differential equations. The equations are solved numerically using a conservative finite volume method. By defining the flux with the Godunov scheme [47, 125], the problem is reduced to solving a Riemann problem at each cell interface. The stability of the Godunov method requires that the time step satisfies the CFL condition (Courant-Friedrichs-Lewy) [32]. We therefore formulate the equations in conservative form, with an explicit expression for the flux.

The equation for the evolution of z , (5.14), is not conservative, however it is possible to recast it in conservative form with an explicit source term,

$$\frac{\partial z}{\partial t} + \nabla \cdot (z\mathbf{u}) = z\nabla \cdot \mathbf{u}. \quad (5.34)$$

The set of partial differential equations is expressed using the vector of conserved variables, \mathbf{U} . For simplicity, only the equations for one dimensional flow are presented:

$$\frac{\partial \mathbf{U}}{\partial t} + \frac{\partial \mathbf{F}(\mathbf{U})}{\partial x} = \mathbf{S}(\mathbf{U}), \quad (5.35)$$

where

$$\mathbf{U} = \begin{pmatrix} z\rho_1 \\ (1-z)\rho_2 \\ \rho u \\ \rho E \\ z \\ (1-z)\rho_2\lambda \end{pmatrix}, \quad \mathbf{F}(\mathbf{U}) = \begin{pmatrix} z\rho_1 u \\ (1-z)\rho_2 u \\ \rho u^2 + p \\ u(\rho E + p) \\ uz \\ (1-z)\rho_2\lambda u \end{pmatrix}, \quad \mathbf{S}(\mathbf{U}) = \begin{pmatrix} 0 \\ 0 \\ 0 \\ 0 \\ z\frac{\partial u}{\partial x} \\ K \end{pmatrix}.$$

The Harten, Lax and van Leer, Contact (HLLC) approximate Riemann solver is used to calculate the fluxes at cell interfaces. It was first presented by Toro, Spruce and Spears [126] and is an extension of the HLL method first published in 1983 [56]. This is extended to second order using MUSCL-Hancock with the van Leer limiter [76, 125].

The numerical methods are implemented in a code developed at the Laboratory of Scientific Computing at the University of Cambridge. This code is capable of

adaptive mesh refinement (AMR) and parallel execution through subdivision of the domain. Simulations of rate stick detonations can be greatly accelerated with adaptive mesh refinement, because the detonation wave has a complex structure, which is very narrow in comparison to the typical distance travelled in the time required to reach steady state. A high resolution is required to resolve the detonation wave, but it is impractical to use such a fine resolution over the whole domain.

5.4 Rotational Symmetry

The detonation of rate sticks is a three dimensional phenomenon. However, the three dimensional symmetry of the rate stick can be exploited to avoid a three dimensional simulation [14, 91, 108]. The source term associated with the geometric effects is

$$\mathbf{S}(\mathbf{U}) = \frac{u_r}{r} \begin{pmatrix} z\rho_1 \\ (1-z)\rho_2 \\ \rho u_r \\ \rho u_z \\ \rho E + p \\ (1-z)\rho_2\lambda \\ z \end{pmatrix}, \quad (5.36)$$

where u_r and u_z are the radial and axial velocities respectively.

5.5 Validation

5.5.1 Riemann Tests

A common method to validate the implementation of numerical methods for compressible inviscid fluid dynamics problems is based on Riemann problems. The solution of a typical Riemann problem will involve a rarefaction wave, a contact discontinuity as well as a shock wave, thus testing multiple aspects of the numerical method at once. Furthermore, the simplicity of the initial conditions means that it is possible to calculate the exact solution of a Riemann problem directly [125].

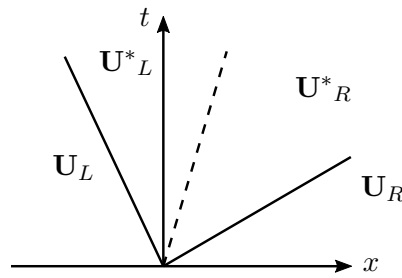


Figure 5.1: The waves originating from the discontinuity of the Riemann problem are plotted in space and time. The contact discontinuity is shown with a dashed line. The solid lines indicate the propagation of rarefaction waves or shock waves across which the flow velocity and pressure change.

Exact solutions provide a reference against which to compare the numerical results. Since the numerical method uses the equation of state to calculate pressures and the speed of sound, Riemann problems also allow us to verify that the equations of state have been implemented correctly.

Figure 5.1 shows the structure of the solution to a Riemann problem. Three waves originate from the origin at $x = 0, t = 0$. The left and right hand waves are either rarefaction waves or shock waves, while the middle wave is a contact discontinuity. The exact solution of a Riemann problem can be calculated using the fact that the flow velocity and pressure are both constant across the contact discontinuity [125].

The two states initially on either side of the discontinuity which define the initial conditions of the Riemann problem are labelled \mathbf{U}_L and \mathbf{U}_R respectively. The states on either side of the contact discontinuity are labelled as \mathbf{U}_L^* and \mathbf{U}_R^* . For each state we refer to the pressure, p , specific volume, v , and flow velocity to the right, u , using the corresponding subscripts and superscripts. For the solution of the Riemann problem we therefore have

$$u_L^* = u_R^* = u^* \quad (5.37)$$

$$p_L^* = p_R^* = p^*. \quad (5.38)$$

The properties of rarefaction waves and shock waves are such that there will always be a pair of waves which solve the problem [125]. To find the solution we must use

5 Detonation Modelling

a root finding method to find the waves such that the change in both pressure and flow velocity across the two waves, are such that equation (5.38) is satisfied.

If a shock wave is travelling to the right, we have from Chapter 4

$$p_R^*(v_R^*, v_R, p_R) = \frac{\frac{p_{\text{REF}}(v_R^*)}{\rho\Gamma} - e_{\text{REF}}(v_R^*) + e_R(v_R, p_R) + \frac{1}{2}p_R(v_R - v_R^*)}{\frac{1}{\rho\Gamma} - \frac{1}{2}(v_R - v_R^*)} \quad (5.39)$$

$$u_R^* = u_R + \sqrt{(p_R^* - p_R)(v_0 - v_R^*)}. \quad (5.40)$$

To calculate the pressure, p_L^* , we can simply replace the subscript R with L in (5.39). Since u is by convention defined as the flow velocity to the right, there is a change in sign when calculating the properties of shock waves propagating to the left, in which case

$$u_L^* = u_L - \sqrt{(p^* - p_L)(v_0 - v_L^*)}. \quad (5.41)$$

For rarefaction waves, we can use the isentropic property of rarefaction waves and calculate the change in pressure by simply calculating the pressure on the isentrope for some candidate new specific volume, v_k^* . This is calculated using equation (3.20),

$$p(v_k^*) = p_{\text{REF}}(v_k^*) + \frac{\Gamma(v_k^*)}{v_k^*} (e_k(v_k, p_k) - e_{\text{REF}}(v_k)) \frac{T_{\text{REF}}(v_k^*)}{T_{\text{REF}}(v_k)}, \quad (5.42)$$

which applies for $k \in \{L, R\}$. For rarefaction waves there is also a restriction on the physically valid choices for v^* ,

$$v_L^* > v_L \quad v_R^* < v_R. \quad (5.43)$$

The change in flow velocity across the rarefaction wave can be calculated using the Riemann invariant,

$$u_L^* = u_L + \int_{v_L}^{v_L^*} \frac{c(v, p(v))}{v} dv \quad (5.44)$$

$$u_R^* = u_R + \int_{v_R^*}^{v_R} \frac{c(v, p(v))}{v} dv, \quad (5.45)$$

where the speed of sound, c , is a function of volume and pressure (3.10), and the pressure is given by equation (5.42).

Test Case	ρ_L	p_L	ρ_R	p_R	t_{final}	x_0
EM120D Products	1600	1.2×10^{10}	1200	1×10^5	8×10^{-5}	0.5
EM120D Reactants	2200	2×10^{10}	1200	1×10^5	5×10^{-5}	0.5

Table 5.1: Initial conditions for Riemann tests in units of kgm^{-3} , Pa, m and s.

The final step is to sample the solution. For each x, t we can sample the solution using the corresponding wave speed, $s = x/t$. By comparing s with the wave speeds of the solution, we can work out which part of the solution we are sampling. The speed of the contact discontinuity is simply u^* . The speed of a shock wave can be calculated using (4.4), which gives us the speed of the wave, D , relative to the unshocked material. Rarefaction waves are more complicated, since they spread out in time. Each point in the rarefaction propagates at a speed $u \pm c$ depending on the direction of the wave. So a rarefaction wave travelling to the left will cover the range

$$u_L - c_L \leq s \leq u_L^* - c_L^*. \quad (5.46)$$

To sample values of s inside this range we must find the value of $v \in [v_L, v_L^*]$ such that

$$u - c = s, \quad (5.47)$$

where u is calculated using (5.44).

Figures 5.2 and 5.3 show the numerical results for Riemann tests overlaid on the exact solutions. Figure 5.2 uses the equation of state for the explosive products, as presented in Chapter 3, while Figure 5.3 uses the equation of state for the reactants. In each case the parameters of the equation of state are those for EM120D. The equations of state parameters are presented in Tables 3.2 and 3.3. The initial conditions are in Table 5.1.

5.5.2 Shock Speed

The equation of state for the reactants can be tested further by verifying that the expected shock velocities are reproduced accurately in the simulations. The reactants equation of state uses the snow plow model to capture the effect of porosity on the properties of the explosive. One of the consequences of the porosity model

5 Detonation Modelling

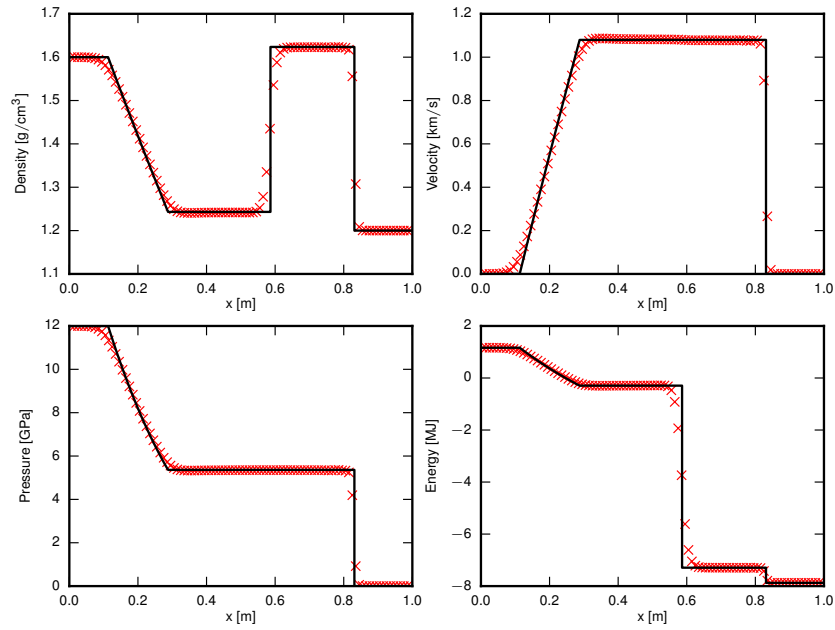


Figure 5.2: Riemann test to verify the implementation of the products equation of state for EM120D. The numerical results (red markers) can be compared with the exact solution (black line).

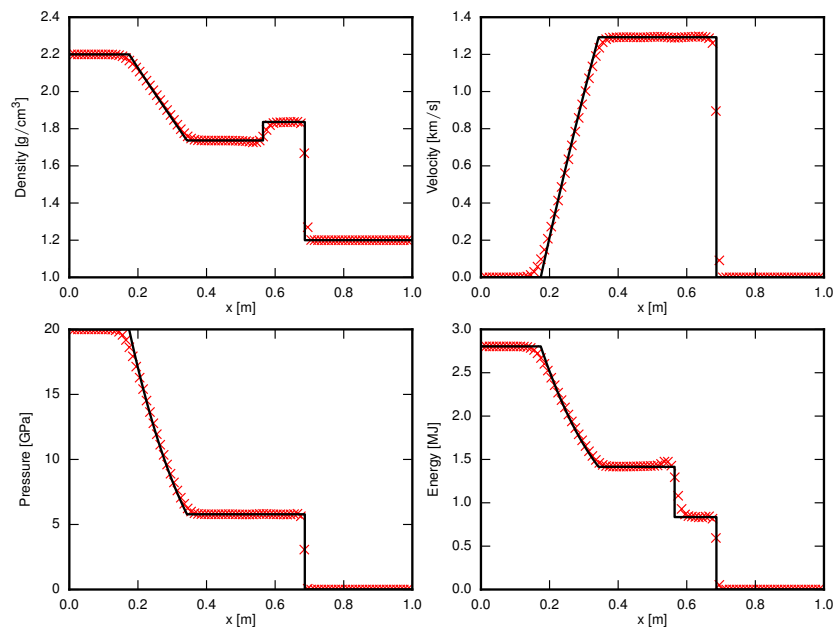


Figure 5.3: Riemann test to verify the implementation of the equation of state for the porous reactants of EM120D. The numerical results (red markers) can be compared with the exact solution (black line).

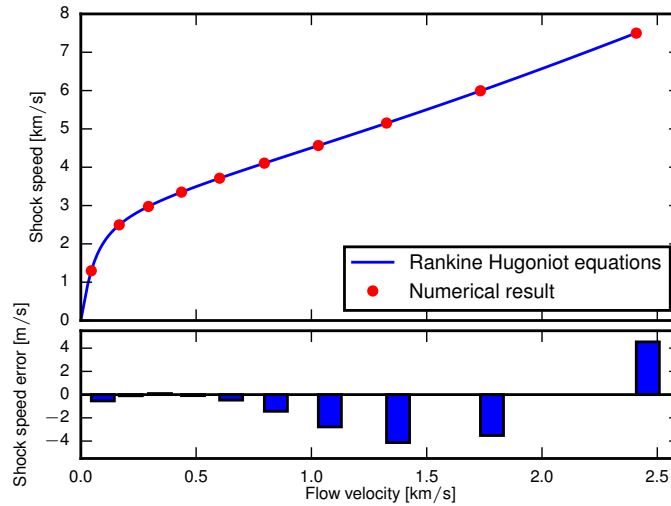


Figure 5.4: Comparison of the shock velocity to flow velocity relationship predicted by the Rankine-Hugoniot conditions with numerical results. The bar chart shows the error between the analytically calculated shock speed and the numerical values.

is that the shock speed is no longer a linear function of the change in flow velocity associated with the shock. This is illustrated in Figure 3.7 in Chapter 3.

To verify that this relationship is reproduced accurately in the simulations, shock waves of varying strengths were initialised. The shock wave speed is evaluated by simply observing the rate at which the wave propagates through the domain. The shock waves are created by initialising the explosive with a uniform flow velocity towards a reflective boundary. The results are shown in Figure 5.4. The x -axis corresponds to the flow velocity, u , used to initialise the explosive. The shock speed, D , is measured relative to the unshocked explosive.

5.5.3 Detonation Waves in 1D

The ZND model for the structure of one dimensional detonation waves can be used to calculate the Rayleigh line, the von Neumann spike, the CJ state and the principal isentrope of the rarefaction wave. This can be done using solely the equations of state (EoS) of the reactants and products, and the Rankine-Hugoniot conditions. Furthermore, using some closure conditions for the mixture of reactants

5 Detonation Modelling

and products, states inside the reaction zone may be evaluated too (see Chapter 4).

ZND waves can also be simulated numerically using the numerical methods presented in this chapter. Here we compare the path of the numerical solution in pressure volume space with that calculated analytically. Figure 5.5 shows the ZND wave for PBX 9502 and compares the numerical simulation of a one-dimensional detonation wave with the calculated ZND wave structure as has been calculated in Chapter 4. Figure 5.6 shows the equivalent validation for EM120D.

The cyan markers indicate the evolution of the state in the explosive as a whole. Across the shock wave (approximately three cells) the state approaches the von Neumann spike in the top left of the plot. As the explosive burns, the state of the explosive (blue) follows the Rayleigh line towards the CJ state. During this stage, the explosive is a mixture of reactants and products, which are at pressure equilibrium but have different specific volumes. The red and green markers represent the states of the reactants and products respectively. After the CJ state, the explosive consists entirely of products and rarefies following the principal isentrope. The plot can be compared those presented in Chapter 4.

The cyan markers lie on the Rayleigh line as expected, and the rarefaction of the detonation products follows the principal isentrope as used for the calibration. This demonstrates that the calibration process is working as expected. The accurate reproduction of the reactant and product specific volumes for states inside the reaction zone serves to validate the numerical implementation of the closure conditions in the code, and in addition corroborates the analysis presented in Chapter 4 which is used to calculate the ZND wave structure directly. Furthermore the speed of propagation of the wave is observed to be equal to the CJ detonation velocity as predicted.

Figures 5.7 and 5.8 show the pressure in the ZND waves as a function of position. These figures serve to demonstrate how much resolution is required for the numerical solution to converge in the reaction zone. The simulation of PBX 9502 requires significantly higher resolution, as is expected given the smaller reaction zone. The required resolution to reach convergence is in the range of 60 to 100 cells per reaction

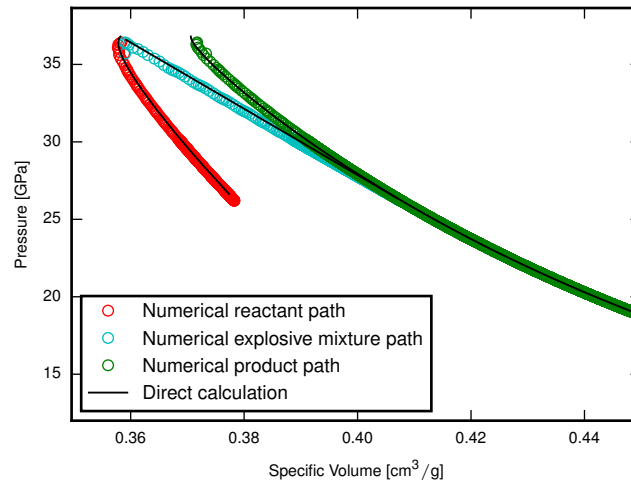


Figure 5.5: The cyan markers indicate the evolution of the state in pressure-volume space across the ZND wave of PBX 9502. The red and green markers represent the state of the reactants and products respectively. The black lines represent the predicted paths which are calculated analytically.

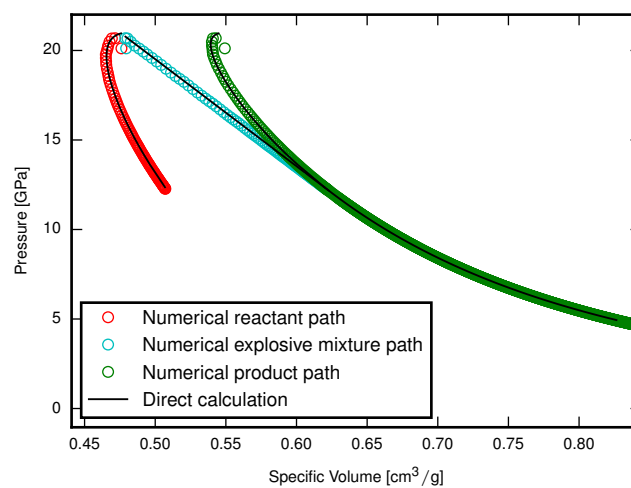


Figure 5.6: The one-dimensional ZND wave for EM120D is presented as for Figure 5.5.

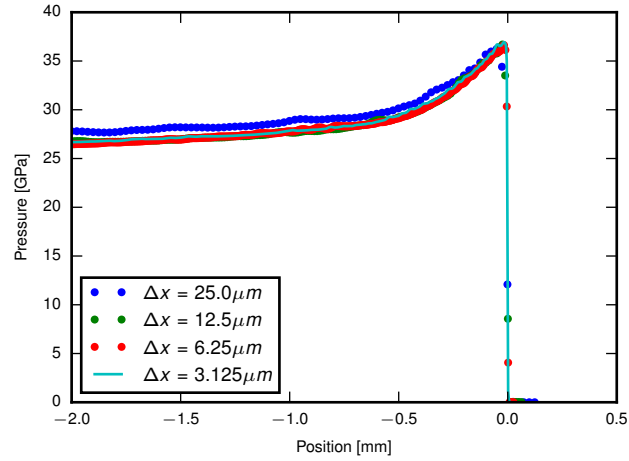


Figure 5.7: The numerical solution for a one dimensional detonation wave in PBX 9502 is plotted for a range of resolutions.

zone length. The results are in broad agreement with the results of Sharpe and Braithwaite [112].

5.6 Evaluating the detonation velocity

In order to compare the simulation results with experimental measurements of the detonation velocity it is necessary to extract wave velocities from the results. This cannot be done accurately from a single time snapshot in multiple dimensions, since any curvature of the shock front means that the one dimensional Rankine-Hugoniot conditions no longer apply. To avoid these complications, we instead measure the wave velocity directly, by using the position of the wave at different times.

In finite volume simulations, the shock wave will naturally be smeared across a number of cells. This smearing of the wave is unavoidable, and as such the precision with which the position of the shock can be measured is limited by the resolution of the simulation. In this work we improve the accuracy by fitting the data to a sharp shock. The position of the fitted shock is chosen such that the integral of the density under the fitted shock wave matches that under the data. This process is illustrated in Figure 5.9.

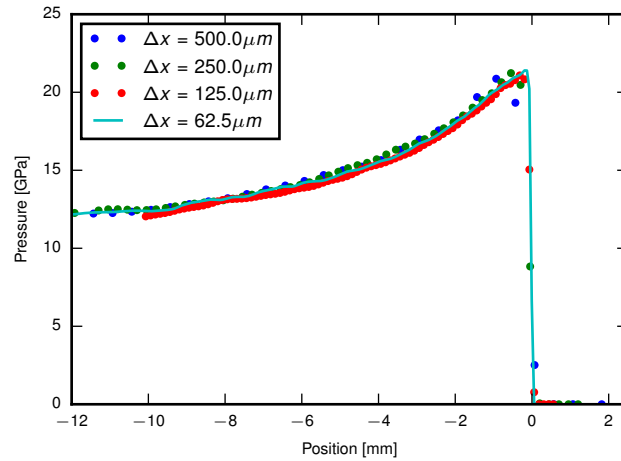


Figure 5.8: The convergence criteria for EM120D is evaluated in the same manner as for PBX 9502 in Figure 5.7.

This procedure allows for the speed of a shock wave or detonation wave to be measured accurately, even over comparatively short time periods.

5.7 Predictive Modelling of Detonation Waves in Rate Sticks and Slabs

5.7.1 Simulation Setup

In one-dimensional domains, the velocity of the detonation wave is the CJ velocity, which depends solely on the EoS of the products and the initial conditions of the explosive. However the velocity of detonation (VoD) measured in rate sticks (cylinders) and slabs is significantly reduced from the ideal VoD, as a result of the loss of energy to the confining material. The measured VoD therefore depends on the geometry and material of the confiner and will also depend on the reaction rate. Near-ideal explosives, with a faster reaction rate, deviate from the ideal VoD to a lesser degree than non-ideal explosives with slower reaction rates. For example, detonation waves in PBX 9502 can deviate in speed by approximately 10%. For EM120D, on the other hand, detonation velocities in rate sticks can be close to 50% slower than the ideal VoD.

5 Detonation Modelling

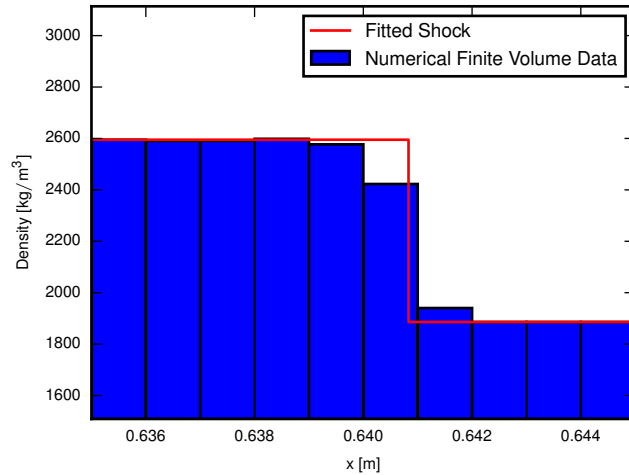


Figure 5.9: Sample data showing the position of a shock wave from a finite volume simulation. The position of the shock wave illustrated by the red line is chosen such that the total mass over the domain is unchanged.

It is currently impractical to model the chemistry of the reaction directly. A one-step reaction model is used to calculate the rate at which reactants transition to products. An approach for calibrating a reaction rate model using shock to detonation transition data will be presented in Chapter 6. In the present chapter, however, the reaction rate is calibrated using direct optimization: the parameters are chosen such that the simulations match the given experimental data. This approach nevertheless permits predictive modelling of detonation waves. It is found in practice that only a few measurements are required for the calibration of the parameters, and that these same parameters can be used to predict detonation velocities in multiple different contexts.

For PBX 9502, the reaction rate is calibrated using VoD data for unconfined rate sticks (air confinement) of multiple radii. The resulting parameters are used to predict the VoD in slabs of varying thickness. For the less ideal explosive, EM120D, data for unconfined rate sticks are used for the calibration. Predictions are then made for rate sticks confined by concrete and steel.

The detonation wave is initiated using a booster - an area of high pressure gas which shocks the explosive, initiating the reaction. After the start of the simulation, the detonation wave must be modelled for some time to allow it to settle to its

5.7 Predictive Modelling of Detonation Waves in Rate Sticks and Slabs

steady speed. Once the wave has converged, the speed can be measured by simply observing the distance covered in some time interval, as described in section 5.6. The measurement of the position of the shock wave introduces an error related to the discretisation of the grid. However the error in the speed measurement can be reduced by measuring the speed over longer time intervals, once the wave is steady.

For unconfined rate sticks and slabs, the confining air is modelled with the ideal gas EoS with adiabatic gamma equal to 1.4. For rate sticks of EM120D with solid confinement, the shock Mie-Grüneisen EoS is used to model concrete and steel with the same parameters as Schoch et al. [108]. Note that while the mathematical formulation uses a temperature equilibrium condition between reactants and products, only pressure equilibrium is used between the explosive and confiner [91]. As such, temperatures in the confiner are inconsequential and use of the shock Mie-Grüneisen EoS is appropriate. This EoS does however neglect the effect of strength in the solid confiner. The pressures generated in the detonation wave are however very large in comparison to the yield stress, which justifies this simplification.

A linear fit of experimental data for the shock speed is used to determine the parameters a and b

$$D = a + bu. \quad (5.48)$$

Using the empirically justified assumption that the relationship is indeed a straight line, the Rankine-Hugoniot conditions can be used to derive the pressure and energy as a function of volume on the Hugoniot locus. The Hugoniot is then used as a reference curve for an EoS of Mie-Grüneisen form:

$$p - p_{\text{REF}}(v) = \rho\Gamma(e - e_{\text{REF}}(v)) \quad (5.49)$$

$$p_{\text{REF}}(v) = \frac{\rho_0\chi a^2}{(1 - b\chi)^2} \quad (5.50)$$

$$e_{\text{REF}}(v) = \frac{1}{2}(v_0 - v)p_{\text{REF}}(v) \quad (5.51)$$

$$\rho\Gamma = \rho_0\Gamma_0, \quad (5.52)$$

where Γ_0 is the ambient Grüneisen gamma, $\rho_0 = 1/v_0$ is the initial density and χ is defined as

$$\chi = 1 - \frac{v}{v_0}. \quad (5.53)$$

The parameters for modelling concrete and steel are given in Table 5.2.

5 Detonation Modelling

	ρ_0 [kgm ⁻³]	a [ms ⁻¹]	b	Γ_0
Steel [127]	7840	3670	1.645	2.0
Concrete [30]	2340	2235	1.745	2.0

Table 5.2: Parameters for the shock Mie-Grüneisen EoS for modelled confinement.

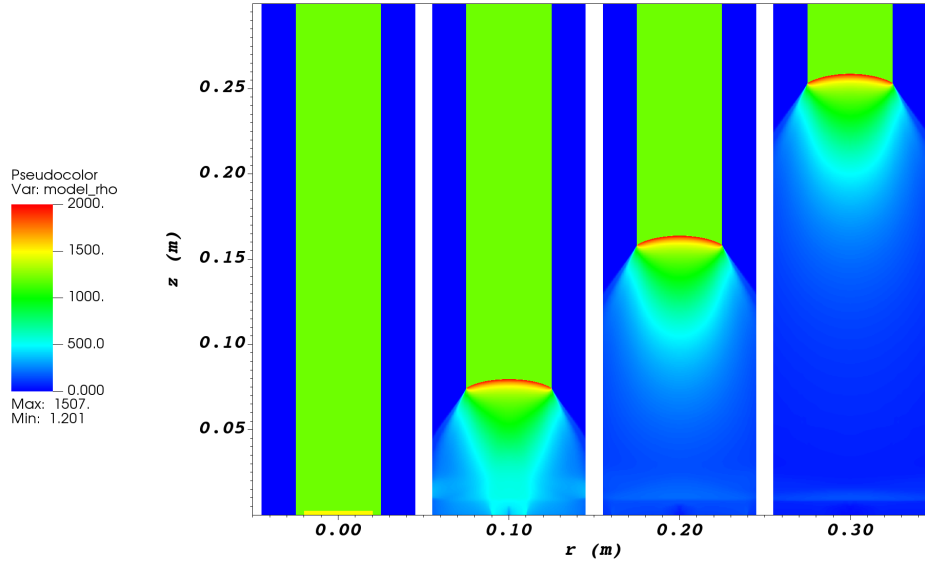


Figure 5.10: Time progression of air confined EM120D. Times are 0, 16 μ s, 32 μ s, 50 μ s.

Figure 5.10 shows four snapshots of a slice through the centre of a cylindrical rate stick. In the left-most plot, the unreacted rate stick is visible as the green rectangle, while the blue, lower-density area shows the confining air. The thin yellow rectangle at the bottom of the domain is the high pressure booster which initiates the detonation. In the subsequent plots, the detonation wave, which can be identified as the red area of highest density propagates upwards through the domain. Note that the simulations are done in half the domain with a reflective boundary through the middle and a cylindrical symmetry source term (see Section 5.4).

The acoustic impedance of air is low, meaning rate sticks confined by only air are ‘weakly’ confined. This means that the sonic locus intersects the shock front at the

explosive confiner interface. This is clearly visible in Figure 5.11. For solid confiners with higher acoustic impedance which provide ‘strong’ confinement, on the other hand, the sonic locus intersects the explosive confiner interface behind the shock front. This regime change is discussed in detail by Bdzil and Stewart [16]. Figures 5.12 and 5.13 show strongly confined detonation waves for EM120D confined by concrete and steel respectively. In contrast to Figure 5.11, the shock wave in the confining material has a higher pressure, and the product gases depressurize much more slowly. Furthermore the shockfront is less curved. In each case the sonic locus can be identified as the back boundary of the detonation driving zone (DDZ).

The cell size of the coarsest grid for these simulations was 0.5mm with two levels of adaptive mesh refinement of factor 2 and 4 respectively. The finest grid, which covered the whole detonation driving and the material interface thus had a cell width of $62.5\mu\text{m}$. This corresponds to approximately 80 cells per reaction zone width.

Figure 5.14 shows a detonation wave in a PBX 9502 rate stick. Note that the rate stick is much narrower with radius 8mm, and yet the shock front is flatter than what was observed in a 25mm radius rate stick of EM120D (Figure 5.11). In PBX 9502 the lengthening of the reaction zone in the rate stick is quite pronounced in comparison to a one dimensional detonation wave. In comparison to EM120D, the detonation velocity ($7516 \pm 10\text{ms}^{-1}$) is much closer to the ideal detonation velocity of 7755ms^{-1} .

For PBX 9502 the resolution of the coarsest grid was doubled with respect to the simulations of EM120D, and two levels of adaptive mesh refinement of factor 4 were used, such that the finest grid had a cell width of $15.625\mu\text{m}$. This corresponds to approximately 65 cells per reaction zone width.

5.7.2 Calibration of the Reaction Rate for EM120D

The reaction rate is very difficult to measure experimentally or to evaluate on the basis of chemical arguments. In reality the explosive does not transition directly from reactants to products but undergoes many intermediate reactions associated with varying amounts of energy. For the purposes of the simulation, these processes

5 Detonation Modelling

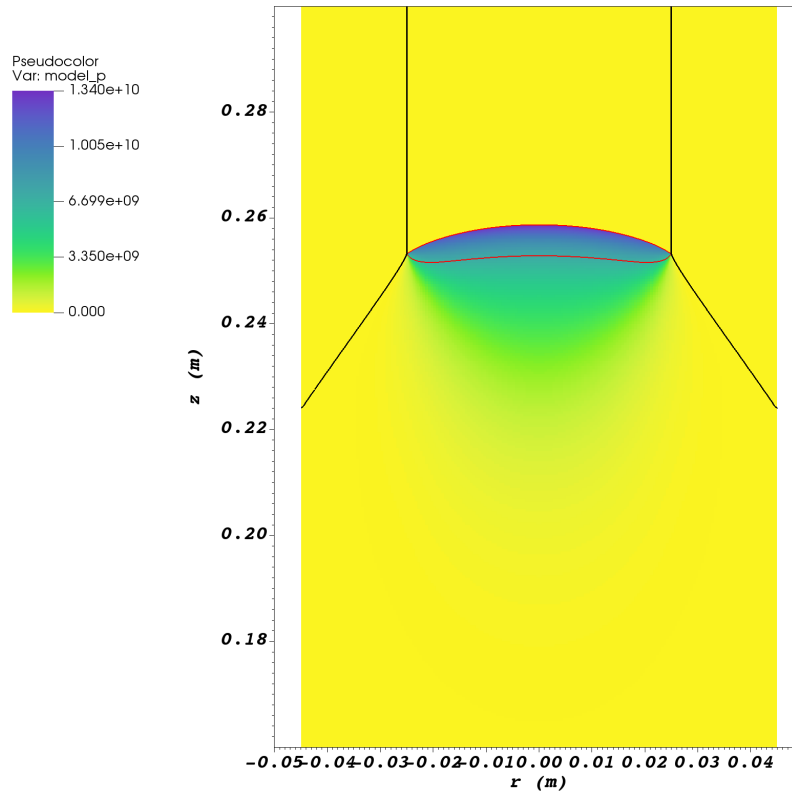


Figure 5.11: The pressure is plotted for a detonation wave propagating upwards in a EM120D rate stick of radius 25mm confined by air. The black line indicates the explosive-air interface, while the red contour serves to show the boundary of the detonation driving zone (DDZ). The detonation velocity was measured to be $5274 \pm 10\text{ms}^{-1}$, significantly slower than the ideal detonation velocity of 6389ms^{-1} .

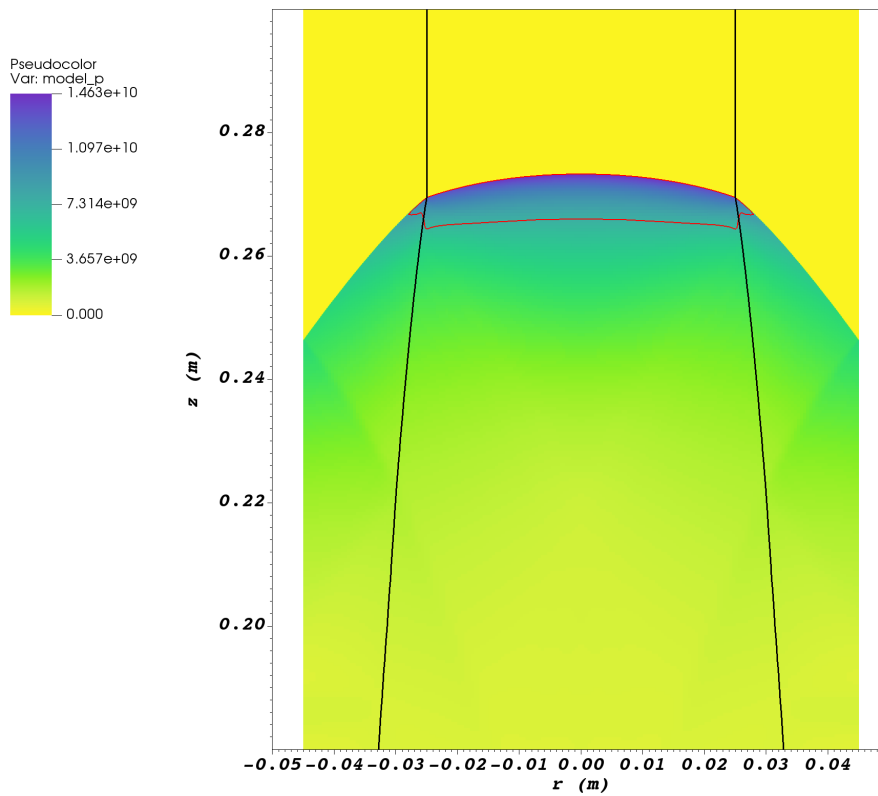


Figure 5.12: The pressure is plotted for a detonation in EM120D confined by concrete. The interface between explosive and confiner is shown in black, while the red line shows the boundary of the DDZ. The detonation wave speed for this radius (25mm) was $5486 \pm 10\text{ms}^{-1}$, faster than the rate stick confined by air (Figure 5.11).

5 Detonation Modelling

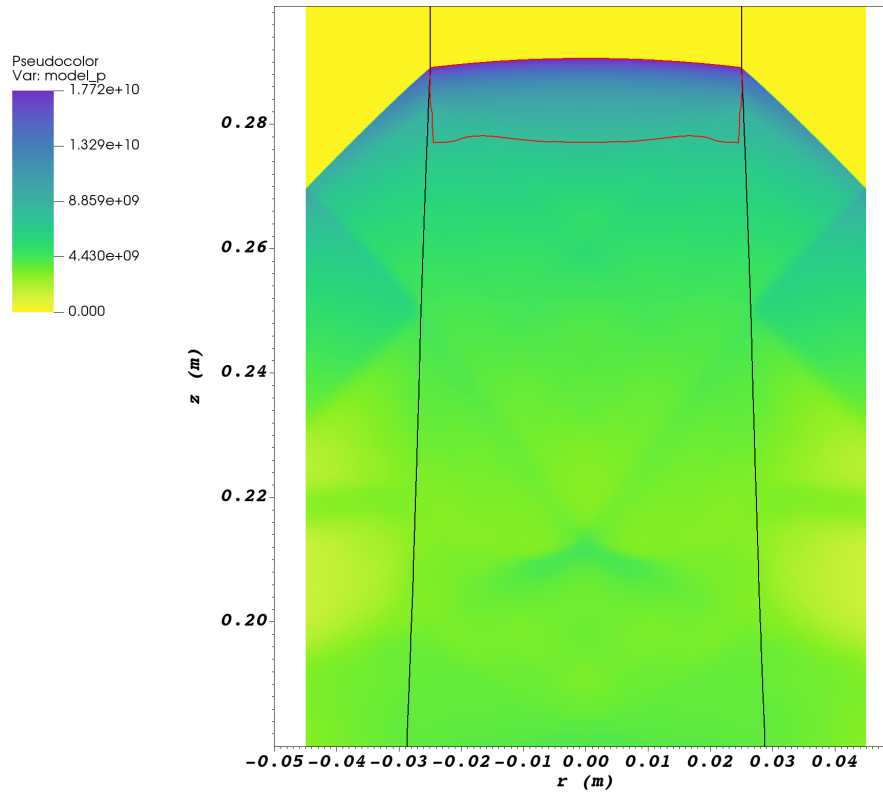


Figure 5.13: This plots shows a detonation wave in a rate stick of EM120D confined by steel. The wave is qualitatively similar to Figure 5.12, however the deflection of the explosive-confiner interface (black) is even less, due to the higher acoustic impedance of steel. The detonation wave was faster still at $5940 \pm 10 \text{ms}^{-1}$.

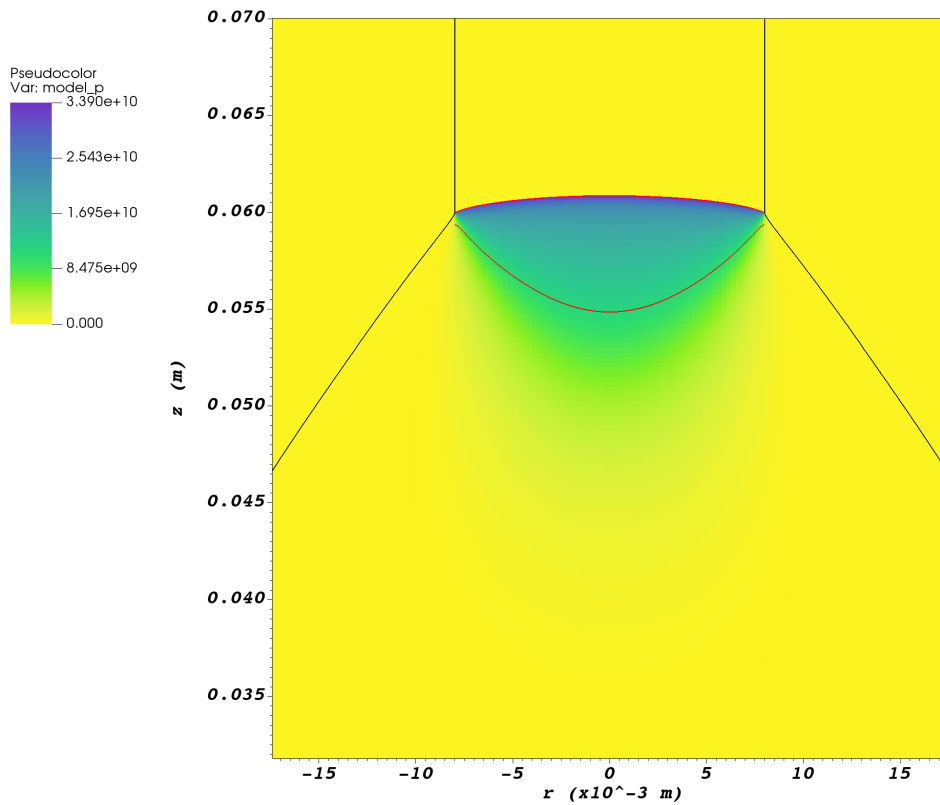


Figure 5.14: The pressure distribution in a detonation rate stick of PBX 9502 with radius 8mm confined by air is plotted. The wave is qualitatively similar to what was observed for EM120D (Figure 5.11), however the pressure is significantly larger, and the shock front is noticeably flatter despite the rate stick having a lower diameter.

5 Detonation Modelling

are combined into a single pressure-dependent expression, K , for the reaction rate as is used by Schoch et al. [108],

$$K = \frac{d\lambda}{dt} = -\lambda^{indx} \left(p \frac{1 - a_h}{\tau_s} + H(p - p_h) \frac{a_h}{\tau_h} \left(\frac{p[\text{Pa}]}{10^9} \right)^{N_p} \times 10^9 \right), \quad (5.54)$$

where

$$a_h = \exp \left(- \left(\frac{1 - \lambda}{\omega_h} \right)^{N_a} \right).$$

The leading coefficient causes the reaction rate to slow as the reaction nears completion. The regression index of the reaction is *indx*. The second term represents the hotspot reaction, where $H(x)$ is the Heaviside function, and p_h is the critical pressure required for ignition. The first term is a bulk burning term which determines the reaction rate once the explosive is fully ignited. The parameter a_h is initially 1, causing the hotspot reaction term to dominate. As the reaction progresses, a_h approaches zero, and the equation becomes dominated by the bulk burning term.

ω_h determines the degree to which the hotspot process consumes the available explosive. τ_s and τ_h determine the time scales of the reaction, and the constant N_a controls the speed at which the hotspots transition to a bulk burning process. Note that it is the pressure in GPa which is raised to the power of N_p .

The calibration was carried out using data from Dremin [39] (which is also used by Schoch et al. [108]) for the rate sticks confined by air. It is then demonstrated that the same parameters allow for predictions to be made for detonation waves in rate sticks confined by solids. The only input required for the predictions is the EoS of the confining material.

It was found that the principal parameters affecting the VoD were τ_h and N_p . The other parameters were assigned the same values as were used by Schoch et al. [108]. This was done purely because it was found that changing these parameters was not necessary to achieve the desired predictive capability.

Since there were only two degrees of freedom in the calibration process, only two data points were required to fully constrain the system. These were chosen to be the detonation velocities for 20 mm and 30 mm rate sticks which were 4920 ms^{-1}

5.7 Predictive Modelling of Detonation Waves in Rate Sticks and Slabs

and 5470 ms^{-1} respectively [39]. The merit function was simply the sum of the absolute difference of the VoD between experiments and simulations for the two radii.

A two-dimensional implementation of the secant method was applied to minimize the difference between the numerical results and the experimental data. For each radius three evaluations of the velocity with different parameters are required to construct a two-dimensional plane in three dimensional space relating the values of the parameters with the VoD. The intersection of this plane with the experimental VoD constitutes a line through the two-dimensional parameter space. The final step is to find the intersection between this line and a similarly calculated line for the second value of the radius.

This process is repeated iteratively until good agreement with the experimental velocities is found. The results of the calibration along with the other parameters are presented in Table 5.3.

τ_h	13 μsGPa
τ_s	20 μsGPa
p_h	1.51 GPa
$indx$	0.667
ω_h	0.95
N_a	9.0
N_p	1.11

Table 5.3: Parameters for the reaction rate model for EM120D. See equation (5.54).

Figure 5.15 shows the simulation results as squares for the calibrated reaction rate. These results are fit using the empirical Eyring equation [27]

$$D = D_{CJ} \left(1 - \frac{A}{R - R_C} \right). \quad (5.55)$$

The resulting values for A and R_C are in Table 5.4.

Figure 5.15 shows good agreement between the predictions from the Eyring fits and the experimental data [39]. The magenta markers represent the experimental measurements which are used to inform the reaction rate parameters. The blue

Confiner	A [mm]	R_C [mm]
Air	3.73	3.5
Concrete	3.61	-0.6
Steel	1.94	-2.8

Table 5.4: Parameters for the fits of the radial dependence of the VoD with rate stick radius for EM120D, with ideal VoD $D_{C,J} = 6.3895 \text{ km s}^{-1}$.

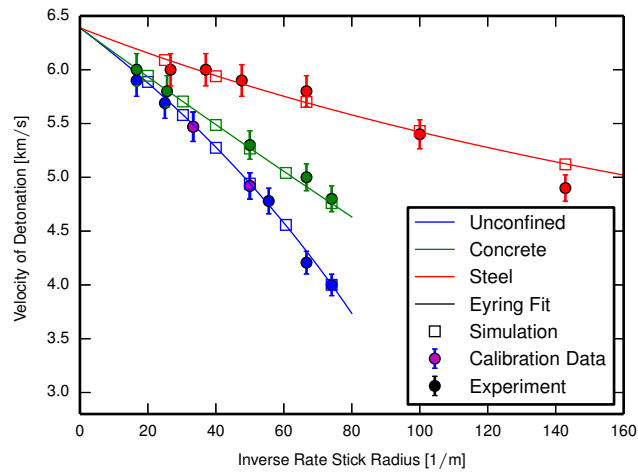


Figure 5.15: The plot shows the radial dependence of the VoD for rate sticks of EM120D. The lines interpolate the numerical results (square markers) using Eyring fits. The circular markers with error bars are the experimental data [39]. The experimental data for unconfined rate sticks that were used for the calibration are highlighted with magenta markers.

markers are measurements of unconfined rate sticks with other radii. The box markers represent individual simulations. The lines are the Eyring fits through the simulation results. The lines for steel and concrete show good agreement over a wide range of radii with the exception of the narrowest steel confined rate stick. This is consistent with the results of Schoch et al. [108]. Furthermore the detonation velocities for unconfined rate sticks show good agreement for all radii despite the calibration having been done using the data points for 20 mm and 30 mm radius only. The Eyring equation fits the simulation data well, indicating that the simulations are converging towards the ideal VoD in the large radius limit as is expected.

The fact that the calibration was successful using just two parameters and two data points demonstrates that the physics of the detonation waves is being captured well by the EoS models and the MiNi16 formulation.

5.7.3 Calibration of the Reaction Rate for PBX 9502

For PBX 9502 we use a simplified version of the ignition and growth model presented by Tarver and McGuire [124] and used by Wescott et al. [129]. We calibrate the reaction rate model using VoD data for unconfined rate sticks [63]. The model is used to predict the VoD in slabs of varying thickness. The predictions are then compared with experimental data [63].

The form of the reaction rate was chosen to be

$$K = r_{DG}S_G(\lambda), \quad (5.56)$$

where

$$r_{DG} = k_{DG}(1 - \lambda)^{1/3}\lambda^{N_\lambda} \quad (5.57)$$

$$S_G = \frac{1}{2}(1 - \tanh(30(0.1 - \lambda))). \quad (5.58)$$

However the results presented here are not necessarily incompatible with a pressure dependent model. This could be achieved through modification of the form of the reaction rate or adjustment of the exponents.

5 Detonation Modelling

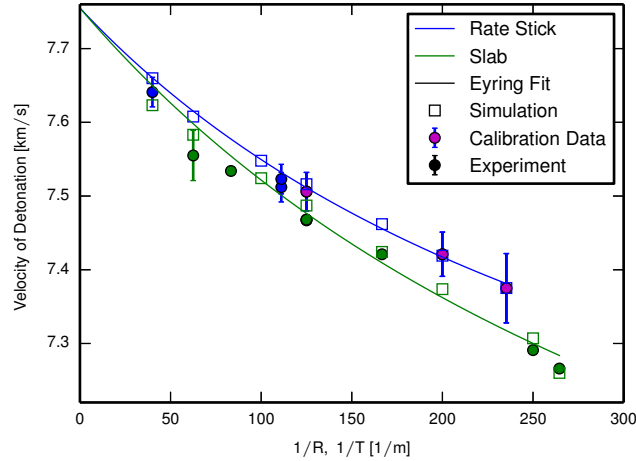


Figure 5.16: The dependence of the VoD with size is presented for both rate sticks and slabs. The lines are Eyring fits through the simulation data (square markers), while the markers represent the experimental data [63]. Note that for slabs the x axis represents the inverse thickness, where the thickness is measured across the whole slab, while for rate sticks the radius, not the diameter, is used.

Confiner	A [mm]	R_C [mm]
Rate sticks	0.34	-2.8
Slabs	0.37	-2.3

Table 5.5: Parameters for the fits of the radial dependence or thickness dependence of the VoD of PBX 9502, with $D_{CJ} = 7.755 \text{ kms}^{-1}$.

The calibration was carried out using the same methodology as was applied for the emulsion in section 5.7.2. In this case the two free parameters are k_{DG} and N_λ . The final value for k_{DG} was $60.65 \mu\text{s}^{-1}$, while N_λ was 1.56.

The results are shown in Figure 5.16. The parameters for the Eyring fits are given in Table 5.5. The simulations match the experimental measurements for rate sticks across the whole range of radius. The predictions for detonation velocities in slabs of varying thickness are also in good agreement with the experimental data.

5.8 Conclusions

In this chapter we have presented the MiNi16 mathematical formulation [91] for modelling an explosive and its interaction with other materials. The interface between the explosive and the confiner is modelled using a diffuse interface model. Furthermore the explosive is modelled using pressure and temperature equilibrium, which can be applied irrespective of the presence of shock waves. The resulting formulation is thus agnostic to the state of the material within a particular cell; the same algorithm can be applied across the whole domain of the simulation.

The implementation of the numerical methods has been validated using Riemann tests. The numerical methods have also been tested by simulating one dimensional detonation waves. This allows us to confirm that we can successfully reproduce the detonation wave structure predicted by the ZND theory. This validates the work presented in Chapter 4. It also tests the implementation of the closure conditions which affect the evolution of the state in the reaction zone.

We have also demonstrated that given some experimental data with which to calibrate parameters for the reaction rate, it is possible to predict the detonation velocity in a variety of situations. Due to the loss of energy to the confiner, detonation waves in rate sticks and slabs propagate at a velocity slower than the ZND velocity. The deviation between the actual detonation velocity and that predicted by the ZND theory depends on the geometry of the explosive, the material properties of the confiner and the reaction rate. Having determined suitable values for the parameters of the reaction rate model, the same parameters have been used to predict the detonation velocity. For both PBX 9502 and EM120D, we have taken this approach to predict detonation velocities and found good agreement with experimental data. These predictions serve to validate the equations of state presented in Chapter 3.

6 Direct Calibration of Reaction Rate Models

6.1 Introduction

In the previous chapters a methodology has been presented to calibrate equations of state and a reaction rate model, which collectively constitute a model for the explosive. We have shown that an explosive model calibrated in this way can be used to predict detonation velocities. This calibration process involves application of an optimization algorithm in order to determine the parameters of the reaction rate model. The objective function of this optimization is the difference between the hydrocode results and the experimental measurements of the detonation velocity. Given the computationally intensive nature of the hydrocode simulations, the optimization quickly becomes intractable for large datasets or a large number of calibration parameters.

In this chapter, an approach is presented with which to determine reaction rate parameters directly. In other words without resorting to the use of the hydrocode. This is done by exploiting the gauge data from shock to detonation transition experiments. These experiments use embedded gauges in the explosive to measure the flow velocity and/or the pressure to study the shock to detonation transition which occurs following an impact of a projectile with the explosive. The flow is naturally dependent on the reaction rate, and thus we can analyse the data and extract information about the reaction rate.

The approach taken here builds on the Lagrangian analysis presented by Seaman [109]. Similar analysis was also carried out in the development of the DAGMAR (Direct Analysis Generated Modified Arrhenius Rate) reaction rate model [3, 45,

128]. The method presented here is built around the observation that, unlike a shock wave in an inert material, a shock wave in a reactive material will accelerate. This acceleration results from the exothermic chemical reaction which is induced by the increase of pressure and temperature behind the shock wave. This phenomenon is of course closely related to the mechanism by which a shock wave in a reactive material will transition to detonation.

Shock to detonation transition has been studied experimentally, theoretically as well as numerically. The exact mechanism by which the transition occurs can be split into two regimes. These two mechanisms were first observed experimentally by Campbell et al. [25, 26].

In each case the impact of a projectile creates a shock wave which propagates from the projectile explosive interface into the explosive. On the one hand, for homogeneous explosives it has been observed that following some induction time, thermal runaway occurs at the interface [31, 113, 114]. This occurs since the part of the explosive closest to the interface was shocked earliest, and thus has been undergoing chemical reaction for longest. Following thermal runaway, a detonation wave develops at the interface. This detonation wave is propagating in material which has already been subject to a shock wave. The detonation wave therefore propagates faster than it would otherwise, and is described as a ‘super-detonation’. The super-detonation propagates faster than the initial shock wave and eventually overtakes it. It is the overtake time which is typically considered the point at which the wave transitions to detonation.

In heterogeneous explosives, on the other hand, experiments show that the initial shock wave will gradually accelerate until it eventually transitions to detonation [49, 133]. Detailed analysis of the dynamics of this process is presented by James [64]. This dichotomy of behaviour is discussed by Menikoff [83], and has also been reproduced numerically by Mi et al. [89].

The methodology presented in this chapter is most suitable for heterogeneous explosives, since in this case the shock wave exhibits a faster acceleration, which can be evaluated more accurately from the experimental data. A shock wave propagating through a reactive material will accelerate, and the shape of such an accelerating wave cannot be the same as that of a shock wave in an inert material. From exper-

imental measurements it is clear that the flow behind the shock wave is not steady, as it would be in an inert material [49]. Instead, during the ignition stage, the flow velocity and pressure increase continuously following the initial discontinuity.

Given information about the flow field and reaction rate at a given instance, the Euler equations can be applied to calculate the evolution of the flow and the acceleration of the wave. Furthermore, it follows that this calculation can be inverted; experimental observations of the evolution of the wave permit direct calculation of the reaction rate. Naturally this process relies on the accuracy of the equations of state for both the reactants and products. In the analysis presented here, we apply the equations of state calibrated for PBX 9502 in Chapter 3. We therefore consider the parameters of the equation of state fixed. Nevertheless it should be noted that errors involved in the equation of state calibration will contribute to further errors in the calculation of the reaction rate.

There are two principal sources of data which can be used, firstly measurements obtained from Lagrangian gauges which measure flow velocity or pressure as a function of time and move with the flow. We can also make use of data from a shock tracker to directly measure the velocity and acceleration of the shock wave. Details of the methodology for these experimental techniques are given by Gustavsen et al. [49].

Values for the reaction rate calibrated in this way can be applied in two ways. Firstly, values for the reaction rate can be used to quantitatively assess the suitability of a given reaction rate model. For example, shock to detonation transition experiments can be carried out at different initial temperatures thus sampling states which are offset from the Hugoniot curve corresponding to ambient initial conditions [8]. Application of the method presented in this chapter to such data would permit us to quantitatively assess the validity of a pressure rate law in this situation. This would be done by directly comparing the calculated reaction rate at some fixed pressure for various initial temperatures. It is already well known that a pressure dependent rate law is inadequate in these circumstances [8]. However it is still unclear how a temperature dependent rate law such as that presented by Aslam [8] compares to an entropy dependent model such as CREST [51]. The method presented here offers an opportunity to answer such questions.

Secondly, the results can be applied to calibrate the parameters for a given reaction rate law. The data obtained from shock to detonation transition experiments corresponds to the reaction rate in the pure reactants immediately following a shock wave (at $\lambda = 1$). In this work we make the assumption that the reaction rate, a function of both the thermodynamics and the reactant mass fraction, λ , is separable,

$$\frac{D\lambda}{Dt} = f(T, p, S)g(\lambda). \quad (6.1)$$

In this case the method presented here can be used to fully determine the parameters of the thermodynamic dependence, f . The parameters of g must be determined separately. Significantly, the parameters of g can be determined by global optimization significantly more efficiently than an equivalent optimization involving the parameters of both f and g .

For some applications, it may be desirable to avoid the use of optimization entirely, in which case the parameters of g may be determined using data for the width of the reaction zone. This can be done following the method presented in Section 6.6.

On the other hand, it may be required to use optimization in order to achieve a greater degree of accuracy. In this case, parameters calculated using this method can serve as a starting point, dramatically reducing the time required for the optimization.

In this chapter we present the methodology behind this approach and demonstrate that the method can be applied in practice using sample data which has been generated for an idealized explosive. The method is then applied to the TATB based explosive PBX 9502. Finally we present simulations that were carried out to compare our model with experiments of detonations of both rate sticks and slabs.

6.2 Methodology

The key idea behind this method is to analyse the flow which is measured by experimental gauges in the explosive material directly following the shock wave. An inert, supported shock wave will cause a gauge to accelerate, and then continue to be carried by the flow at a steady velocity. In shock to detonation experiments,

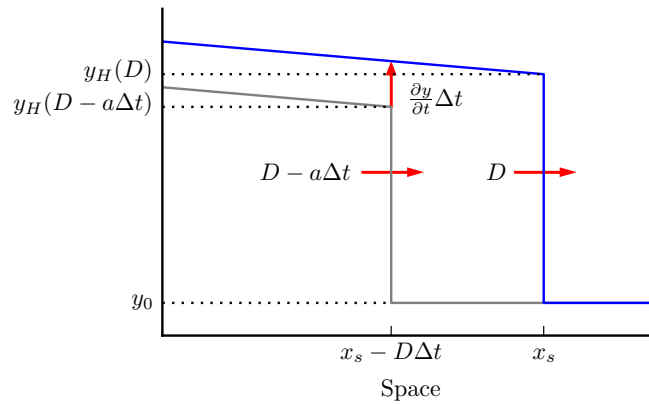


Figure 6.1: This figure shows two time snapshots of an accelerating shock wave with velocity, D , and acceleration, a , as a function of space. The grey line shows the shock wave Δt before the blue line.

on the other hand, gauges are observed to accelerate following the shock [49, 133]. This acceleration can be explained by considering two properties of the flow. Firstly, the shock wave is itself accelerating as it propagates. Secondly, following the passing of the shock wave, the material will begin to react.

With knowledge of the equations of state and the rate law, it is possible to calculate the properties of the flow field. And similarly if the properties of the shocked material can be measured experimentally, this gives us information about the rate of the chemical reaction.

The key step for this analysis is to observe that for the flow behind the shock wave, for any thermodynamic variable, we can relate the spatial derivative, with the acceleration of the shock wave, and the time derivative. This relationship is dependent on the Rankine-Hugoniot conditions and thus also dependent on the equation of state.

Figure 6.1 shows two time snapshots of an accelerating shock wave in space, using some thermodynamic variable y (y could represent pressure, density or flow velocity). The subscript H is used to represent the value immediately after the shock, which can be calculated using the Rankine-Hugoniot conditions and the shock speed, D . Since the shock is accelerating, the post-shock state $y_H(D)$ is reduced for the grey line.

6 Direct Calibration of Reaction Rate Models

The wave is travelling to the right at a speed D , so the distance covered by the wave in time Δt is to first order $D\Delta t$. As such, we can write

$$\begin{aligned}\frac{\partial y}{\partial x} &= \lim_{\Delta t \rightarrow 0} \frac{y_H(D) - \left(y_H(D - a\Delta t) + \frac{\partial y}{\partial t} \Delta t \right)}{D\Delta t} \\ &= \lim_{\Delta t \rightarrow 0} \frac{\frac{\partial y_H}{\partial D} a\Delta t - \frac{\partial y}{\partial t} \Delta t}{D\Delta t} \\ &= \frac{1}{D} \left(a \frac{\partial y_H}{\partial D} - \frac{\partial y}{\partial t} \right).\end{aligned}\tag{6.2}$$

where $a = \frac{\partial D}{\partial t}$ is the acceleration of the wave and $\frac{\partial y}{\partial x}$ is the space derivative immediately to the left of the shock wave.

It is convenient to write the equation using the material derivative, which is defined as

$$\frac{D}{Dt} = \frac{\partial}{\partial t} + u \frac{\partial}{\partial x},\tag{6.3}$$

where u is the flow velocity. This can be done by considering the system in Figure 6.1 in a reference frame where the flow velocity behind the shock is zero. Equation (6.2) is equivalent to

$$\frac{\partial y}{\partial x} = \frac{1}{u_s} \left(a \frac{\partial y_H}{\partial D} - \frac{Dy}{Dt} \right),\tag{6.4}$$

where $u_s = D - u_H(D)$ is the propagation velocity of the wave in the boosted reference frame.

An equation of the form of (6.4) is required for the flow velocity, u , and the pressure, p ,

$$\frac{\partial u}{\partial x} = \frac{1}{u_s} \left(a \frac{\partial u_H}{\partial D} - \frac{Du}{Dt} \right)\tag{6.5}$$

$$\frac{\partial p}{\partial x} = \frac{1}{u_s} \left(a \frac{\partial p_H}{\partial D} - \frac{Dp}{Dt} \right).\tag{6.6}$$

The derivatives of the Hugoniot functions are dependent on the equation of state. The pressure, $p_H(v)$, on the Hugoniot is given by equation (4.9) in Chapter 4. The expression for p_H can be substituted into equation (4.5) and equation (4.4) to calculate $u_H(v)$ and the shock speed, D , as a function of post-shock specific volume,

v ,

$$u_H(v) = \sqrt{(p_H(v) - p_0)(v_0 - v)} \quad (6.7)$$

$$D(v) = v_0 \sqrt{\frac{p_H(v) - p_0}{v_0 - v}}. \quad (6.8)$$

We can now calculate the derivatives using

$$\frac{\partial u_H}{\partial D} = \frac{\partial u_H}{\partial v} / \frac{\partial D}{\partial v} \quad (6.9)$$

$$\frac{\partial p_H}{\partial D} = \frac{\partial p_H}{\partial v} / \frac{\partial D}{\partial v}. \quad (6.10)$$

Note that these derivatives are done entirely via analytic methods, even for complex non-linear equations of state.

The Euler equations can be expressed using material derivatives as

$$\frac{D\rho}{Dt} + \rho \frac{\partial u}{\partial x} = 0 \quad (6.11)$$

$$\rho \frac{Du}{Dt} + \frac{\partial p}{\partial x} = 0 \quad (6.12)$$

$$\frac{DE}{Dt} + (E + p) \frac{\partial u}{\partial x} = 0, \quad (6.13)$$

where ρ is the density and E is the total specific energy. Note that we have implicitly made the assumption that there is a single value for the flow velocity and the pressure in the reactant product mixture.

Using a general equation of state for the explosive,

$$e = e(\rho, p, \lambda), \quad (6.14)$$

which defines the specific internal energy, e , as a function of the density, ρ , pressure, p , and the mass fraction of the explosive which is unreacted, λ , we can relate the material derivatives of the thermodynamic variables using

$$\begin{aligned} \frac{DE}{Dt} &= \frac{D}{Dt}(\rho e(\rho, p, \lambda)) \\ &= \left(e + \rho \frac{\partial e}{\partial \rho} \right) \frac{D\rho}{Dt} + \rho \frac{\partial e}{\partial p} \frac{Dp}{Dt} + \rho \frac{\partial e}{\partial \lambda} \frac{D\lambda}{Dt}. \end{aligned} \quad (6.15)$$

Since we are operating in a reference frame where the flow velocity is zero, the energy has no first order kinetic energy contribution. In this equation $\frac{D\lambda}{Dt}$ is nothing but the reaction rate.

6 Direct Calibration of Reaction Rate Models

Equations (6.5),(6.6),(6.11),(6.12),(6.13),(6.15) constitute a system of six linear equations with eight unknowns:

$$\frac{D\rho}{Dt}, \frac{Du}{Dt}, \frac{Dp}{Dt}, \frac{DE}{Dt}, \frac{D\lambda}{Dt}, a, \frac{\partial u}{\partial x}, \frac{\partial p}{\partial x}.$$

The remaining terms and coefficients can all be calculated using the equations of state of the reactants and products and the strength of the shock wave. Given two of these eight unknowns, the system is fully constrained and we can calculate the remaining six unknowns.

Flow velocity data from gauges in shock to detonation transition experiments can be used to evaluate the strength of the shock (via measurement of u_H) and the material derivative $\frac{Du}{Dt}$. Using the data from neighbouring gauges in the explosive, it is furthermore possible to evaluate the acceleration of the shock wave. Note that for this purpose, data from a shock tracker could also be used and may potentially offer greater accuracy if the number of gauges is small. The most accurate way of doing this was found to be through evaluating the derivative of an interpolating cubic spline for $u_H(t)$, constructed using the u_H values from gauges shocked at different times. As such the accuracy of this method is dependent on having many gauges with sufficiently small separation from each other. However if data from pressure gauges were available, $\frac{Dp}{Dt}$ could be used to constrain the system in place of the acceleration.

It is interesting to consider the physical significance of the fact that this system of equations has two degrees of freedom. It means that the acceleration of a shock wave in the explosive is not solely a function of the reaction rate – the acceleration is dependent on the gradients behind the shock, and is thus dependent on the history of the shock wave (the speeds of the shock wave at previous times).

This is significant since it means that it is not possible in general to construct a function which describes the acceleration of a shock wave in terms of the shock wave strength. While we can construct such a function using the data from a single experiment, we cannot expect the same function to work for a different experiment which is carried out in different conditions, for example with a different initial pressure.

6.3 Proof of Concept

To demonstrate the validity of the approach presented above, we begin by applying it to an idealized explosive. We simulate shock to detonation transition in an ideal, gas phase explosive, and generate flow velocity data as would be measured by experimental gauges. The idea is to create some gauge data, which is free of experimental error, for a case where the reaction rate is known. We will then apply the methodology developed above to calculate the reaction rate in the explosive and verify the applicability of the method in practice.

For this purpose we model the explosive with the inviscid Euler equations and an ideal gas equation of state,

$$p = \rho(\gamma - 1)(e + (1 - \lambda)Q), \quad (6.16)$$

which is dependent on the reactant mass fraction, λ , ($\lambda = 1$ for reactants, and $\lambda = 0$ for products). In this case, if the reaction rate is to be positive, it must be defined as $-\frac{D\lambda}{Dt}$. The specific heat of combustion is Q . The adiabatic gamma, γ , is chosen to be 1.4 throughout. For this idealized explosive we have

$$\frac{\partial e}{\partial \lambda} = Q \quad (6.17)$$

$$\frac{\partial e}{\partial p} = \frac{1}{\rho(\gamma - 1)} \quad (6.18)$$

$$\frac{\partial e}{\partial \rho} = -\frac{p}{\rho^2(\gamma - 1)}. \quad (6.19)$$

The Hugoniot pressure, $p_H(v)$, is expressed in terms of specific volume as

$$p_H(v) = \frac{p_0 v_0 + \frac{\gamma-1}{2} p_0 (v_0 - v)}{v - \frac{\gamma-1}{2} (v_0 - v)}, \quad (6.20)$$

where v_0 and p_0 are the initial specific volume and initial pressure respectively. For the present objectives we can work in dimensionless variables, and so we define the temperature, T , as

$$T = p/\rho. \quad (6.21)$$

The initial conditions for the explosive are chosen to be $\rho = p = T = 1$.

We employ an Arrhenius form for the reaction rate

$$-\frac{D\lambda}{Dt}(T, \lambda) = \lambda A \exp\left(-\frac{T_A}{T}\right) \quad (6.22)$$

6 Direct Calibration of Reaction Rate Models

We define the parameters A and T_A in terms of the dimensionless activation temperature, \tilde{T}_A , the initial post-shock temperature, T_H , and \tilde{A} .

$$T_A = \tilde{T}_A T_H \quad (6.23)$$

$$A = \frac{\tilde{A}}{Q} \exp(\tilde{T}_A) \frac{1}{\tilde{T}_A} \quad (6.24)$$

The form of these equations has been chosen such that the initial post-shock rate of change of the temperature is

$$\begin{aligned} \frac{DT}{Dt} &= \left. \frac{\partial T}{\partial \lambda} \right|_{\rho, e} \frac{D\lambda}{Dt} \\ &= (\gamma - 1) Q \lambda \frac{\tilde{A}}{Q} \exp(\tilde{T}_A) \frac{1}{\tilde{T}_A} \exp\left(-\frac{\tilde{T}_A T_H}{T_H}\right) \\ &= (\gamma - 1) \lambda \tilde{A} \frac{1}{\tilde{T}_A} \end{aligned} \quad (6.25)$$

With this choice, the induction time is to a first approximation a function of \tilde{A} only.

We use $Q = 11.6269$ and $\tilde{A} = 9.3765$. These values have been chosen such that if we were to use $\tilde{T}_A = 14.99$ and a Mach 3 ignition shock wave, the dynamics of the system would be the same as that modelled by Nikiforakis and Clarke [95]. However the high activation temperature used in that study leads to ignition behaviour which is not conducive to application of the method presented in this work. For higher activation energies, the shock propagates through the explosive with very little acceleration. After some induction time, thermal runaway occurs at the boundary, and a super-detonation wave develops.

In the present work, we use a lower activation temperature of $\tilde{T}_A = 10$. The behaviour is qualitatively different in this case. We have done two simulations, one with an ignition shock of Mach 3, and the other with an ignition shock of Mach 3.25. However T_H is kept fixed at the value corresponding to a Mach 3 wave, so that the reaction rate is the same for the two simulations. The ignition shock wave is created in the simulation using a reflective boundary condition and by initializing the explosive with a non-zero velocity towards the boundary, u_0 . The parameters are summarized in Table 6.1. Figures 6.2 and 6.3 show the gauge data for an initial shock of Mach number 3 and 3.25 respectively. For clarity, only 15 of the 45 gauges are shown in the plot.

Q	11.6269	
\tilde{A}	9.3765	
\tilde{T}_A	10	
T_H	2.6790	
Initial Mach number	3	3.25
u_0	2.6294	2.9012

Table 6.1: Parameters for ignition to detonation of an idealized explosive.

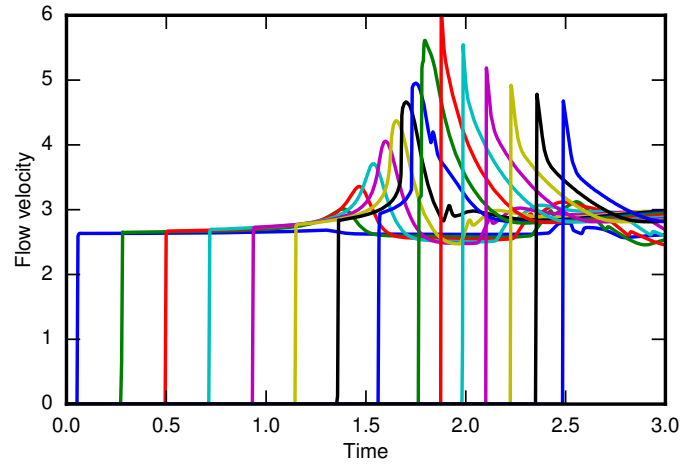


Figure 6.2: Gauge data for shock to detonation transition for an idealized explosive, with a Mach 3 ignition shock. The units are dimensionless.

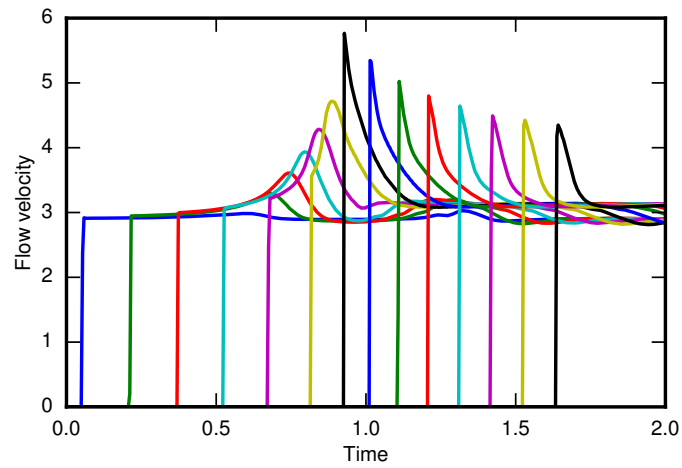


Figure 6.3: Gauge data for shock to detonation transition for an idealized nondimensionalised explosive, with a Mach 3.25 ignition shock. Each line corresponds to a particular gauge.

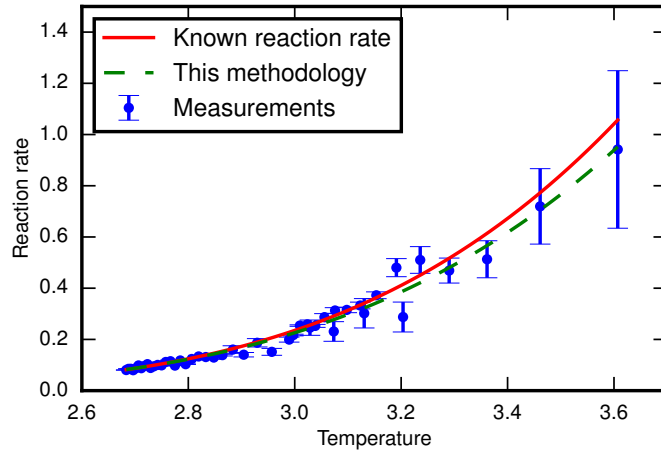


Figure 6.4: Reaction rate data extracted from simulated gauge output for an ideal explosive is compared with the known rate law used to generate the data.

Figure 6.4 shows the reaction rate data which was extracted from the gauges. The error bars correspond to the uncertainty in measurement of the post-shock derivative. The errors are larger for higher temperatures, since these gauges measure the shock close to the detonation transition. The velocity profile of these gauges is more curved, which increases the uncertainty associated with measuring the derivative.

The majority of the data points are collected around two temperatures values (one at 2.7 and the other at 3.05). These correspond to the initial post-shock temperatures for the two simulations. Using multiple simulations with differing initial shock strength thus allows us to sample a wider temperature range, and significantly improve the accuracy of the resulting fit.

The line of best fit to the extracted data has parameters $\tilde{A} = 9.0329$ and $\tilde{T}_A = 9.5681$. These values can be compared to the exact parameters in Table 6.1. We note that the resulting parameters do not exactly match the chosen values used to generate the data. This is because the results are affected by numerical errors, despite the absence of experimental error. These arise from the numerical errors in the simulation itself, which was carried out with a hydrocode. Furthermore the data generated for the gauges is of finite resolution, which leads to errors in the evaluation of the shock strength and post-shock derivatives.

6.4 Application to PBX 9502

The methodology presented above is applied here to the TATB based explosive PBX 9502. The application of this method first requires equations of state for each of the reactants and products. We further require closure rules with which to evaluate the derivative $\frac{\partial e}{\partial \lambda}$.

We use equations of state of Mie-Grüneisen form for the reactants, α , and the products, β ,

$$p_k - p_{k,\text{REF}}(v_k) = \rho_k \Gamma_k(v_k)(e_k - e_{k,\text{REF}}(v_k)) \quad \text{for } k \in \{\alpha, \beta\}. \quad (6.26)$$

The reference functions and their parameters are those developed in Chapter 3. Evaluation of states in the reaction zone where both reactants and products coexist requires mixture rules and closure conditions. In this chapter we use pressure equilibrium and temperature equilibrium,

$$v = \lambda v_\alpha + (1 - \lambda)v_\beta \quad (6.27)$$

$$e(v, p, \lambda) = \lambda e_\alpha(v_\alpha, p) + (1 - \lambda)e_\beta(v_\beta, p) \quad (6.28)$$

$$T_\alpha(v_\alpha, p) = T_\beta(v_\beta, p), \quad (6.29)$$

where pressure equilibrium means we have a single value for the pressure, p . The methodology to use these closure rules to evaluate states with non-integer values of λ is discussed in Chapter 3. A heat isolation closure rule may be implemented in place of temperature equilibrium, in which case the entropy of the reactants is kept fixed following the shock wave.

The state immediately behind the shock consists of reactants only, and so using only the equation of state of the reactants we can evaluate

$$\frac{\partial e}{\partial p} = \frac{1}{\rho \Gamma}, \quad (6.30)$$

$$\begin{aligned} \frac{\partial e}{\partial \rho} &= \frac{\partial v}{\partial \rho} \frac{\partial e}{\partial v} = -\frac{1}{\rho^2} \frac{\partial e}{\partial v} \\ &= -\frac{1}{\rho^2} \left[\frac{\partial e_{\text{REF}}}{\partial v} - \frac{p - p_{\text{REF}}}{(\rho \Gamma)^2} \frac{\partial \rho \Gamma}{\partial v} - \frac{1}{\rho \Gamma} \frac{\partial p_{\text{REF}}}{\partial v} \right]. \end{aligned} \quad (6.31)$$

Similarly the Hugoniot pressure, $p_H(v)$, can be calculated using the equation of state of the reactants with the expression given in equation (4.9) in Chapter 4.

6 Direct Calibration of Reaction Rate Models

The remaining term $\frac{\partial e}{\partial \lambda}$ also depends on the equation of state used to model the products, and the closure rules used to describe the mixture of reactants and products in the reaction zone. Evaluating the energy at states with non-integer λ requires the solution of a nonlinear equation. The equation of state for the mixture cannot be written as an explicit function of λ and involves the solution of a nonlinear equation, and so we cannot differentiate the equation of state for the mixture explicitly. The derivative with respect to λ is instead evaluated using finite differences,

$$\left(\frac{\partial e}{\partial \lambda}\right)_{v,p} = \frac{e(v,p,1-\Delta\lambda) - e(v,p,1)}{-\Delta\lambda}. \quad (6.32)$$

The value of λ is always one immediately after the shock, because the reactants do not burn prior to the passing of the shock. A value of 10^{-4} for $\Delta\lambda$ was found to give an accurate value for the derivative.

We calculate values for the reaction rate for the experiments which are presented by Gustavsen [49]. Some of the experiments were not included due to the small number of gauges. We used experiments denoted by the codes 2s-85, 2s-86, 2s-116 and 2s-117, for which additional gauge data is available in Wescott et al. [129] and Aslam[8]. The reaction rate values are presented in Table 6.2. Data such as this can be used to quantitatively assess the suitability of the thermodynamic dependence of a proposed reaction rate model for modelling the experiments under consideration.

The resulting reaction rate values are plotted with the post-shock temperature in Figure 6.5. We fit an Arrhenius reaction rate form for the thermodynamic dependence,

$$-\frac{D\lambda}{Dt}(T, \lambda = 1) = A \exp\left(-\frac{T_A}{T}\right). \quad (6.33)$$

With the limited experimental data employed here, an Arrhenius function provides a good fit to the data. However a more complex rate form may be required in order to fit a more wide-ranging data set. The parameters for the best fit to the data are $A = 365.88\mu\text{s}^{-1}$, $T_A = 6729.7\text{K}$.

It is emphasised that the data in Table 6.2 can be used to determine parameters for alternative rate models with very little additional work required. For example the same data can be used to calibrate a pressure dependent rate law,

$$-\frac{D\lambda}{Dt}(p, \lambda = 1) = 10^6 \left(\frac{p}{17.36 \text{ GPa}}\right)^{6.66}. \quad (6.34)$$

Experiment	v cm ³ /kg	p GPa	T K	$-\frac{D\lambda}{Dt}$ μs^{-1}	u_H mm μs^{-1}	$\frac{du_H}{dt}$ ms ⁻²	$\frac{Du}{Dt}$ ms ⁻²
2s-86	0.3925	13.23	864.5	0.1113	1.349	1.908e+08	2.899e+08
2s-86	0.3905	13.87	905.7	0.3221	1.392	4.144e+08	4.606e+08
2s-86	0.3875	14.89	972.1	0.3562	1.458	4.628e+08	5.496e+08
2s-86	0.3848	15.91	1041	0.3885	1.521	5.724e+08	8.161e+08
2s-86	0.3806	17.70	1167	0.9954	1.627	9.711e+08	8.776e+08
2s-85	0.3839	16.29	1068	0.5882	1.544	6.576e+08	6.778e+08
2s-85	0.3791	18.43	1219	1.579	1.669	1.353e+09	9.869e+08
2s-117	0.4028	10.49	701.7	5.286e-04	1.156	7.339e+07	2.186e+08
2s-117	0.4007	11.01	730.9	0.04844	1.194	1.185e+08	2.256e+08
2s-117	0.3983	11.61	765.9	0.07739	1.238	1.630e+08	2.836e+08
2s-117	0.3944	12.68	830.2	0.2548	1.312	3.666e+08	4.528e+08
2s-117	0.3915	13.54	884.2	0.2231	1.370	3.870e+08	5.977e+08
2s-117	0.3888	14.43	941.8	0.3047	1.428	4.485e+08	6.073e+08
2s-116	0.3930	13.08	855.1	0.1998	1.339	3.391e+08	5.085e+08
2s-116	0.3891	14.33	935.1	0.3337	1.422	4.175e+08	4.556e+08
2s-116	0.3862	15.38	1005	0.4152	1.488	5.132e+08	5.833e+08
2s-116	0.3824	16.90	1110	0.9822	1.581	8.906e+08	6.152e+08

Table 6.2: Reaction rate values for PBX 9502 as calculated from shock to detonation transition experiments using the methodology presented in this chapter. The thermodynamic values correspond to the state immediately following the shock wave and are calculated using the experimental post-shock flow velocity, u_H , and the previously calibrated equation of state for the reactants (Chapter 3). The final two columns of data are obtained from analysis of the experimental gauge data and are used to calculate the reaction rate, $\frac{D\lambda}{Dt}$, using the method presented in this chapter.

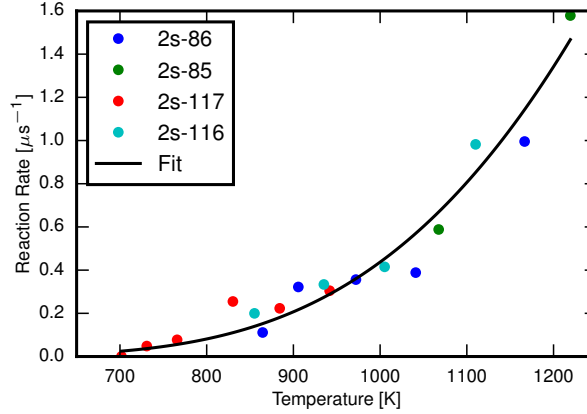


Figure 6.5: Data extracted from experimental data from shock to detonation transition experiments of PBX 9502.[8, 49, 129]

6.5 Validation

The above work demonstrates how we can use gauge data from shock to detonation transition experiments to directly evaluate the rate. However these values apply to the rate immediately following the shock wave. The method does not give us any information regarding the reaction rate in partially burnt explosive. We can make the assumption that the reaction rate model can be expressed as

$$\frac{D\lambda}{Dt} = f(T)g(\lambda) \quad (6.35)$$

where f may be a function of various thermodynamic functions of state. The function g controls the evolution of the reaction rate as the concentration of the reactants is reduced. We may define $g(\lambda)$ such that $g(1) = 1$ and $g(0) = 0$, since any constant multiple in g may be factored out and included in f .

The form and parameters of $g(\lambda)$ may be determined using experimental data for the length of the reaction zone in detonation waves. Such an approach could be used to constrain the reaction rate as a whole. However it would not be possible to evaluate the temperature dependence or pressure dependence of the reaction rate directly from an experimental measurement of the reaction zone width, since for a given explosive ZND waves pass through a fixed path in temperature and pressure space.

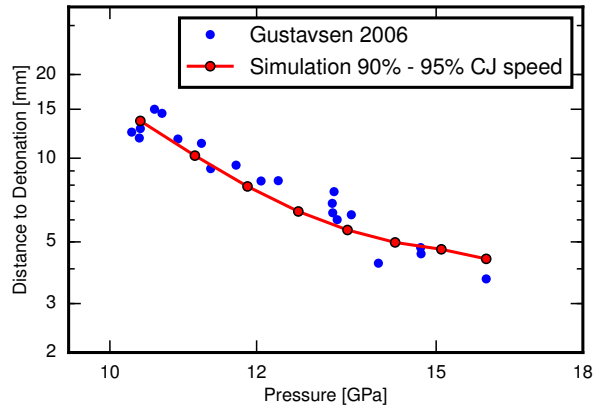


Figure 6.6: Simulation results for shock to detonation transition are compared with experimental data from Gustavsen et al. [49]. Only one degree of freedom was used for optimization, and yet the calibrated rate law fits the experimental data over a range of impact pressures. The vertical red lines correspond to individual simulations.

In this section we use the pop-plot data from Gustavsen [49] and optimization to determine the remaining free parameter, n , in the rate law

$$-\frac{D\lambda}{Dt}(T, \lambda) = A\lambda^n \exp\left(-\frac{T_A}{T}\right). \quad (6.36)$$

The parameters for the thermodynamic dependence are fixed at $A = 365.88\mu\text{s}^{-1}$, $T_A = 6729.7\text{K}$. Only the value of n is adjusted during the calibration. The value of n found to best fit the experimental data was 1.69. The resulting pop-plot is shown in Figure 6.6 along with the experimental data from Gustavsen et al. [49]. The simulations show good agreement to the experimental data despite using only a single parameter for the calibration. This demonstrates that the thermodynamic dependence of the reaction rate is correctly capturing the change in the reaction rate which occurs as a result of different projectile velocities and impact pressures.

Figure 6.6 plots the average of the positions corresponding to a wave velocity of 90% and 95% of the CJ velocity. This is necessary because particularly for high impact pressures the transition to detonation is gradual and ill-defined. This is expected to some degree since PBX 9502 is heterogeneous, and this behaviour is typical for heterogeneous explosives.

Note that the impact pressure is recalculated using the projectile velocity reported by Gustavsen, and the equation of state for PBX 9502 which was developed and calibrated in the present work. The equation of state for the Kel-F projectile was the same as that used by Gustavsen et al. [49].

6.6 Reaction Zone Width

An alternative approach to determine the parameters of the function g is presented in this section. This method uses data for the width of the reaction zone, and allows parameters for $g(\lambda)$ to be determined without resorting to optimization using hydrocode simulations for any parameters.

For PBX 9502, we use the values for the width of the reaction zone from Seitz et al. [111]. In this paper the width of the reaction zone is measured in terms of the time it takes a gauge to be traversed by the wave. This is done by matching a ZND model directly with experimental data. To calculate the size of the reaction zone in time, we can simply integrate the rate over the reaction zone. This is the integral defined in equation (4.41) in Chapter 4. This corresponds to the amount of time it takes for the reaction zone to propagate past a particle embedded in the explosive. The procedure for evaluating this integral is explained fully in Chapter 4.

From Seitz et al. [111] the explosive is 85% burnt ($\lambda = 0.15$) after 25ns and 98% burnt after 300ns. The substantial reduction of the reaction rate at around $\lambda = 0.1$ is a distinguishing feature of PBX 9502 arising from the comparatively time scales associated with the coagulation of solid carbon. It makes sense therefore to construct $g(\lambda)$ such as to account for this behaviour. While the precise value of λ at which the reaction rate is reduced employs some degree of speculation, this value is largely consistent with the literature [8, 63, 70, 123, 129].

Following Aslam [8], the chosen form for g was

$$g(\lambda) = \lambda^n \left(f_s + \frac{1 - f_s}{2} \left(1 + \tanh \left(\frac{\lambda - 0.1}{0.02} \right) \right) \right), \quad (6.37)$$

with free variables n and f_s . $g(1)$ is almost exactly 1, and $g(\lambda)$ approaches $f_s \lambda^n$ for small λ .

A	$365.88\mu\text{s}^{-1}$
T_A	6729.7K
$T_{transition}$	2000K
T_{A_2}	7877K
n	0.5
f_s	0.036

Table 6.3: Parameters for the calibrated rate law of PBX 9502.

Unfortunately, it was found that the form of f , which was determined using shock to detonation transition experiments, is too slow when evaluated at the von Neumann spike. In other words, no matter the choice of parameters for g , it is not possible to reach $\lambda = 0.15$ within 25ns. Since the temperature of the von Neumann spike is well above the temperature range which is sampled (see Figure 6.5), this does not necessarily indicate that the previous results are incorrect. It merely indicates that we are extrapolating beyond the regime of data which was used to calibrate the model. To match the data we introduce a new parameter to $f(T)$.

$$f(T) = \begin{cases} A \exp\left(-\frac{T_A}{T}\right) & \text{if } T \leq T_{transition} \\ A_2 \exp\left(-\frac{T_{A_2}}{T}\right) & \text{if } T > T_{transition} \end{cases} \quad (6.38)$$

$$A_2 = \exp\left(\frac{T_{A_2}}{T_{transition}}\right) A \exp\left(-\frac{T_A}{T_{transition}}\right)$$

A_2 is chosen such that f will be continuous at the transition temperature, which is chosen to be 2000K, a value well below the von Neumann temperature, 2730K, but significantly higher than the temperatures in Figure 6.5. Since A and T_A for the low temperature regime have already been determined, the only new free parameter is T_{A_2} .

It is now possible to achieve a good fit with the experimental data from Seitz et al. [111]. This is shown in Figure 6.7. The parameters are summarized in Table 6.3.

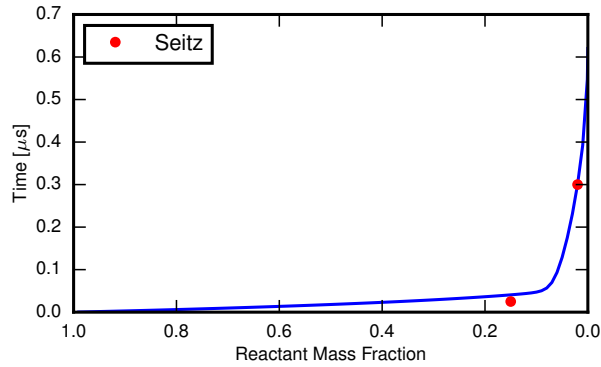


Figure 6.7: The plot shows the time taken for a piece of material to evolve from the initial condition of $\lambda = 1$ following the passing of a ZND wave. The red markers represent the experimental results from Seitz et al. [111].

6.7 Results

The rate law presented above can be tested by modelling both shock to detonation transition and the detonation of confined rate sticks. The rate law, along with the equations of state are used in the MiNi16 Eulerian formulation [91], which was described in Chapter 5.

It is important to emphasize that the parameters of the model (the parameters of the equation of state and the parameters of the reaction rate model) are all fully determined without the use of the hydrocode. No optimization is required where the objective function involves execution of the hydrocode.

The pop-plot is generated by simulating the shock to detonation transition of the explosive in one dimension. The results are compared with the experimental data from Gustavsen et al. [49] in Figure 6.8. The simulations predict distances to detonation slightly below the spread of the experimental data. However these are genuine predictions in the sense that the pop-plot data is not used at all to determine the various parameters. Even in the case where it is desirable to use any available pop-plot data with the aim of producing a more accurate model, it is apparent that the parameters calibrated here would serve as a more than adequate starting point from which to begin an optimization algorithm.

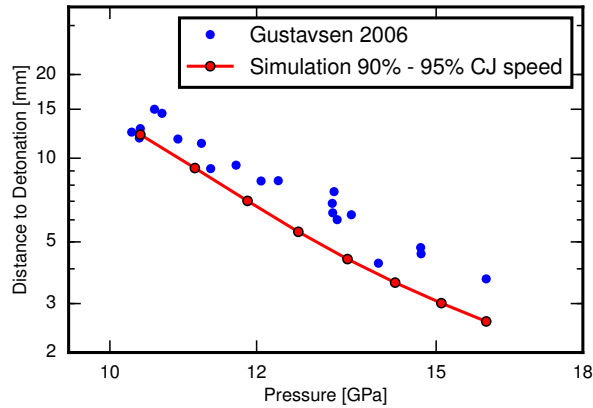


Figure 6.8: Pop-plot using the reaction rate parameters for the best fit to the data in Figure 6.5. The lower and upper red lines indicate transition to detonation defined as the point where the wave velocity first exceeds 90% and 95% of the CJ velocity respectively. The vertical red lines correspond to specific simulations.

Detonation waves of the confined explosive are also simulated using two geometries - cylindrical rate sticks, and two dimensional slabs. In each case we may take advantage of the symmetry of the system to do the simulation in two dimensions. The velocity of detonation is measured as a function of the rate stick radius, and the slab thickness. In either case the confining material is air, modelled with an ideal gas equation of state with adiabatic gamma 1.4.

The results are compared with the experimental measurements of Jackson and Short[63] in Figure 6.9. The model does not reproduce the curvature in the velocity of detonation dependence on the radius which is observed experimentally. This curvature has been reproduced in this work (Figure 5.16). However there is an important distinction which is that the model presented in this chapter has been calibrated without the use of any detonation velocity data. Similar predictions could therefore be made even for explosives for which no detonation velocity experimental data is available. Note that for rate sticks with $1/R > 200\text{m}^{-1}$, and slabs with $1/T > 200\text{m}^{-1}$, the detonation failed. This manifests as a gradual deceleration of the detonation wave until the pressures and temperatures reduce to the point where chemical reactions cease entirely.

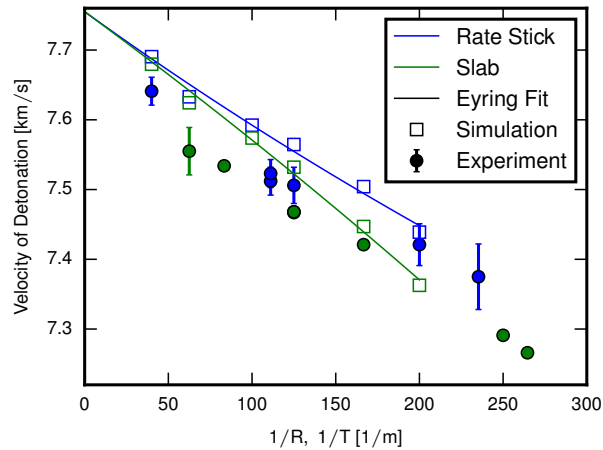


Figure 6.9: Predictions for the velocity of detonation in PBX 9502 rate sticks and slabs. The graph plots the velocity against the inverse radius, R , for rate sticks, and thickness, T , for slabs. The square markers represent individual simulations, while the lines are Eyring fits [27] through the simulation results. The circular markers represent experimental data from Jackson and Short [63].

Once again it is emphasised that the detonation velocity data is not used at all in the calibration process, and as such the simulation results in Figure 6.9 are genuine predictions. This is in contrast to the results presented in Chapter 5, where the rate stick data is used in the calibration procedure. The resulting model is then used to predict the detonation velocity of the slabs and for rate sticks of differing radii.

6.8 Conclusions

A methodology has been presented to calculate reaction rate values directly from the gauge data which is generated in shock to detonation transition experiments. By relating the acceleration of the igniting shock wave with the derivatives of the flow field, a linear system is constructed. Measurement of the acceleration of the shock wave itself and the post-shock acceleration of a gauge fully constrains the system. We can thus determine the reaction rate in the material after the passing of the shock wave.

This method offers an opportunity to avoid the global optimization of parameters through a direct comparison of simulation results with experimental data. The reaction rate parameters can instead be calibrated independently of the hydrocode, an approach which is dramatically more efficient.

Direct calculation of the reaction rate with this method can form the basis for a direct evaluation of the thermodynamic dependence of the reaction rate. This can be used to motivate the choice of mathematical function used to express the reaction rate.

The method relies on the accuracy of the equations of state. The method also uses a closure condition to evaluate the partial derivative of the specific internal energy with respect to the progress variable, $\frac{\partial e}{\partial \lambda}$. The accuracy of the predicted reaction rate values are therefore dependent on the extent to which the temperature equilibrium condition is physically justified. The method can however be trivially modified to use a heat isolation condition instead.

The method has been validated using simulated gauge data for an idealized explosive. This demonstrates that the method can work in principle. The method is further validated by correctly capturing the thermodynamic dependence of the reaction rate of PBX 9502. This is demonstrated by reproducing the thermodynamic dependence exhibited in the pop-plot experimental data, despite the use of a fairly small dataset.

Use of experimental values for the width of the reaction zone, allows the model to be further extended to the detonation regime. The accuracy of the predictions is necessarily limited by the accuracy of the experimental data. In Chapter 5, the calibration of the reaction rate uses measurements of the detonation velocity. Since detonation waves eventually converge to a steady wave, their velocity can be measured with comparatively high accuracy. In contrast, the data from embedded gauges which is used in this chapter, is subject to more experimental error. Nevertheless predictions of the velocity of confined detonation waves using this method match the experimental data with reasonable accuracy.

The results presented in this chapter show the potential of the method which has been presented, and motivate a future investigation using more experimental

6 Direct Calibration of Reaction Rate Models

data. Furthermore the method can evidently serve as an excellent tool for reducing the amount of time required to calibrate a reaction rate model by determining a suitable set of parameter values from which to start the optimization.

7 Conclusions

This thesis develops a comprehensive methodology for modelling ignition and detonation of explosives. The objective was to be able to simulate the combustion of explosives and their interaction with the environment in complex geometries. In particular, the aim was to develop robust models, which are applicable in a wide range of scenarios and make accurate, quantitative predictions. The work has been presented in the form of a methodology which can be applied to construct a model for any condensed phase high explosive.

The methodology has been applied to construct explosive models for two condensed-phase explosives, PBX 9502 and EM120D. The TATB based explosive, PBX 9502, is an insensitive high explosive which is comparatively ideal. EM120D, on the other hand, is an ammonium nitrate based emulsion, which is significantly porous and is also non-ideal. The explosive model is of a form suitable for implementation in a hydrocode and consists of two independent equations of state, a reaction rate model and mixture rules. Application of the methodology to both of these explosives serves to validate the methodology for both ideal and non-ideal explosives.

In Chapter 3, the form of the equation of state models was developed with the aim of improving the robustness of the explosive model with particular focus on the mixture rules of pressure equilibrium and temperature equilibrium and the applicability of the equations of state in this context. Reliable and robust solution of the temperature equilibrium condition requires equations of state which behave according to the physical requirements of thermodynamics.

Furthermore the equations of state were developed to be applicable to a wide variety of explosives; they do not rely on experimental data which is rarely available. Many explosives are significantly porous, and therefore the equations of state

7 Conclusions

were developed such as to be able to incorporate the porosity explicitly. Finally the mathematical forms were chosen to be as simple as possible, with the aim of developing equations of state which can be used in efficient hydrocode simulations.

The reactant equation of state is an adaptation of the equation of state of Davis [35]. The reference functions are altered such as to incorporate the snow plow porosity model. The porosity model has been shown to successfully reproduce the curved D,u relationship that has been measured experimentally in PBX 9502. A simple modification to the mathematical form for the Grüneisen gamma widens the range of validity of the equation of state, while avoiding the complexity of the WSD model. The temperatures are derived solely from the Hugoniot data and the thermodynamics of the explosive in ambient conditions, since there is very limited thermal data available for the reactants of many explosives.

The product equation of state is an adaptation of the JWL equation of state which accommodates evaluation of the temperature. As is the case for the Williamsburg equation of state, the reference curves are calibrated to data for the principal isentrope from a thermochemical code. However this data is used to calibrate parameters for reference curves which are based on the simple empirical form used by the standard JWL equation of state. This takes advantage of the additional accuracy offered by the ideal detonation code, while preserving the simplicity and efficiency of JWL.

A methodology has been presented to determine all the various parameters required to use the equations of state for a specific explosive. The methodology was applied to the non-ideal explosive emulsion EM120D and the ideal TATB based explosive PBX 9502.

In Chapter 4, the equations of state are used to directly calculate the structure of one dimensional detonation waves using the ZND theory. This permits us to calculate states inside the reaction zone, and make a direct comparison between candidate closure rules. Evaluation of the state in the reaction zone allows us to quantify how much heat transfer must occur if the reactants and products are to remain at temperature equilibrium.

The equations of state for the explosives were also used in the context of the MiNi16 formulation [91] to perform direct numerical simulation of the detonation wave and its interaction with the confiner. The numerical implementation was validated using one dimensional Riemann tests. The equation of state models and numerical method were also validated by simulating one dimensional detonation waves, which can be compared with the predictions of the ZND theory.

An accurate reaction rate model is still required in order to make predictions. The most common approach is to use an empirical form for the reaction rate with free parameters. The values of the free parameters are determined by optimizing the accuracy of the hydrocode predictions using experimental data. This involves many executions of the hydrocode and is a computationally intensive process. In Chapter 5 this approach was used to calibrate a reaction rate model for both EM120D and PBX 9502.

For EM120D, the predictive capability demonstrated by Schoch et al. [108] was successfully reproduced. The methodology was shown to be capable of predicting the effect of strong confinement on the detonation velocity, despite only using data for weakly confined rate sticks in the calibration process. For PBX 9502, the methodology was applied to predict the dependence of the detonation velocity on the geometry. The model was calibrated using rate stick data, and used to predict the detonation velocity in a slab geometry. In each case, the accuracy of the predictions was verified using experimental data. The results demonstrate that the equations of state are both accurate and robust in practice.

A method has also been presented to directly calculate values for the reaction rate from experimental data, and thus avoid the expensive optimization procedure. This exploits the experimental data from gauges embedded in an explosive which is ignited by shock to detonation transition. By relating the acceleration of the igniting shock wave with the derivatives of the flow field, a linear system is constructed. Measurement of the acceleration of the shock wave itself and the post-shock acceleration of a gauge fully constrains the system. We can thus determine the reaction rate in the material after the passing of the shock wave. The method has been validated by applying it to simulated gauge data for an idealized explosive with a known reaction rate.

7 Conclusions

The principal advantage of the proposed method to directly calculate values for the reaction rate is that the resulting values can be used to establish the thermodynamic dependence of the reaction rate. Given data for an explosive which samples states other than the single shock Hugoniot, this method can quantitatively evaluate the relative accuracy of pressure dependent forms in comparison to temperature or entropy dependent forms.

This method also offers an opportunity to avoid the global optimization of parameters through a direct comparison of simulation results with experimental data. The reaction rate parameters can instead be calibrated independently of the hydrocode, an approach which is significantly more efficient. Furthermore, the resulting explosive model is independent of the numerical methods used in the hydrocode. This approach therefore serves to further validate the numerical methods used, since in this case there is no scope for errors in the explosive model to be compensated for in the optimization process.

This method has been applied to the insensitive high explosive PBX 9502 to calculate reaction rate values directly. The resulting values justify an empirical reaction rate model, which has been developed to match the resulting reaction rate values as well as experimental data for the width of the reaction zone in a ZND wave.

The resulting model can be used to simulate both ignition and detonation of PBX 9502. While the predictions (Figure 6.9) are not as precise as those achieved via optimization (Figure 5.16), the calibration procedure is much less computationally intensive. Furthermore the calibration presented in Chapter 6 relies on a limited set of experimental data and is completely independent of the experimental confined detonation velocity measurements. Detonation velocities of rate sticks can be measured much more precisely than the acceleration of the shock wave during ignition. As such, it is to be expected that the direct optimization of parameters approach presented in Chapter 5 will yield a more precise model.

The best approach may be to use a combination of the two methods. The analysis of embedded gauge data can be used to motivate the form of the reaction rate model, and provide a first guess to the parameters of the model. The parameters could then be refined further by optimization of the simulation results with respect to

experimental measurements. This will still lead to a significant increase in efficiency, since the number of iterations required for optimization is strongly dependent on the accuracy of the initial guess.

A Derivation of the Shock Mie-Grüneisen Equation of State

As a shock wave passes a piece of material, the flow velocity of the material is increased. The relation between this velocity, u , and the shock velocity, D , is empirically found to be approximately linear for many solids [5, 131],

$$D = a + bu, \quad (\text{A.1})$$

where a is the ambient speed of sound, and b is an empirically determined constant. Note that the shock velocity is measured with respect to the unshocked material.

Using the Rankine-Hugoniot condition for mass conservation,

$$\rho(D - u) = \rho_0 D \quad (\text{A.2})$$

$$u = \left(1 - \frac{\rho_0}{\rho}\right) D = \chi D \quad (\text{A.3})$$

where χ has been defined such that

$$\chi = \left(1 - \frac{\rho_0}{\rho}\right). \quad (\text{A.4})$$

The shock velocity can then be expressed as a function of volume only,

$$D = a + bu \quad (\text{A.5})$$

$$= a + b\chi D \quad (\text{A.6})$$

$$= \frac{a}{1 - b\chi}. \quad (\text{A.7})$$

Using the Rankine-Hugoniot condition for conservation of momentum (4.2) we can calculate the pressure on the Hugoniot curve, p_H ,

$$p_H - p_0 = u\rho_0 D \tag{A.8}$$

$$= \rho_0 \chi D^2 \tag{A.9}$$

$$= \frac{\rho_0 \chi a^2}{(1 - b\chi)^2}. \tag{A.10}$$

The final step is to determine the energy reference function. This is most easily done using the Hugoniot equation,

$$e_H - e_0 = \frac{1}{2}(p_H + p_0)(v_0 - v). \tag{A.11}$$

For the applications which are the subject of the present thesis, typical shock waves are such that the pressure increases by several orders of magnitude. The initial pressure, p_0 , and initial energy, e_0 , can therefore be neglected to obtain the pressure and energy on the Hugoniot curve,

$$p_H = \frac{\rho_0 \chi a^2}{(1 - b\chi)^2} \tag{A.12}$$

$$e_H = \frac{1}{2}(v_0 - v)p_H. \tag{A.13}$$

B Derivation of Davis Equation of State

This derivation follows that presented by Davis [35]. Experimentally, the relation between shock velocity, D , and post-shock flow velocity, u , is approximately linear. In the limit of weak shocks, the shock velocity is the ambient speed of sound, a . As such, we may express the shock velocity as

$$D = a + bu, \quad (\text{B.1})$$

where b is a positive dimensionless parameter. The Rankine-Hugoniot condition for momentum can be used to determine the pressure, p ,

$$p = \rho_0 u D = \rho_0 u (a + bu), \quad (\text{B.2})$$

where ρ_0 is the ambient density. By completing the square, we have

$$u = -\frac{a}{2b} + \frac{1}{2} \sqrt{\frac{a^2}{b^2} + \frac{4p}{b\rho_0}}. \quad (\text{B.3})$$

In the limit of weak shock waves, the Hugoniot curve is isentropic. Therefore,

$$\left(\frac{\partial p}{\partial u}\right)_S = a\rho_0 + 2b\rho_0 u \quad (\text{B.4})$$

$$= b\rho_0 \sqrt{\frac{a^2}{b^2} + \frac{4p}{b\rho_0}}. \quad (\text{B.5})$$

Furthermore, the propagation speed, D , of weak shock waves is nothing but the ambient sound speed, a , so

$$\left(\frac{\partial p}{\partial u}\right)_S = \rho_0 a = \rho_0 \sqrt{\left(\frac{\partial p}{\partial \rho}\right)_S} = -\sqrt{\left(\frac{\partial p}{\partial v}\right)_S} \quad (\text{B.6})$$

$$\Rightarrow \left(\frac{\partial p}{\partial v}\right)_S = -(a^2 \rho_0^2 + 4b\rho_0 p). \quad (\text{B.7})$$

This is a first order differential equation with solution

$$p_S(v) = e^{-4b\rho_0 v} \int (-a^2 \rho_0^2) e^{4b\rho_0 v} dv \quad (\text{B.8})$$

$$= \frac{-a^2 \rho_0}{4b} + ce^{-4b\rho_0 v}. \quad (\text{B.9})$$

The pressure at the initial specific volume, $v_0 = 1/\rho_0$, is orders of magnitude smaller than the shock pressure for typical applications, and so can be assumed to be zero. This determines the value of the integration constant, c . The isentropic pressure can finally be expressed in terms of specific volume as

$$p_S(v) = \frac{a^2 \rho_0}{4b} \left(-1 + e^{4b} e^{-4b\rho_0 v} \right) \quad (\text{B.10})$$

$$= \frac{a^2 \rho_0}{4b} \left(e^{4b(1-v/v_0)} - 1 \right) \quad (\text{B.11})$$

C Volume and Mass Fractions for Parametrising Multiphase Fluids

The method used in this thesis frequently refers to both the mass fraction and volume fraction of a multiphase fluid. Consider a two phase fluid. Let each fluid have N_k particles of mass m_k and occupy a volume V_k where k is a label. The overall density of the fluid is

$$\rho = \frac{\sum_k N_k m_k}{\sum_k V_k}. \quad (\text{C.1})$$

The density of each phase is

$$\rho_k = \frac{N_k m_k}{V_k}. \quad (\text{C.2})$$

The volume fraction, z_k , and mass fraction, λ_k , of each phase are defined to be

$$\begin{aligned} z_k &= \frac{V_k}{\sum_i V_i} & \lambda_k &= \frac{N_k m_k}{\sum_i N_i m_i} \\ 1 &= \sum_i z_i & 1 &= \sum_i \lambda_i. \end{aligned} \quad (\text{C.3})$$

We wish to find mixture rules which define the overall density as a function of the densities of the fluid's constituents using either the volume fraction or mass fraction as a parameter. Firstly, consider

$$\sum_k V_k = \frac{\sum_k N_k m_k}{\rho} = \sum_k \frac{N_k m_k}{\rho_k} \quad (\text{C.4})$$

$$\frac{1}{\rho} = \sum_k \frac{\lambda_k}{\rho_k} \quad (\text{C.5})$$

On the other hand we have

$$\sum_k N_k m_k = \rho \sum_k V_k = \sum_k \rho_k V_k \quad (\text{C.6})$$

$$\rho = \sum_k z_k \rho_k. \quad (\text{C.7})$$

In terms of the specific volume, v , these relations are

$$v = \sum_k \lambda_k v_k \quad (\text{C.8})$$

$$\frac{1}{v} = \sum_k \frac{z_k}{v_k}. \quad (\text{C.9})$$

It also possible to relate the volume fraction with the mass fraction for an individual phase,

$$z_k = \frac{V_k}{\sum_i V_i} = \frac{N_k m_k / \rho_k}{(\sum_i N_i m_i) / \rho} = \frac{\lambda_k \rho}{\rho_k}. \quad (\text{C.10})$$

Bibliography

- [1] A. N. Afanasev, V. M. Bogomolov, and I. M. Voskoboinikov. “Generalized shock hughoniot of condensed substances”. *Journal of Applied Mechanics and Technical Physics* 10.4 (1969), pp. 660–664.
- [2] G. Allaire, S. Clerc, and S. Kokh. “A Five-Equation Model for the Simulation of Interfaces between Compressible Fluids”. *Journal of Computational Physics* 181.2 (2002), pp. 577–616.
- [3] A. B. Anderson, M. J. Ginsberg, W. L. Seitz, and J. Wackerle. “Shock initiation of Porous TATB”. *Seventh Symposium (International) on Detonation*. Annapolis, MD, 1981, p. 385.
- [4] M. Arienti, E. Morano, and J. E. Shepherd. *Shock and detonation modeling with the Mie-Grüneisen equation of state*. Tech. rep. California Institute of Technology, 2004.
- [5] J. R. Asay and M. Shahinpoor. “Equation of State”. *High-Pressure Shock Compression of Solids*. Springer-Verlag New York, 1993, pp. 75–113.
- [6] T. D. Aslam. “Investigations on Detonation Shock Dynamics”. PhD thesis. University of Illinois, Urbana-Champaign, 1996.
- [7] T. D. Aslam. “The reactants equation of state for the tri-amino-tri-nitrobenzene (TATB) based explosive PBX 9502”. *Journal of Applied Physics* 122.3 (2017), p. 035902.
- [8] T. D. Aslam. “Shock temperature dependent rate law for plastic bonded explosives”. *Journal of Applied Physics* 123.14 (2018), p. 145901.
- [9] T. D. Aslam and J. B. Bdzil. “Numerical and theoretical investigations on detonation-inert confinement interactions”. *12th Symposium (International) on Detonation*. San Diego, California, 2002, pp. 483–488.

- [10] T. D. Aslam, R. L. Gustavsen, N. J. Whitworth, H. J. Lacy, B. D. Lambourn, C. A. Handley, H. R. James, and S. Root. “Multi-shock and isentropic compression of the tri-amino-tri-nitro-benzene based explosive PBX 9502 : Evaluation of reactive flow models”. *Fifteenth Symposium (International) on Detonation*. 2014.
- [11] T. D. Aslam, R. L. Gustavsen, N. J. Whitworth, R. Menikoff, C. M. Tarver, C. A. Handley, and B. D. Bartram. “Shock, release and reshock of PBX 9502: Experiments and modeling”. *AIP Conference Proceedings*. Vol. 1979. 2018, p. 100001.
- [12] M. R. Baer and J. W. Nunziato. “A two-phase mixture theory for the deflagration-to-detonation transition (ddt) in reactive granular materials”. *International Journal of Multiphase Flow* 12.6 (1986), pp. 861–889.
- [13] J. W. Banks, W. D. Henshaw, D. W. Schwendeman, and A. K. Kapila. “A study of detonation propagation and diffraction with compliant confinement”. *Combustion Theory and Modelling* 12.4 (2008), pp. 769–808.
- [14] J. W. Banks, D. W. Schwendeman, A. K. Kapila, and W. D. Henshaw. “A high-resolution Godunov method for compressible multi-material flow on overlapping grids”. *Journal of Computational Physics* 223.1 (2007), pp. 262–297.
- [15] G. Baudin and R. Serradeill. “Review of Jones-Wilkins-Lee equation of state”. *EPJ Web of Conferences* 10 (2010), p. 00021.
- [16] J. B. Bdzil and D. S. Stewart. “The Dynamics of Detonation in Explosive Systems *”. en. *Annual Review of Fluid Mechanics* 39.1 (2007), pp. 263–292.
- [17] John B. Bdzil. “High-Explosives Performance”. *Los Alamos Science* 28 (2003), pp. 96–110.
- [18] Stephen J Blundell and Katherine M Blundell. *Concepts in thermal physics*. OUP Oxford, 2009.
- [19] N. K. Bourne and J. E. Field. “Explosive ignition by the collapse of cavities”. *Proceedings of the Royal Society A: Mathematical, Physical and Engineering Sciences* 455.1987 (1999), pp. 2411–2426.

Bibliography

- [20] N. K. Bourne and J. E. Field. “Shock-induced collapse and luminescence by cavities”. *Philosophical Transactions of the Royal Society A: Mathematical, Physical and Engineering Sciences* 357.1751 (1999), pp. 295–311.
- [21] M. Braithwaite, W. B. Brown, and A. Minchinton. “The use of ideal detonation computer codes in blast modelling”. *Fragblast 5*. Balkema: Rotterdam, 1996, pp. 37–44.
- [22] M. Braithwaite and G. J. Sharpe. “Reduced, Chemistry Implicit, Equations of State for Explosion and Detonation Products”. *15th International Detonation Symposium*. 2014, pp. 869–877.
- [23] W. Byers Brown. *Williamsburg Equation of State for Fluids at Very High Density*. Tech. rep. Contract Report for ICI plc Explosives Group Technical Centre. 1994.
- [24] W. Byers Brown, Z. Feng, and M. Braithwaite. “Williamsburg Equation of State for Modelling Non-Ideal Detonation”. *Journal de Physique IV* 5.4 (1995), pp. 209–214.
- [25] A. W. Campbell, W. C. Davis, J. B. Ramsay, and J. R. Travis. “Shock Initiation of Solid Explosives”. *Physics of Fluids* 4.4 (1961), p. 511.
- [26] A. W. Campbell, W. C. Davis, and J. R. Travis. “Shock Initiation of Detonation in Liquid Explosives”. *Physics of Fluids* 4.4 (1961), p. 498.
- [27] A. W. Campbell and R. Engelke. “Diameter effect in high-density heterogeneous explosives”. *6th Symposium on Detonation*. 1976.
- [28] M. Carroll and A. C. Holt. “Suggested Modification of the P - α Model for Porous Materials”. *Journal of Applied Physics* 43.2 (1972), pp. 759–761.
- [29] D. L. Chapman. “On the rate of explosion in gases”. *Philosophical Magazine Series 5* 47.284 (1899), pp. 90–104.
- [30] L. C. Chhabildas, L. N. Kmetyk, W. D. Reinhart, and C. A. Hall. “Enhanced hypervelocity launcher - capabilities to 16 km/s”. *International Journal of Impact Engineering* 17.1-3 (1995), pp. 183–194.
- [31] J. F. Clarke. “Fast flames, waves and detonation”. *Progress in Energy and Combustion Science* 15.3 (1989), p. 241.

- [32] R. Courant, K. Friedrichs, and H. Lewy. “Über die partiellen Differenzengleichungen der mathematischen Physik”. German. *Mathematische Annalen* 100.1 (1928), pp. 32–74.
- [33] L. L. Davis and L. G. Hill. “ANFO Cylinder Tests”. *AIP Conference Proceedings* 620 (2002), pp. 165–168.
- [34] W. C. Davis. “Equation of state for detonation products”. *11th Detonation Symposium*. 1998, pp. 303–308.
- [35] W. C. Davis. “Complete equation of state for unreacted solid explosive”. *Combustion and Flame* 120.3 (2000), pp. 399–403.
- [36] G. DeOliveira, A. K. Kapila, D. W. Schwendeman, J. B. Bdzil, W. D. Henshaw, and C. M. Tarver. “Detonation diffraction, dead zones, and the ignition-and-growth model.” *The Thirteenth Symposium (International) on Detonation*. Norfolk, Virginia, 2006, pp. 13–23.
- [37] J. J. Dick, C. A. Forest, J. B. Ramsay, and W. L. Seitz. “The Hugoniot and shock sensitivity of a plastic-bonded TATB explosive PBX 9502”. *Journal of Applied Physics* 63.10 (1988), p. 4881.
- [38] W. Döring. “Über den Detonationsvorgang in Gasen”. *Annalen der Physik* 435.6-7 (1943), pp. 421–436.
- [39] A. N. Dremin. *Results from Detonic Research Contract II*. Tech. rep. 1999.
- [40] J. D. Dunnett, D. C. Swift, and M. Braithwaite. “Comparison of Williamsburg and JWL Equations of State for Nitromethane”. *11th Detonation Symposium*. 1998.
- [41] J. O. Erkman and D. J. Edwards. *Computed and Experimental Hugoniots for Unreacted Porous High Explosives*. Tech. rep. White Oak, Maryland, US: Naval Ordnance Laboratory, 1974.
- [42] R. P. Fedkiw, T. D. Aslam, B. Merriman, and S. Osher. “A Non-oscillatory Eulerian Approach to Interfaces in Multimaterial Flows (the Ghost Fluid Method)”. *Journal of Computational Physics* 152 (1999), pp. 457–492.
- [43] Eric N. Ferm and Fesseha Mariam. “Proton Radiography Observations of the Failure of a Detonation Wave to Propagate to the End of a Conical Explosive Charge”. *AIP Conference Proceedings*. Vol. 845. 1. AIP, 2006, p. 968.

Bibliography

- [44] W. Fickett and W. C. Davis. *Detonation: Theory and Experiment*. Dover Publications, 2000.
- [45] C. A. Forest, J. Wackerle, J. J. Dick, S. A. Sheffield, and D. R. Pettit. “Lagrangian Analysis of MIV Gauge Experiments on PBX 9502 using the Mass-displacement Moment function”. *Ninth Symposium (International) on Detonation*. Portland, OR, 1989.
- [46] T. R. Gibbs and A. Popolato. *LASL Explosive Property Data*. University of California Press, 1980.
- [47] S. K. Godunov. “A difference method for numerical calculation of discontinuous solutions of the equations of hydrodynamics”. *Matematicheskii Sbornik* 89.3 (1959), pp. 271–306.
- [48] R. L. Gustavsen, S. A. Sheffield, and R. R. Alcon. “Shock Initiation of “Virgin” and “Recycled” PBX 9502 Measured with Embedded Electromagnetic Particle Velocity Gauges”. *AIP Conference Proceedings* 706 (2004), p. 973.
- [49] R. L. Gustavsen, S. A. Sheffield, and R. R. Alcon. “Measurements of shock initiation in the tri-amino-tri-nitro-benzene based explosive PBX 9502: Wave forms from embedded gauges and comparison of four different material lots”. *Journal of Applied Physics* 99.11 (2006), p. 114907.
- [50] R. L. Gustavsen, S. A. Sheffield, R. R. Alcon, J. W. Forbes, C. M. Tarver, and F. Garcia. “Embedded Electromagnetic Gauge Measurements and Modelling of Shock Initiation in the TATB based Explosives PBX 9502 and LX-17”. *AIP Conference Proceedings* 620 (2002), p. 1019.
- [51] C. A. Handley. “The CREST Reactive Burn Model”. *13th Symposium (International) on Detonation*. Norfolk, Virginia, 2006.
- [52] C. A. Handley and H. R. James. “A comparison between entropy, temperature and pressure-dependent reactive-burn models”. *AIP Conference Proceedings* 1426.1 (2012), p. 519.
- [53] C. A. Handley and B. D. Lambourn. “Predicting the Effect of Porosity on the Shock Sensitivity of Explosives”. *AIP Conference Proceedings* 1195 (2010), p. 221.

- [54] C. A. Handley, N. J. Whitworth, H. R. James, B. D. Lambourn, and M-A. Maheswaran. “The CREST reactive-burn model for explosives”. *EPJ Web of Conferences* 10 (2010), p. 00004.
- [55] C. A. Handley, B. D. Lambourn, N. J. Whitworth, H. R. James, and W. J. Belfield. “Understanding the shock and detonation response of high explosives at the continuum and meso scales”. *Applied Physics Reviews* 5.1 (2018), p. 011303.
- [56] A. Harten, P. D. Lax, and B. van Leer. “On upstream differencing and Godunov-type schemes for hyperbolic conservation laws”. *SIAM review* 25.1 (1983), pp. 35–61.
- [57] W. Herrmann. “Constitutive Equation for the Dynamic Compaction of Ductile Porous Materials”. *Journal of Applied Physics* 40.6 (1969), pp. 2490–2499.
- [58] C. W. Hirt and B. D. Nichols. “Volume of fluid (VOF) method for the dynamics of free boundaries”. *Journal of Computational Physics* 39.1 (1981), pp. 201–225.
- [59] E. Ioannou, S. Schoch, N. Nikiforakis, and L. Michael. “Detonation propagation in annular arcs of condensed phase explosives”. *Physics of Fluids* 29.11 (2017), p. 116102.
- [60] S. I. Jackson. “An analytic method for two-dimensional wall motion and product isentrope from the detonation cylinder test”. *Proceedings of the Combustion Institute* 35.2 (2015), p. 1997.
- [61] S. I. Jackson. “The dependence of Ammonium-Nitrate Fuel-Oil (ANFO) detonation on confinement”. *Proceedings of the Combustion Institute* 36.2 (2017), pp. 2791–2798.
- [62] S. I. Jackson and M. Short. “Experimental measurement of the scaling of the diameter- and thickness-effect curves for ideal, insensitive, and non-ideal explosives”. en. *Journal of Physics: Conference Series* 500.5 (2014), p. 052020.
- [63] S. I. Jackson and M. Short. “Scaling of detonation velocity in cylinder and slab geometries for ideal, insensitive and non-ideal explosives”. *Journal of Fluid Mechanics* 773 (2015), pp. 224–266.

Bibliography

- [64] H. R. James and B. D. Lambourn. “On the systematics of particle velocity histories in the shock-to-detonation transition regime”. *Journal of Applied Physics* 100.8 (2006), p. 084906.
- [65] Jouguet. “Sur la propagation des réactions chimiques dans les gaz”. fre. *Journal de Mathématiques Pures et Appliquées* (1905), pp. 347–425.
- [66] A. K. Kapila, R. Menikoff, J. B. Bdzil, S. F. Son, and D. S. Stewart. “Two-phase modeling of deflagration-to-detonation transition in granular materials: Reduced equations”. *Physics of Fluids* 13.10 (2001), p. 3002.
- [67] D. L. Kennedy. “The Challenge of Non-Ideal Detonation”. en. *Le Journal de Physique IV* 05.C4 (1995), pp. C4–191–C4–207.
- [68] D. E. Kittell and C. D. Yarrington. “A physically-based Mie–Grüneisen equation of state to determine hot spot temperature distributions”. *Combustion Theory and Modelling* 20.5 (2016), pp. 941–957.
- [69] D. E. Kittell, C. D. Yarrington, J. B. Lechman, and M. R. Baer. “Letter: Modeling reactive shock waves in heterogeneous solids at the continuum level with stochastic differential equations”. *Physics of Fluids* 30.5 (2018), p. 051701.
- [70] C. B. Kiyanda and M. Short. “Modelling of Detonation in PBX 9502 using a Stiffened-gas EOS Mixture Model”. *AIP Conference Proceedings* 955.1 (2007), p. 393.
- [71] M. J. Klein and P. H. E. Meijer. “Principle of Minimum Entropy Production”. *Physical Review* 96.2 (1954), p. 250.
- [72] B. D. Lambourn and C. A. Handley. “A two-temperature model for shocked porous explosive”. *AIP Conference Proceedings* 1793 (2017), p. 120025.
- [73] LD Landau and EM Lifshitz. *Fluid Mechanics*, Pargamon. 1987.
- [74] E. L. Lee and C. M. Tarver. “Phenomenological model of shock initiation in heterogeneous explosives”. *Physics of Fluids* 23.12 (1980), p. 2362.
- [75] J. H. S. Lee. *The Detonation Phenomenon*. Cambridge University Press, 2008.

- [76] B. van Leer. “Towards the ultimate conservative difference scheme. V. A second-order sequel to Godunov’s method”. *Journal of Computational Physics* 32.1 (1979), pp. 101–136.
- [77] G. A. Levesque and P. Vitello. “The Effect of Pore Morphology on Hot Spot Temperature”. *Propellants, Explosives, Pyrotechnics* 40.2 (2015), pp. 303–308.
- [78] G. A. Levesque, P. Vitello, and W. M. Howard. “Hot-spot contributions in shocked high explosives from mesoscale ignition models”. *Journal of Applied Physics* 113 (2013), p. 233513.
- [79] C. Matignon, N. Desbiens, R. Sorin, and V. Dubouis. “Theoretical study of the influence of the equation of state mixture properties on the velocity-curvature relationship for heterogeneous solid explosives”. *AIP Conference Proceedings* 1426 (2012), p. 319.
- [80] S. D. McGrane, T. D. Aslam, T. H. Pierce, S. J. Hare, and M. E. Byers. “Temperature of shocked plastic bonded explosive PBX 9502 measured with spontaneous Stokes/anti-Stokes Raman”. *Journal of Applied Physics* 123.4 (2018), p. 045902.
- [81] R. Menikoff. “Empirical Equations of State for Solids”. *Shock Wave Science and Technology Reference Library, Vol. 2*. Ed. by Y. Horie. Springer Berlin Heidelberg, 2007. Chap. 4, pp. 143–188.
- [82] R. Menikoff. *Complete EOS for PBX 9502*. Tech. rep. Los Alamos National Laboratory, 2009.
- [83] R. Menikoff. “On Beyond the Standard Model for High Explosives: Challenges & Obstacles to Surmount”. *AIP Conference Proceedings* 1195 (2010), p. 18.
- [84] R. Menikoff. *JWL Equation of State*. Tech. rep. Los Alamos National Laboratory, 2015.
- [85] R. Menikoff. *Complete Mie-Gruneisen Equation of State*. Tech. rep. Los Alamos National Laboratory, 2016.
- [86] R. Menikoff and E. Kober. “Equation of state and Hugoniot locus for porous materials: P- α model revisited”. *AIP Conference Proceedings* 505 (2000), pp. 129–132.

Bibliography

- [87] R. Menikoff and M. S. Shaw. “Reactive burn models and ignition & growth concept”. *EPJ Web of Conferences* 10 (2010), p. 00003.
- [88] R. Menikoff and M. S. Shaw. “Modeling detonation waves in nitromethane”. *Combustion and Flame* 158.12 (2011), pp. 2549–2558.
- [89] X. Mi, A. J. Higgins, E. Ioannou, L. Michael, N. Nikiforakis, J. Loiseau, H. D. Ng, and C. B. Kiyanda. “Shock-induced Collapse of Multiple Cavities in Liquid Nitromethane”. *16th International Detonation Symposium (in press)*. Cambridge, MD, 2018.
- [90] L. Michael. “Numerical Simulations of Shock-Induced Void Collapse in Liquid Explosives”. PhD thesis. University of Cambridge, 2012.
- [91] L. Michael and N. Nikiforakis. “A hybrid formulation for the numerical simulation of condensed phase explosives”. *Journal of Computational Physics* 316 (2016), pp. 193–217.
- [92] L. Michael and N. Nikiforakis. “The evolution of the temperature field during cavity collapse in liquid nitromethane. Part I: inert case”. *Shock Waves* (2018), pp. 1–20.
- [93] A. Minchinton. “On the Influence of Fundamental Detonics on Blasting Practice”. *11th International Symposium on Rock Fragmentation by Blasting*. Sydney, 2015, pp. 41–54.
- [94] John von Neumann. *Theory of detonation waves*. Tech. rep. DTIC Document, 1942.
- [95] N. Nikiforakis and J. F. Clarke. “Numerical studies of the evolution of detonations”. *Mathematical and Computer Modelling* 24.8 (1996), pp. 149–164.
- [96] O. E. Petel, D. Mack, A. J. Higgins, R. Turcotte, and S.K. Chan. “Minimum propagation diameter and thickness of high explosives”. *Journal of Loss Prevention in the Process Industries* 20.4-6 (2007), pp. 578–583.
- [97] O.E. Petel, D. Mack, A.J. Higgins, R. Turcotte, and S.K. Chan. “Comparison of the detonation failure mechanism in homogeneous and heterogeneous explosives”. *Proceedings of the 13th International Detonation Symposium, IDS 2006*. 2006, pp. 2–11.

- [98] F. Petitpas, R. Saurel, E. Franquet, and A. Chinnayya. “Modelling detonation waves in condensed energetic materials: multiphase CJ conditions and multidimensional computations”. *Shock Waves* 19.5 (2009), pp. 377–401.
- [99] F. Peugeot and M. W. Sharp. *Nimic Nations Collaborative Efforts in Shock Modelling Reactive Models for Hydrocodes : Past , Present and Future*. Tech. rep. December. Brussels, Belgium: NATO, 2002.
- [100] N. K. Rai, M. J. Schmidt, and H. S. Udaykumar. “High-resolution simulations of cylindrical void collapse in energetic materials: Effect of primary and secondary collapse on initiation thresholds”. *Physical Review Fluids* 2.4 (2017), p. 043202.
- [101] J. B. Ramsay. “Effect of Confinement on Failure in 95 TATB/5 KEL-F”. *8th Symposium (International) on Detonation*. Albuquerque, New Mexico, 1985, pp. 372–379.
- [102] T. R. Salyer and L. G. Hill. “The Dynamics of Detonation Failure in Conical PBX 9502 Charges”. *13th Symposium (International) on Detonation*. Norfolk, Virginia, 2006, pp. 24–34.
- [103] J. A. Sanchidrián, R. Castedo, L. M. López, P. Segarra, and A. P. Santos. “Determination of the JWL Constants for ANFO and Emulsion Explosives from Cylinder Test Data”. *Central European Journal of Energetic Materials* 12.2 (2015), pp. 177–194.
- [104] R. Saurel and R. Abgrall. “A Multiphase Godunov Method for Compressible Multifluid and Multiphase Flows”. *Journal of Computational Physics* 150.2 (1999), pp. 425–467.
- [105] R. Saurel, F. Fraysse, D. Furfaro, and E. Lapebie. “Multiscale multiphase modeling of detonations in condensed energetic materials”. *Computers & Fluids* 159 (2017), pp. 95–111.
- [106] R. Saurel, F. Petitpas, and R. A. Berry. “Simple and efficient relaxation methods for interfaces separating compressible fluids, cavitating flows and shocks in multiphase mixtures”. *Journal of Computational Physics* 228.5 (2009), pp. 1678–1712.
- [107] S. Schoch. “Multi-phase detonations in elastic-plastic confinement”. PhD thesis. University of Cambridge, 2012.

Bibliography

- [108] S. Schoch, N. Nikiforakis, B. J. Lee, and R. Saurel. “Multi-phase simulation of ammonium nitrate emulsion detonations”. *Combustion and Flame* 160.9 (2013), pp. 1883–1899.
- [109] L. Seaman. “Lagrangian analysis for multiple stress or velocity gages in attenuating waves”. *Journal of Applied Physics* 45.10 (1974), pp. 4303–4314.
- [110] S. B. Segletes. “Thermodynamic stability of the Mie–Grüneisen equation of state, and its relevance to hydrocode computations”. *Journal of Applied Physics* 70.5 (1991), pp. 2489–2499.
- [111] W. L. Seitz, H. L. Stacy, R. Engelke, P. K. Tang, and J. Wackerle. “Detonation Reaction-Zone Structure of PBX 9502”. *Proceedings of the Ninth Symposium (International) on Detonation*. Portland, OR, 1989, p. 657.
- [112] G. J. Sharpe and M. Braithwaite. “Steady Non-ideal Detonations in Cylindrical Sticks of Explosives”. *Journal of Engineering Mathematics* 53.1 (2005), pp. 39–58.
- [113] G. J. Sharpe and M. Short. “Shock-induced ignition of thermally sensitive explosives”. *IMA Journal of Applied Mathematics* 69.5 (2004), pp. 493–520.
- [114] G. J. Sharpe and M. Short. “Ignition of thermally sensitive explosives between a contact surface and a shock”. *Physics of Fluids* 19.12 (2007), p. 126102.
- [115] S. A. Sheffield and R. Engelke. “Condensed-Phase Explosives: Shock Initiation and Detonation Phenomena”. *Shock Wave Science and Technology Reference Library, Vol. 3*. Ed. by Y. Horie. Springer Berlin Heidelberg, 2009. Chap. 1, pp. 1–64.
- [116] S. A. Sheffield, R. L. Gustavsen, and R. R. Alcon. “In-situ magnetic gauging technique used at LANL-method and shock information obtained”. *AIP Conference Proceedings* 505 (2000), p. 1043.
- [117] S. A. Sheffield, R. L. Gustavsen, L. G. Hill, and R. R. Alcon. “Electromagnetic Gauge Measurements of Shock Initiating PBX9501 and PBX9502 Explosives”. *11th Detonation (International) Symposium*. Snowmass, CO, 1998, pp. 451–458.
- [118] J. E. Shepherd and D. R. Begeal. “Transient compressible flow in porous materials”. *NASA STI/Recon Technical Report N 88* (Jan. 1988).

- [119] M. Short and J. J. Quirk. “High Explosive Detonation–Confiner Interactions”. *Annual Review of Fluid Mechanics* 50 (2018), p. 215.
- [120] M. Short, J. Quirk, C. B. Kiyanda, S. I. Jackson, M. E. Briggs, and M. A. Shinas. “Simulation of detonation of ammonium nitrate fuel oil mixture confined by aluminum: Edge angles for DSD”. *Fourteenth (International) Detonation Symposium*. 2010, pp. 769–778.
- [121] D. S. Stewart, S. Yoo, and W. C. Davis. “Equation of State for modelling the detonation reaction zone”. *12th Symposium (International) on Detonation*. Vol. 64. 2002, p. 624.
- [122] D. S. Stewart, S. Yoo, and B. L. Wescott. “High-order numerical simulation and modelling of the interaction of energetic and inert materials”. *Combustion Theory and Modelling* 11.2 (2007), pp. 305–332.
- [123] P. K. Tang, W. W. Anderson, J. N. Fritz, R. S. Hixson, and J. E. Vorthman. “A Study of the Overdriven Behaviors of PBX 9501 and PBX 9502”. *11th International Detonation Symposium*. Snowmass, CO, 1998, pp. 1058–1064.
- [124] C. M. Tarver and E. M. McGuire. “Reactive flow modeling of the Interaction of TATB Detonation Waves with Inert Materials”. *12th Symposium (International) on Detonation*. San Diego, California, 2002.
- [125] E. F. Toro. *Riemann Solvers and Numerical Methods for Fluid Dynamics: A Practical Introduction*. 2009.
- [126] E. F. Toro, M. Spruce, and W. Speares. “Restoration of the contact surface in the HLL-Riemann solver”. English. *Shock Waves* 4.1 (1994), pp. 25–34.
- [127] M. Van Thiel, J. Shaner, and E. Salinas. *Compendium of Shock Wave Data*. Tech. rep. Livermore: Lawrence Livermore National Lab, 1977.
- [128] J. E. Vorthman, G. Andrews, and J. Wackerle. “Reaction Rates from Electromagnetic Gauge Data”. *8th Symposium (International) on Detonation*. Albuquerque, New Mexico, 1985.
- [129] B. L. Wescott, D. S. Stewart, and W. C. Davis. “Equation of state and reaction rate for condensed-phase explosives”. *Journal of Applied Physics* 98.5 (2005), p. 053514.

Bibliography

- [130] N. J. Whitworth. “CREST modelling of PBX 9502 corner turning experiments at different initial temperatures”. *Journal of Physics: Conference Series* 500.5 (2014), p. 052050.
- [131] M. L. Wilkins. *Computer Simulation of Dynamic Phenomena*. Springer Berlin Heidelberg, 2013.
- [132] S. D. Wilkinson, M. Braithwaite, N. Nikiforakis, and L. Michael. “A complete equation of state for non-ideal condensed phase explosives”. *Journal of Applied Physics* 122.22 (2017), p. 225112.
- [133] R. E. Winter, S. S. Sorber, D. A. Salisbury, P. Taylor, R. L. Gustavsen, S. A. Sheffield, and R. Alcon. “Experimental study of the shock response of an HMX-based explosive”. *Shock Waves* 15.2 (2006), p. 89.
- [134] Y. B. Zeldovich. “On the Theory of the Propagation of Detonation in Gaseous Systems”. *Zh. Eksp. Teoret. Fiz.* 10 (1940), p. 542.
- [135] Y. B. Zeldovich. “Regime classification of an exothermic reaction with nonuniform initial conditions”. *Combustion and Flame* 39.2 (1980), p. 211.
- [136] Y. B. Zeldovich and Y. P. Raizer. *Physics of Shock Waves and High-Temperature Hydrodynamic Phenomena*. Dover Publications, 1965.
- [137] J. A. Zukas and W. P. Walters. *Explosive Effects and Applications*. High pressure shock compression of condensed matter. Springer New York, 2002.